

CHEMICAL LABELING STRATEGIES FOR MASS SPECTROMETRY-BASED
BIOMOLECULAR IDENTIFICATION, CHARACTERIZATION AND QUANTIFICATION

By

Shuai Nie

A DISSERTATION

Submitted to
Michigan State University
in partial fulfillment of the requirements
for the degree of

Chemistry – Doctor of Philosophy

2015

ABSTRACT

CHEMICAL LABELING STRATEGIES FOR MASS SPECTROMETRY-BASED BIOMOLECULAR IDENTIFICATION, CHARACTERIZATION AND QUANTIFICATION

By

Shuai Nie

Advances in the development of mass spectrometry (MS) and tandem mass spectrometry (MS/MS) instrumentation have made this technique a versatile analytical tool to identify, characterize and quantify biomolecules including peptides, proteins, lipids, nucleic acids, oligosaccharides and other metabolites. However, based on the individual physicochemical properties of various biomolecules, biomolecular MS or MS/MS on its own may not necessarily give the desired analytical information. Therefore, chemical labeling strategies which alter the behavior of analytes with respect to their ionization, fragmentation and mass analysis are commonly used to facilitate MS-based analysis of biomolecules. This dissertation focuses on the development of biomolecular chemical labeling strategies for lipids, peptides and proteins, to provide improved capabilities for MS-based qualitative and quantitative analysis.

Structural labeling via gas phase ion chemistry provides a convenient and rapid modification method for structural and reactivity characterization of modified biomolecular ions. Here, a novel photo-induced inter-molecular gas-phase cross-linking reaction has been developed to investigate the cross-linking reactivity of individual triacylglyceride (TG) molecules as a function of their structures. Ultraviolet photodissociation tandem mass spectrometry (UVPD-MS/MS) of non-covalent complex ions consisting of TG dimers and protonated diiodoaniline resulted in the formation of multiple cross-linked TG products via homolysis of carbon-iodine bonds, hydrogen

abstraction and radical recombination. The efficiency of the UVPD reaction depended on the number of unsaturation sites present within the TG lipids.

For MS-based quantification, an approach for the multiplexed relative quantification of aminophospholipids from within two different crude lipid extracts was developed. Relative quantification at the 'sum composition' and/or 'molecular lipid' levels was achieved using high resolution/accurate mass MS/MS by ratiometric measurement of pairs of 'reporter' ions formed via the neutral loss from isobaric stable isotope-labeled d_6 -'heavy' and d_6 -'light' S,S'-dimethylthiobutanoylhydroxysuccinimide and iodine/methanol derivatized aminophospholipid ions.

In addition, absolute quantification of full length parathyroid hormone (PTH 1-84), a clinical protein biomarker of secondary hyperparathyroidism, and its *in vivo* oxidized and truncated variants was achieved using a dual stable isotope-labeled internal standard approach coupled with immunocapture and high resolution LC-MS and MS/MS. Analysis of clinical PTH samples using this strategy revealed that no oxidation or PTH 7-84 occurred *in vivo*. However, several novel sites of *in vivo* PTH truncation were discovered. At last, stable isotope-containing dimethyl labeling and multi-dimensional LC-MS/MS were applied for proteomic profiling of human RPMI-8226 cells treated with competitive (i.e., Bortezomib) and non-competitive (i.e., TCH-013) proteasome inhibitors to evaluate their distinct mechanisms of action. Four proteins closely related to the regulation of mitochondrial functions and growth and division of cancer cells were observed to be selectively down-regulated after TCH-013 treatment compared to Bortezomib or vehicle control treatment.

ACKNOWLEDGEMENTS

The experience of study and research in the methodology and application development of bioanalytical mass spectrometry and related chemical derivatization strategies in the past four and half years is the most exciting and challenging adventure I've ever had in my life so far. I would like to thank all the people mentioned below for their generous help and support during the life-changing experience.

First, I want to give special thanks to my advisor, Dr. Gavin Reid, who introduced me to the amazing world of bioanalytical mass spectrometry and provided me the guidance toward becoming an independent analytical chemist. Your enthusiasms for scientific discoveries, broad knowledge and meticulous thinking have been always inspiring me. Also, thanks for letting me have the opportunity to conduct my research and collaborate with other talented scientists at both Michigan State University and the University of Melbourne. For my previous and current committee members, Dr. Merlin Bruening, Dr. Marcos Dantus, Dr. Jetze Tepe and Dr. Xuefei Huang, I sincerely appreciate your help to my research projects, especially for providing professional advices in fields that I was not familiar with before.

I greatly appreciate my collaborators, Evert Njomen and Dr. Jetze Tepe at Michigan State University, for providing the cell lysates of drug-treated RPMI-8226 cells for the TCH-013 drug action mechanism study. Also, thank DiaSorin for providing the clinical patient samples for the quantitative analysis of PTH proteins.

I would like to greatly thank the current and former Reid lab members, Dr. Eileen Ryan, Dr. Todd Lydic and Dr. Li Cui for supporting me and proofreading my dissertation. I also thank all the other Reid lab members who have helped me with my experiments,

scientific writing and exams. Thanks for Dr. Cassie Phaner who taught me the sample handling and derivatization techniques for lipids and lipidomic analysis. I deeply appreciate all the help I received from the Dr. Nicholas Williamson, Dr. Ching-Seng Ang and Dr. David Perkins during my one-year visit in the Bio21 Molecular Science & Biotechnology Institute at the University of Melbourne. Thanks for helping me with the instrument setup and data analysis using bioinformatic tools.

Finally, I want to thank my parents. I can always feel their unconditional love and support even though most of the time I was thousands of miles away from them. Thanks also to my girlfriend for supporting and understanding me when I was busy doing experiments or writing. Finally, thanks to all my other friends who will always give me warm encouragement or just simply listen to me when I was having a bad day.

TABLE OF CONTENTS

LIST OF TABLES.....	x
LIST OF FIGURES.....	xi
KEY TO ABBREVIATIONS	xv
CHAPTER ONE	
An Overview of Chemical Labeling Strategies for Mass Spectrometry Analysis of Biomolecules.....	1
1.1 Introduction to Mass Spectrometry Analysis of Natural Biomolecules	1
1.1.1 Ionization Techniques	1
1.1.2 Mass Analyzers	2
1.1.3 Fragmentation Techniques.....	5
1.1.3.1 Collision-Induced Dissociation.....	5
1.1.3.2 Electron Capture Dissociation and Electron Transfer Dissociation.....	6
1.1.3.3 Photodissociation.....	7
1.1.4 Applications for Identification and Quantification of Natural Biomolecules.....	7
1.1.4.1 Peptides and Proteins.....	8
1.1.4.2 Lipids	10
1.1.4.3 Nucleic Acids	14
1.1.4.4 Oligosaccharides and Other Small Molecule Metabolites.....	14
1.2 Chemical Labeling Strategies for Improved Identification, Characterization and Quantification of Biomolecules Using Mass Spectrometry.....	15
1.2.1 Applications of Structural Labeling for Improved Identification and Structural Characterization	16
1.2.1.1 Ionization Efficiency	16
1.2.1.2 Structural Characterization of Peptides and Proteins.....	19
1.2.1.2.1 Sequence of Amino Acid Residues.....	19
1.2.1.2.2 Post-Translational Modifications	21
1.2.1.2.3 Tertiary and Quaternary Structures of Proteins	22
1.2.1.3 Structural Characterization of Lipids	24
1.2.1.3.1 Lipid Classes and Sum Compositions	24
1.2.1.3.2 Identities and Linkage Positions of Glycerol Backbone Substituents.....	25
1.2.1.3.3 Positions and Stereochemistry of Carbon-Carbon Double Bonds.....	27
1.2.1.4 Intra- and Inter-Molecular Interactions of Nucleic Acids.....	28
1.2.1.5 Structural Characterization of Oligosaccharides.....	28
1.2.2 Applications of Stable Isotope Labeling for Improved Structural Characterization and Quantification	29
1.2.2.1 Structures of Large Biomolecules and Mechanisms of Gas Phase Biomolecular Ion Fragmentation.....	29
1.2.2.2 Quantification of Biomolecules	31
1.2.2.2.1 Stable Isotope-Labeled Analogue Internal Standards	32
1.2.2.2.2 Metabolic Labeling.....	33

1.2.2.2.3 Chemical Labeling	35
1.3 Aims of this Dissertation.....	37

CHAPTER TWO

Photo-Induced Inter-Molecular Cross-Linking of Gas Phase Triacylglycerol Lipids Ions	39
2.1 Introduction.....	39
2.2 Results and Discussion.....	42
2.2.1 Photo-Induced Dissociation of Protonated Diiodoaniline-TG Dimer Complex Ions	42
2.2.2 Proposed Mechanisms and Structures of Covalently Cross-linked TG Dimer Product Ions.....	45
2.2.3 Proposed Fragmentation Mechanisms of TG Dimer Product Ion Structures 1a , 1b and 1c	48
2.2.4 Effects of Structures of the Cross-Linker and TG Lipids on the Formation of Cross-Linked TG Dimer Product Ions	59
2.2.5 Solution Phase Cross-Linking of TG lipids	60
2.3 Conclusions.....	62

CHAPTER THREE

Characterization and Multiplexed Quantification of Derivatized Aminophospholipids ...	63
3.1 Introduction.....	63
3.2 Results and Discussion.....	66
3.2.1 Characterization of the Gas Phase Fragmentation Reactions of DMBNHS Derivatized Aminophospholipids.....	66
3.2.1.1 Diacyl-Aminophospholipids.....	66
3.2.1.2 Alkyl Ether-Aminophospholipids	74
3.2.1.3 Plasmalogen-Aminophospholipids	76
3.2.2 Characterization and Quantification of Isobaric Stable Isotope Containing DMBNHS Derivatized Aminophospholipid Standards	77
3.2.3 Multiplexed Quantification of Selected Aminophospholipid Ion Abundance Changes Between a Metastatic Colorectal Cancer Cell Line, SW620 and its AlkyGlycerone Phosphate Synthase (AGPS) siRNA Knockdown	81
3.3 Conclusions.....	91

CHAPTER FOUR

Experimental Methods for Chapters Two and Three	92
4.1 Materials	92
4.2 siRNA Knockdown of Alkyglycerone Phosphate Synthase (AGPS) in SW620 Colorectal Cancer Cells and Lipid Extraction.....	92
4.3 Derivatization of Lipid Standards and Crude Lipid Extracts	93
4.3.1 Synthesis of Saturated TG Lipids from Unsaturated TG Lipid Standards	93
4.3.2 Photo-Induced Solution Phase Cross-linking of TG Lipid Standards.....	93
4.3.3 Derivatization of Aminophospholipids Using d ₆ -Heavy/light DMBNHS and Iodine/Methanol Methods	94
4.4 Mass Spectrometry.....	95

4.4.1	Photo-Induced Gas Phase Cross-linking MS/MS and CID-MS ⁿ Structural Analysis of TG Dimer Complex Ions.....	95
4.4.2	ESI-MS, -MS/MS and -MS ³ Analysis of Derivatized Aminophospholipid Standards.....	96
4.4.3	ESI-MS and -MS/MS Analysis of Derivatized Crude Lipid Extracts from Combined Control and AGPS siRNA Knockdown of the SW620 Colorectal Cancer Cells	97

CHAPTER FIVE

Quantitative Immuno LC-MS/MS of Parathyroid Hormone and Its *In Vivo* Heterogeneous Post-Translational Protein Modifications: Oxidation and Truncation.... 99

5.1	Introduction.....	99
5.2	Results and Discussion.....	105
5.2.1	Quantitative Immuno LC-MS/MS Workflow with Optimized Sample Preparation, High Resolution/Accurate Mass HCD-MS/MS and Near Full Sequence Coverage.....	105
5.2.2	Quantitative Analysis of <i>In Vivo</i> Full Length, Oxidized and Truncated PTH Tryptic Peptides in Patient Samples.....	112
5.2.3	Identification of Novel Truncation Sites of PTH Proteins.....	120
5.3	Conclusions.....	122

CHAPTER SIX

Quantitative Proteomic Analysis Using Dimethyl Labeling and Two Dimensional LC-MS/MS to Study the Mechanism of Action of the Non-Competitive Proteasome Inhibitor, TCH-013..... 123

6.1	Introduction.....	123
6.2	Results and Discussion.....	126
6.2.1	Quantitative Proteomic Analysis Workflow	126
6.2.2	Coverage of Protein Identification and Selection Criteria During Protein Quantification.....	129
6.2.3	Protein Regulation in Human RPMI-8226 Cells Induced by TCH-013.....	132
6.3	Conclusions.....	136

CHAPTER SEVEN

Experimental Methods for Chapters Five and Six 137

7.1	Materials	137
7.2	Biological Samples	138
7.2.1	Patient Information and Immuno-Affinity Enrichment of PTH Proteins	138
7.2.2	Cell Culture and Treatment Using TCH-013, Bortezomib and DMSO.....	138
7.3	Protein Digestion	139
7.3.1	Trypsin Digestion of PTH Standards and Immuno-Enriched Samples from Patient Plasmas.....	139
7.3.2	Trypsin Digestion of Proteins in Lysates of TCH-013, Bortezomib and DMSO Treated RPMI-8226 Cells	140
7.4	Dimethyl Labeling of Digested Proteins from TCH-013, Bortezomib and DMSO Treated RPMI-8226 Cells	140

7.5 Basic pH Reversed-Phase Fractionation of Digested and Dimethyl Labeled Proteins.....	141
7.6 Mass Spectrometry.....	141
7.6.1 LC-MS/MS Analysis of Digested PTH standards and Immuno-Affinity Enriched Samples from Patient Plasmas.....	141
7.6.2 LC-MS/MS Analysis of Digested, Dimethyl Labeled and Fractionated Proteins from TCH-013, Bortezomib and DMSO Treated RPMI-8226 Cells.....	143
7.7 Data Analysis.....	144
7.7.1 Quantification of Full Length, Oxidized and Truncated PTH Variants in Patient Plasma.....	144
7.3.3 Bioinformatic Analysis for Proteomic Profiling of Proteins in TCH-013, Bortezomib and DMSO Treated RPMI-8226 Cells.....	145
BIBLIOGRAPHY	147

LIST OF TABLES

Table 5.1	HCD-MS/MS precursor/fragment ion transitions, optimized HCD normalized collision energy (NCE) and retention times for quantitatively monitored PTH peptides.	109
Table 5.2	Concentration of full length, oxidized and truncated PTH tryptic peptides in patient plasma determined by quantitative immuno LC-MS/MS with near full sequence coverage. Concentrations of oxidized PTH peptides were corrected to remove <i>ex vivo</i> oxidation. ND indicates that the peptide was not detectable.	118
Table 6.1	Protein down-regulation (near 2 folds) expressed in \log_2 heavy/light protein ratios in three biological replicates of TCH-013 (heavy) treated RPMI-8226 cells compared to that treated with Bortezomib (light) and DMSO control (light).....	135

LIST OF FIGURES

Figure 1.1	Structural complexity of glycerophospholipids lipids. PC, PE, PS, PA, PG, CL and PI indicate glycerophosphocholine, glycerophosphoethanolamine, glycerophosphoserine, glycerophosphate, glycerophosphoglycerol, glycerophosphoglycerophosphoglycerol and glycerophosphoinositol, respectively.	13
Figure 2.1	Ion trap 266 nm UVPD-MS/MS of mono-unsaturated and saturated TG homodimer complex ions with protonated diIA. (A) $2TG_{(14:0/16:1/14:0)}$ + 3,4-diIA (complex 1), (B) $2TG_{(14:0/16:0/14:0)}$ + 3,4-diIA (complex 2) and (C) $2TG_{(14:0/16:1/14:0)}$ + 2,4-diIA (complex 3). Note, that high mass ion complexes are fragile ions and as such exhibit an apparent mass-shift to lower m/z (see explanation provided in the text).....	44
Figure 2.2	Proposed mechanisms for the photo-induced cross-linking reactions of TG dimer complex ions $[2TG_{(14:0/16:1/14:0)} + 3,4-diIA + H]^+$ (complex 1).....	47
Figure 2.3	Ion trap CID-MS ³ analysis of cross-linked mono-unsaturated and saturated TG homodimer complex ions with protonated 3,4-diIA or 2,4-diIA, formed by 266 nm UVPD-MS/MS. (A) [complex 1 - 2I] ⁺ from Figure 2.1A, (B) [complex 2 - 2I] ⁺ from Figure 2.1B, and (C) [complex 3 - 2I] ⁺ from Figure 2.1C. The major product ions formed from proposed structures 1a , 1b and 1c in Figure 2.2 are labeled in Figure 2.3A.	49
Figure 2.4	Ion trap CID-MS ⁴ analysis of cross-linked mono-unsaturated TG homodimer complex ions from Figure 2.3A. (A) [complex 1 - 2I - aniline] ⁺ , (B) [complex 1 - 2I - $TG_{(14:0/16:1/14:0)}$] ⁺ , and (C) [complex 1 - 2I - 14:0 FA] ⁺	52
Figure 2.5	Proposed mechanisms for the CID-MS ³ and -MS ⁴ fragmentation reactions of [complex 1 - 2I] ⁺ ions corresponding to structure 1a in Figure 2.2.....	53
Figure 2.6	Proposed mechanisms for the CID-MS ³ and -MS ⁴ fragmentation reactions of [complex 1 - 2I] ⁺ ions corresponding to structure 1b in Figure 2.2.....	55
Figure 2.7	Ion trap CID-MS ³ analysis of the cross-linked saturated/mono-unsaturated TG heterodimer complex ion [complex 4 - 2I] ⁺ , formed by 266 nm UVPD-MS/MS.....	56
Figure 2.8	Proposed mechanisms for the CID-MS ³ and -MS ⁴ fragmentation reactions of [complex 1 - 2I] ⁺ ions corresponding to structure 1c in Figure 2.2. MG denotes monoacylglyceride.	58
Figure 2.9	Ion trap MS and MS/MS analysis of products in solution phase inter-molecular cross-linking reactions of TG lipids. (A) MS analysis of products in	

	the solution containing TG _(14:0/16:1/14:0) and 3,5-diiodoaniline after 9 min of irradiation with 266 nm UV photons; (B) CID-MS/MS analysis of the product ions at m/z 1496 from Figure 2.9A.....	61
Figure 3.1	HCD-MS/MS analysis of DMBNHS derivatized (A) PE _(18:0/18:1) and (B) PS _(16:0/18:1)	69
Figure 3.2	Proposed CID-MS/MS fragmentation mechanisms for DMBNHS derivatized PE _(18:0/18:1) and PS _(16:0/18:1)	70
Figure 3.3	HCD-MS ³ analysis of the S(CH ₃) ₂ neutral loss (NL) product ions formed by linear ion trap CID-MS/MS of the DMBNHS derivatized (A) PE _(18:0/18:1) and (B) PS _(16:0/18:1)	72
Figure 3.4	Proposed HCD-MS ³ fragmentation mechanisms for DMBNHS derivatized PE _(18:0/18:1) after the neutral loss of 271 Da.	73
Figure 3.5	CID-MS/MS analysis of a DMBNHS derivatized monoalkyl-ether PE lipid PE _(O-16:0_18:1) from a crude lipid extract of SW620 colorectal cancer cells. The inset shows the HCD-MS ³ spectrum of the S(CH ₃) ₂ neutral loss (NL) product ion.....	75
Figure 3.6	CID-MS/MS, HCD-MS ³ and HCD-MS/MS of a 1:1 mixture of d ₆ -heavy/light DMBNHS and iodine/methanol derivatized PE lipids. (A) CID-MS/MS of pooled d ₆ -heavy/light DMBNHS derivatized PE _(14:0/14:0) . The inset shows the HCD-MS ³ spectrum of the S(CD ₃) ₂ neutral loss product ion from the d ₆ -heavy DMBNHS derivatized lipid as well as the structures and initial fragmentation sites for the d ₆ -heavy/light DMBNHS derivatized lipid species (B) HCD-MS/MS of pooled d ₆ -heavy/light DMBNHS and iodine/methanol derivatized PE _(P-18:0/22:6)	80
Figure 3.7	Ultra-high resolution/accurate mass ESI-MS of a 1:1 mixture (normalized to protein concentration) of isobaric d ₆ -heavy/light DMBNHS and iodine/methanol derivatized crude lipid extracts from a metastatic colorectal cancer cell line, SW620 and its alkyglycerone phosphate synthase (AGPS) siRNA knockdown. The insets show expanded m/z regions containing the lipids PE _(35:1) and PE _(O-36:1) , PS _(O-28:2) , and PE _(P-35:1) . The ion labeled with a # corresponds to a diisooctyl phthalate contaminant ion.	83
Figure 3.8	HCD-MS/MS of the isobaric d ₆ -heavy/light DMBNHS derivatized PE _(35:1) and PE _(O-36:1) lipids from Figure 3.5. The inset shows expanded m/z regions of the spectrum containing the characteristic S(CH ₃) ₂ /S(CD ₃) ₂ neutral loss product ions.....	85
Figure 3.9	HCD-MS/MS of the isobaric d ₆ -heavy/light DMBNHS derivatized PS _(O-28:2) lipid from Figure 3.7. The inset shows an expanded m/z region of the	

spectrum containing the characteristic $S(CH_3)_2/S(CD_3)_2$ neutral loss product ions..... 87

Figure 3.10 HCD-MS/MS of the isobaric d_6 -heavy/light DMBNHS and iodine/methanol derivatized $PE_{(P-35:1)}$ lipid from Figure 3.7. The inset shows an expanded m/z region of the spectrum containing the characteristic O-alkenyl-chain neutral loss product ions..... 90

Figure 5.1 Summary of (A) previously identified full length PTH 1-84, N-terminally truncated PTH X-84 (X=7, 28, 34, 37, 38, 45 and 48) and mid-molecular fragment PTH X-77 (X= 34, 37 and 38) [248-250]; (B) full length, oxidized and truncated PTH protein-unique tryptic peptides monitored quantitatively during LC-MS/MS in this study; (C) truncated PTH protein-unique tryptic peptides monitored qualitatively during LC-MS/MS in this study. The dashed lines represent the variable lengths of truncated forms of PTH. 103

Figure 5.2 Oxidation percentages of PTH in different sets of patient samples [264]. The percentage of oxidation was calculated by taking the sum concentration of PTH 1-13 M(O), PTH 7-13 M(O) and PTH 14-20 M(O) divided by the sum concentration of all full length, truncated and oxidized tryptic peptides quantified. There were 41 blood samples in set A collected from site 1 and stored at least a week before sample analysis, and 29 samples in set B and 4 samples in set C collected from site 2 and stored at most 2 days before sample analysis. 104

Figure 5.3 Quantitative immuno LC-MS/MS workflow with optimized sample preparation, high resolution/accurate mass HCD-MS/MS and near full sequence coverage. Pmp indicates paramagnetic particles..... 107

Figure 5.4 HCD-MS/MS spectra of (A) ^{15}N -labeled PTH 1-13 ($z = +3$); (B) $^{13}C_6^{15}N_1Leu$ -labeled PTH 1-13 M(O) ($z = +3$); (C) ^{15}N -labeled PTH 7-13 ($z = +3$); (D) $^{13}C_6^{15}N_1Leu$ -labeled PTH 7-13 M(O) ($z = +3$); (E) ^{15}N -labeled PTH 14-20 ($z = +2$); (F) $^{13}C_6^{15}N_1Leu$ -labeled PTH 14-20 M(O) ($z = +2$) with optimized charge states of precursor ions and HCD normalized collision energy (NCE) for sensitivity..... 108

Figure 5.5 Resolving monitored fragment ions from artefact ions with isobaric m/z in a patient sample using high resolution/accurate mass HCD-MS/MS (A) extracted ion current (XIC) chromatogram of y_{11}^{2+} (m/z 643.3320) from PTH 1-13 M(O) (m/z 491.2576); (B) XIC chromatogram of y_{11}^{2+} (m/z 651.3080) from ^{15}N -labeled PTH 1-13 M(O) (m/z 497.2396); (C) XIC chromatogram of y_{11}^{2+} (m/z 646.8404) from $^{13}C_6^{15}N_1Leu$ -labeled PTH 1-13 M(O) (m/z 493.5968). Resolution for Figure 5.5A-C was at 17,500 (at $m/\Delta m = 200$). The inset shows expanded m/z region of the HCD-MS/MS of PTH 1-13 M(O) averaged across the XIC peak in Figure 5.5A at resolution of 17,500 (dotted line) and 140,000 (solid line) 111

Figure 5.6	Extracted ion current (XIC) chromatograms from a patient sample for (A) base peak in MS data and for monitored HCD-MS/MS fragment ions of (B) PTH 1-13, (C) ¹⁵ N-labeled PTH 1-13, (D) PTH 1-13 M(O), (E) ¹⁵ N-labeled PTH 1-13 M(O), (F) ¹³ C ₆ ¹⁵ N ₁ Leu-labeled PTH 1-13 M(O), (G) PTH 7-13, (H) ¹⁵ N-labeled PTH 7-13, (I) PTH 7-13 M(O), (J) ¹⁵ N-labeled PTH 7-13 M(O), (K) ¹³ C ₆ ¹⁵ N ₁ Leu-labeled PTH 7-13 M(O), (L) PTH 14-20, (M) ¹⁵ N-labeled PTH 14-20, (N) PTH 14-20 M(O), (O) ¹⁵ N-labeled PTH 14-20 M(O) and (P) ¹³ C ₆ ¹⁵ N ₁ Leu-labeled PTH 14-20 M(O) as listed in Table 5.1.	114
Figure 5.7	Extracted ion current (XIC) chromatograms of representative HCD-MS/MS fragment ions from truncated PTH peptides in a patient sample (A) XIC chromatogram of γ_7^+ (m/z 681.4042) from PTH 34-44 (m/z 556.3348); (B) XIC chromatogram of γ_5^{2+} (m/z 277.1765) from PTH 37-44 (m/z 397.7478); (C) XIC chromatogram of γ_5^{2+} (m/z 277.1765) from PTH 38-44 (m/z 341.2058); (D) XIC chromatogram of γ_{10}^+ (m/z 1017.4847) from PTH 66-77 (m/z 609.3040).	119
Figure 5.8	Identification of novel truncation sites of PTH by LC-HCD-MS/MS analysis of (A) PTH 53-66 (z = +4) and (B) PTH 66-74 (z = +2) from a representative patient sample.	121
Figure 6.1	A workflow using tryptic digestion, dimethyl labeling, basic reversed-phase fractionation, LC-MS/MS and bioinformatic analysis for quantitative proteomic analysis of TCH-013, Bortezomib and DMSO (vehicle control) treated human RPMI-8226 cells.	128
Figure 6.2	Overlapping of identified heavy/light proteins in three biological replicate sample mixtures consisting of (A) a heavy-labeled TCH-013 (10 μ M) treated sample mixed with a light-labeled Bortezomib (0.1 μ M) treated sample; (B) a heavy-labeled TCH-013 (10 μ M) treated sample mixed with a light-labeled DMSO (0.1%, v/v) treated sample. The influence of selection criteria (i.e., minimum of peptides assigned to each protein) on the number of relatively quantified proteins common in three biological replicates of sample mixture A (C) and B (D).....	131
Figure 6.3	Histograms of averaged log ₂ heavy/light proteins ratios (n=3) for quantified proteins after (A) TCH-013 (heavy) treatment vs Bortezomib (light) treatment and (B) TCH-013 (heavy) treatment vs DMSO (light) treatment.....	134

KEY TO ABBREVIATIONS

AGPS: alkyglycerone phosphate synthase

CI: chemical ionization

CID: collision-induced dissociation

CL: glycerophosphoglycerophosphoglycerol

DAG: diacylglyceride

diIA: diiodoaniline

DMBNHS: S,S'-dimethylthiobutanoylhydroxysuccinimide ester iodide

DNA: deoxyribonucleic acid

ECD: electron capture dissociation

EI: electron ionization

ESI: electrospray ionization

ETD: electron transfer dissociation

FA: fatty acid

FT-ICR: Fourier transform ion cyclotron resonance

GC: gas chromatography

HCD: higher-energy collisional dissociation

HDX: hydrogen-deuterium exchange

HPLC: high performance liquid chromatography

ICAT: isotope-coded affinity tags

IDMS: isotope dilution mass spectrometry

iTRAQ: isobaric tags for relative and absolute quantification

MALDI: matrix-assisted laser desorption/ionization

MM: multiple myeloma

MRM: multiple reaction monitoring

MS: mass spectrometry

MS/MS: tandem mass spectrometry

MSⁿ: multi-stage tandem mass spectrometry

m/Δm: the m/z value of a peak divided by the full width of the peak at half its maximum height

NHS: N-hydroxysuccinimide

PA: glycerophosphate

PC: glycerophosphocholine

PE: glycerophosphoethanolamine

PG: glycerophosphoglycerol

PI: glycerophosphoinositol

PS: glycerophosphoserine

PTH: parathyroid hormone

PTHrR: PTH related protein

PTM: post-translational modification

RDD: radical-directed dissociation

RNA: ribonucleic acid

SILAC: stable isotope labeling with amino acid in cell culture

siRNA: silencing RNA

TG: triglyceride

TMTs: tandem mass tags

TOF: time-of-flight

UHPLC: ultra-high performance liquid chromatography

UVPD: ultraviolet photodissociation

XIC: extracted ion current

CHAPTER ONE

An Overview of Chemical Labeling Strategies for Mass Spectrometry Analysis of Biomolecules

1.1 Introduction to Mass Spectrometry Analysis of Natural Biomolecules

1.1.1 Ionization Techniques

Mass spectrometry (MS) represents a key analytical method for the analysis of biomolecules, including peptides, proteins [1], lipids [2], nucleic acids [3], oligosaccharides [4] and other small molecule metabolites [5] and is based on the intrinsic and most basic property of any molecule, its molecular weight. Before the advent of MS, which measures the mass to charge ratios (m/z) of ions, molecular weights were indirectly assigned based on molecular size or sedimentation coefficient with low resolution and throughput, using size exclusion chromatography [6], electrophoresis [7] and ultracentrifugation [8]. In a mass spectrometer, electric and/or magnetic fields are used to control the trajectories of ionized molecules. Physical parameters related to analyte ions can be measured by the instrument for calculation of their molecular weight based on rigorous equations of ion motion, with high resolution and accuracy [9]. At the early stage of MS-based biomolecule analysis, electron ionization (EI) and chemical ionization (CI) were the two most widely used ionization techniques which required the analytes to be gasified before ionization and therefore limited the applications to volatile and thermally stable small biomolecules (e.g., oligopeptides and esterified fatty acids) [9]. With the introduction of 'soft' ionization techniques including electrospray ionization (ESI) [10] and matrix-assisted laser desorption ionization (MALDI) [11] in the late 1980s, MS analysis of large biomolecules

became practical. During the process of these two 'soft' ionization techniques, non-volatile and thermally unstable large biomolecules can be directly extracted from solution phase or a mixture of sample and matrix into the gas phase as intact structures due to the negligible amount of internal energy deposited [1-5]. ESI produces multiply or singly charged analyte ions [10]. Due to the very gentle ionization process, even weakly bound complex ions consisting of multiple biomolecules can be preserved and introduced into the mass spectrometer for analysis of the inter-molecular interaction after ESI [12]. MALDI primarily produces singly charged analyte ions and has inherent advantages for application to two dimensional [13] or even three dimensional [14] imaging of various biomolecules in tissue samples.

1.1.2 Mass Analyzers

After ionization, a mixture of analyte ions can be transferred to various types of mass analyzers to directly determine their m/z , or may be further subjected to gas phase ion reactions (e.g., fragmentation) before mass analysis. The functioning mechanisms and applications of commonly used mass analyzers and other related techniques are discussed below.

The earliest types of mass analyzers, magnetic sector and double focusing electromagnetic analyzers, employ magnetic fields alone or magnetic and electric fields in tandem, respectively, to separate analyte ions with different m/z values in space before detection [9]. With a typical source acceleration voltage around 10,000 V, electromagnetic instruments can achieve high energy (~thousands of eV) collision-induced fragmentation of analyte ions which is especially useful in characterization of subtle structural features of biomolecules [15]. Time-of-flight (TOF) analyzers determine

the m/z values of analyte ions by their m/z dependent-flight times after acceleration by high voltage. Operating with moderate m/z resolving power, high energy collision-induced fragmentation and compatibility with pulsed ionization sources can all be achieved using time-of-flight instruments [16]. Quadrupole type analyzers determine the m/z values of analyte ions by their m/z dependent-trajectory stability in an applied oscillating electric field [9]. The triple quadrupole mass spectrometer is widely used for tandem mass spectrometry (MS/MS)-based quantitative analysis [17]. For analysis of complex mixtures containing multiple analytes with isobaric (i.e., same nominal mass) or isomeric (i.e., same exact mass) mass values, MS/MS identification and quantification with high specificity, sensitivity and throughput can be achieved by selection of precursor ions, fragmentation and detection of characteristic product ions [18]. Ion trap analyzers (i.e., three dimensional and linear ion traps) store ions in an oscillating electric field and separate them based on their m/z dependent-resonance frequencies of motion after applying a supplemental radial frequency voltage [9]. Relying on the unique ability of ion trapping, resonance activation and ion ejection, MS/MS and multistage MS/MS (MS^n) can be performed in a single ion trap analyzer in a time-dependent manner. Also, ion trap analyzers are frequently used as a reaction vessel and mass analyzer for the study of gas phase ion chemistry [19]. Fourier transform ion cyclotron resonance (FT-ICR) [20] and Orbitrap analyzers [21] function by trapping ions in an static magnetic or electric field, respectively, and then measuring the m/z dependent-resonance frequency of circulating or oscillating analyte ions. The most unique feature of these two types of mass analyzers is their high resolving power, represented by the m/z value of a peak divided by the full width of the peak at half its

maximum height (i.e., $m/\Delta m$). Currently, $m/\Delta m$ up to 2,000,000 for FT-ICR [22] and 450,000 for Orbitrap [23] can be achieved. During analysis of complex mixtures, overlapping analyte ions at low resolution can be considerably resolved for more confident identification [24] and quantification [25] as long as the exact masses of those analyte ions are different. With the ability to trap low energy electrons, electron-induced activation can be performed in FT-ICR instruments for structural characterization of large biomolecule ions and their fragile post-translational modifications (PTM) [26]. Providing comparable mass resolving power as that of FT-ICR, Orbitrap type instruments have more modest size and cost.

The sensitivity of MS-based analysis has improved considerably due to ongoing technological advancements in ion source/MS interfaces for improved sample desolvation and ion transfer [27-30]. In addition, other platforms are often used in combination with mass spectrometry to further expand its analytical capabilities. For instance, without any enrichment steps, analytes at ng/mL level in blood or tissue can be identified and quantified using a combined ultra-high performance liquid chromatography (UHPLC) - tandem mass spectrometry workflow [31]. For isobaric or isomeric analyte ions which have same nominal or exact m/z value, high performance liquid chromatography (HPLC) and ion mobility spectrometry can be easily coupled to a mass spectrometer to resolve and detect those analyte ions if they have different hydrophobicity and ion mobility [32]. For high throughput analysis, various types of ambient sampling/ionization methods have enabled rapid identification and quantification of individual analytes in complex samples with minimal sample preparation [33]. With the rapid advancement in mass analyzer instrumentation and

related MS technologies as discussed above, MS has become not only a device to separate and analyze gas phase ions, but also a powerful platform to solve various challenging analytical problems with high specificity, sensitivity and throughput.

1.1.3 Fragmentation Techniques

Soft ionization techniques maintain the atomic connectivity of neutral analytes after ionization and thus molecular weight can be easily interpreted from an MS spectrum. However, considering the possible structural isomers and the limited mass resolution of many mass spectrometers, the m/z of precursor ions alone, is usually insufficient for unequivocal biomolecule identification. Thus, one of the methods commonly used for MS-based identification involves activation and fragmentation of the analyte ions, followed by interpretation of the product ions to re-assemble the analyte structures. Various fragmentation techniques which activate ions differently have been developed to provide complementary product ions for comprehensive characterization of analyte structures.

1.1.3.1 Collision-Induced Dissociation

Collision-induced dissociation (CID), one of the most commonly used fragmentation techniques, activates ions by converting kinetic energy to internal energy during the collision of analyte ions and neutral gas molecules in a collision cell such as an ion trap and quadrupole [34]. The amount of energy deposited into ions as internal energy during collision can considerably affect the subsequent fragmentation reactions [35]. Low energy CID, usually with less than 100 eV of available collision energy for conversion into internal energy, breaks the weakest bonds and can have more diverse fragmentation pathways including intra-molecular rearrangements [36]. Commonly used

techniques of low energy CID include resonance excitation in linear and three dimensional ion traps and beam type CID in quadrupoles and collision cells of higher-energy collisional dissociation (HCD). High energy CID with a few thousand eV of available collision energy gives more direct bond cleavage [35]. While low energy CID and HCD are compatible with almost all of the current ionization sources and mass analyzers, high energy CID is usually limited to applications using electromagnetic and time of flight (TOF) instruments in which analyte ions with high kinetic energy can be produced.

1.1.3.2 Electron Capture Dissociation and Electron Transfer Dissociation

Randomization of internal energy in low energy CID usually leads to less bond cleavage or exclusive cleavage of specific weak bonds in large or labile modification-containing analyte ions, resulting in spectra with relatively limited information for structural interpretation [37]. To overcome this drawback, electron capture dissociation (ECD) [38] and electron transfer dissociation (ETD) [37] were developed to provide more random and extensive fragmentation via direct bond cleavage prior to randomization of the internal energy. In both ECD and ETD, an electron is captured by or transferred to a multiply charged cation (charge state >1) to form a distonic cation with a positive charge and a radical. The fast process of electron recombination induces activation resulting in direct bond cleavage and complementary product ions compared to those of CID. ECD is performed in ICR instruments where trapping of low-energy electrons is possible while ETD can be applied in more widely used ion trap instruments through ion/ion reactions between analyte cations and singly charged anthracene anions. ECD and ETD have been widely applied for structural characterization of intact

proteins and labile PTM of peptides, including phosphorylation, glycosylation, sulfonation, and nitrosylation [37, 39]. However, due to the reduced charge state after electron recombination, both ECD and ETD cannot be applied to analysis of singly charged analyte ions.

1.1.3.3 Photodissociation

Another emerging ion activation method is photodissociation (PD), especially ultraviolet photodissociation (UVPD) which has less dependency on charge state of analyte ions due to the photon-based activation and has been employed for structural characterization of a wide range of biomolecular classes [40-44]. Selective activation can also be achieved since only ions (with or without chemical derivatization) that absorb the excitation wavelength can be activated [45]. Various types of lasers have been coupled to mass spectrometers to perform gas phase PD induced by photons with different wavelengths, including 157 nm (F₂ excimer laser), 193 nm (ArF excimer laser), 266 nm (the fourth harmonic of a Nd:YAG laser), 351 nm (XF excimer laser), 355 nm (the third harmonic of a Nd:YAG laser), 800 nm (femtosecond titanium sapphire laser), a tunable range of 205-2550 nm (optical parametric oscillator-Nd:YAG lasers) and 10.6 μm (CO₂ laser) [46].

1.1.4 Applications for Identification and Quantification of Natural Biomolecules

The varied structures and abundances of biomolecules including peptides, proteins, lipids, nucleic acids, oligosaccharides and other metabolites in a living organism at different physiological and pathological states are closely related to their biological activities and functions [47]. Qualitative and quantitative analysis of biomolecules in complex mixtures are critical to understand their functional roles and

further decipher mechanisms associated with both normal cell functioning and the onset and progression of disease, thus aiding in the discovery of novel biomarkers and potential therapeutic drug targets [1, 5, 48, 49]. The merits that MS provides as an analytical tool have been described above. From here the identification and quantification of natural (i.e., without chemical labeling) biomolecules using MS-based methods is discussed while highlighting the limitations of MS-based analysis without chemical labeling for each class of biomolecule.

1.1.4.1 Peptides and Proteins

Proteins or polypeptides are biopolymers of amino acids and frequently modified after their translation. They are responsible for near all cellular functions (e.g., enzymatic catalysis, signaling and transport of molecules) [47]. In MS analysis of proteins, proteolytic peptide-based structural characterization and quantitative analysis, namely 'bottom-up' workflows, are typically performed [50]. Relying on enzymatic digestion, separation techniques, soft ionization methods (i.e., ESI and MALDI), well-understood gas phase fragmentation mechanisms, advanced instrumentation of mass spectrometry and automated data processing softwares, characterization of the primary structure (i.e., sequences of amino acid residues) and PTMs of peptides derived from complex protein mixtures has become much easier compared to using other available methods [50]. Various enzymes (e.g., trypsin, Lys-C, Arg-C, Asp-N, and Glu-C) having different proteolytic specificities are commercially available for cleaving proteins into peptides that have appropriate m/z ranges and adequate ionization efficiency for subsequent MS analysis [51]. Separation techniques including liquid chromatography, electrophoresis and ion mobility separation are often necessary to resolve peptides

based on their hydrophobicity, size and mobility before introducing them into mass spectrometers [50, 52]. Data acquisition during MS/MS analysis may be non-targeted or targeted depending on the desired outcome. For instance, for comprehensive profiling of all peptides and proteins in a complex mixture, non-targeted strategies including data-dependent [53] or data-independent [54] acquisition are usually selected to achieve broad coverage of identification. For targeted analysis of specific peptides or proteins, pre-determined multiple reaction monitoring (MRM) transitions can be applied to achieve optimal sensitivity for detection of peptides even at pg/mL level [55]. Finally, software can be employed for peptide and protein identification during data interpretation using database searching or *de novo* sequencing algorithms [56]. In addition to the classic proteolysis-based 'bottom-up' workflows, 'top-down' approaches employing the gas phase fragmentations of natural intact protein ions have also been developed for the characterization of their primary structures and PTMs [39, 40]. Identities of and interactions (e.g., binding sites and stoichiometry) between components in a natural protein complex at a near native state can also be characterized by 'native mass spectrometry' where non-denaturing buffers and instruments capable of high m/z measurement are employed [39, 57]. For the label free quantification of peptides and proteins, either spectra counting-based or signal intensity-based methods have been developed with data processing softwares (e.g., MaxQuant, Skyline and Progenesis) [58, 59]. These methods are especially advantageous when comparative quantification between large sets of experimental data is required [60].

However, successful identification, characterization and quantification of individual peptides and proteins as well as their PTMs in complex mixtures from

biological samples are still problematic. For example, with an estimated concentration dynamic range of cellular proteome of at least 10^9 , direct MS analysis of low abundance proteins without any enrichment or derivatization to improve the ionization efficiency is very challenging [61]. Also, the chemical properties of peptides derived from cellular proteomes, including hydrophobicity and the ability to acquire charge, have significant effects on their ionization efficiency during ESI and thus affect MS sensitivity [62]. A typical example is the decreased ionization efficiency of peptides with acidic phosphorylated amino acid residues under positive mode ESI compared to their unmodified counterparts [63]. Localization of PTMs on peptides or intact proteins is complex due to their low stoichiometry and possible structural lability depending on the specific modification [64]. As for the quantification of unlabeled peptide and proteins as well as their PTMs, a robust LC-MS/MS setup and complicated data processing workflow are commonly required to ensure reproducibility of quantitative results [60]. Also, since all samples are processed and analyzed through LC-MS separately, systematic errors that may compromise the accuracy of quantitative results are unavoidable through the entire sample preparation and data acquisition stages.

1.1.4.2 Lipids

Lipids play critical roles as structural and functional components of biological membranes, as signaling and targeting molecules, and as a cellular energy resource [47]. The qualitative and quantitative analysis of lipidome profiles under different cellular states has emerged as a complementary alternative to proteomics and genomics to address challenging cell biological questions [49]. Based on the International Lipid Classification and Nomenclature Committee nomenclature, lipids are divided into eight

major categories including fatty acyls, glycerolipids, glycerophospholipids, sphingolipids, sterol lipids, prenol lipids, saccharolipids, and polyketides [65]. Of these, fatty acyls, glycerolipids, glycerophospholipids, sphingolipids and sterol lipids are most often targeted in lipidomic studies [49]. Similar to proteins, structural information of lipids can be hierarchically categorized as different levels, including lipid class, 'sum composition', 'molecular lipids' and 'structurally defined molecular lipids' as proposed in a recent review by Ekroos [66]. Lipids in each of eight major categories can be further divided into lipid subclasses based on the similarity of chemical structures. Then, the 'sum compositions' of lipids in each class or subclass are defined with additional information including the number of carbon elements and carbon-carbon double bonds. Further structural confirmation of the 'molecular lipids' with at least two glycerol backbone substituents requires the determined length and number of unsaturation of the substituents. Finally, 'structurally defined molecular lipids' can be defined with more detailed structural information including the position and stereochemistry of unsaturation on glycerol backbone substituents. To date, identification and quantification at the lipid class, sum composition and molecular lipids levels can be achieved through high resolution mass spectrometry or MS/MS coupled with prior LC separation, or direct infusion [67-70]. For instance, through a combination of spiking in exogenous internal standards, high resolution mass spectrometry and MS/MS, 20 major lipid classes and ~250 molecular lipid species from yeast cells have been absolutely quantified without any chromatography separation and chemical derivatization in order to study effects of external and internal stimuli on the molecular composition profile of yeast lipidome [70].

However, owing to their structural diversity (over 40,000 biologically relevant molecular lipid structures recorded in the LIPID MAPS Structure Database, <http://www.lipidmaps.org/data/structure>), accurate identification and quantification of entire molecular lipids or even the structurally defined molecular lipids in a cellular lipidome with an estimated dynamic range of at least 10^6 is still challenging [71]. For example, the structural complexity of glycerolphospholipids is highlighted in Figure 1.1 [65]. Different lipid classes are differentiated based on the chemical structure of the head group. Identity of the sn substituent on the glycerol backbone (i.e., acyl, plasmalogen alkenyl and alkyl chain or no substituent) indicates the specific subclass. Other structural features of the sn substituent are also variable (e.g., the length, the unsaturation (number, sites and stereochemistry) and the site of linkage to the glycerol backbone of the fatty acyl chains in the diacyl glycerophosphocholine (PC)). Although methods employing high energy CID [15] and MSⁿ [72-74] have been developed to locate the site of unsaturation and the linkage site of sn substituent for a range of glycerolipids and fatty acids with no chemical derivatization, complicated spectra for interpretation and low sensitivity make it difficult to apply those methods for analysis of complex lipid mixtures. The accuracy of quantitative analysis of cellular lipidomes is also limited by the lack of enough commercially available exogenous lipids as internal standards to represent the structural diversity of endogenous lipids, as well as possible error that can be introduced during separate analysis of a given lipid mixture at different polarities (i.e., both positive and negative ionization mode) during mass spectrometry analysis.

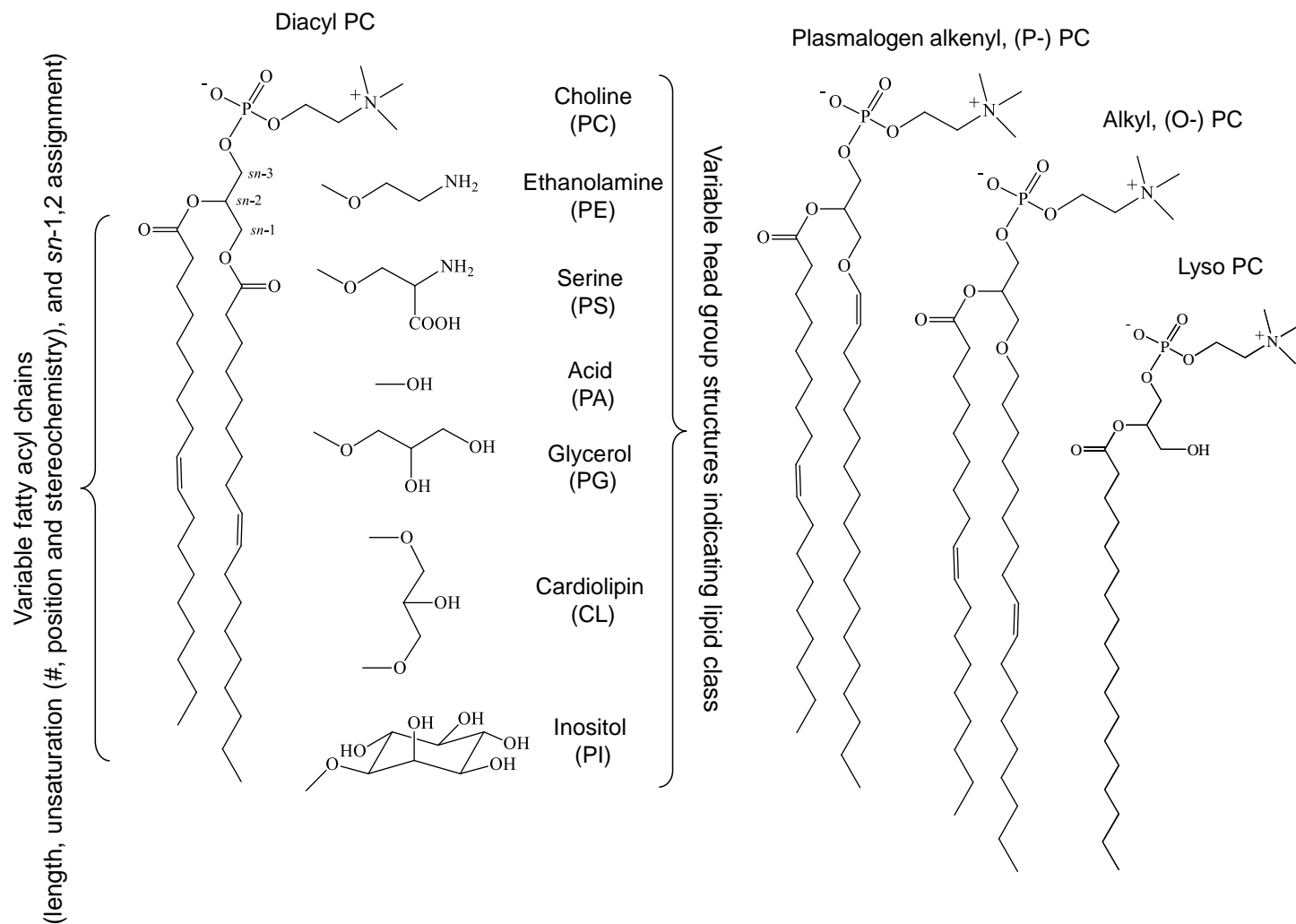


Figure 1.1 Structural complexity of glycerophospholipids lipids. PC, PE, PS, PA, PG, CL and PI indicate glycerophosphocholine, glycerophosphoethanolamine, glycerophosphoserine, glycerophosphate, glycerophosphoglycerol, glycerophosphoglycerophosphoglycerol and glycerophosphoinositol, respectively.

1.1.4.3 Nucleic Acids

Nucleic acids including deoxyribonucleic acids (DNA) and ribonucleic acids (RNA) are biopolymers consisting of nucleotides [47]. Similar to the amino acids as basic building blocks of peptides and proteins, different nucleotides consisting of five-carbon sugars, phosphate group(s) and nucleobases are polymerized in various sequences as the primary structure of nucleic acids and the coded genetic information. To date, MS has played an important role in qualitative and quantitative analysis of nucleic acids, especially for structural characterization of post-transcriptionally modified transfer RNA [75], quantitative analysis of DNA damage [76] and stoichiometry of the nucleic acid/ligand complex [77]. However, without any functional modification to the naturally synthesized nucleic acids, direct analysis of their secondary or tertiary structures and interactions between components in a nucleic acid/ligand complex are still challenging [3].

1.1.4.4 Oligosaccharides and Other Small Molecule Metabolites

Oligosaccharides are biopolymers of simple sugars responsible for various important cellular events including the modulation of protein functions, cell adhesion and cell signaling [78]. They can exist alone or be covalently bonded to proteins or lipids as a modification (i.e., glycosylation) [47]. Although the methodologies and technologies of MS-based analysis of oligosaccharides keep evolving, it remains a challenge to structurally characterize and quantify this type of molecules. Natural oligosaccharides have low ionization efficiency in positive ionization mode due to the lack of basic sites [4]. Also, unlike proteins and nucleic acids that have linear primary structures, oligosaccharides can have extremely high structural complexity due to the possible

branching of the simple sugar monomer, isomeric positions of glycosidic bonds and stereochemical properties [47]. These two facts lead to the limited sensitivity and complicated MS/MS spectra during MS-based analysis of natural oligosaccharides.

Other biological relevant small molecule metabolites including but not limited to nucleotides, amino acids, fatty acids, organic acids and their derivatives are also targets of MS-based analysis [5].

Given the limitations of direct analysis of natural biomolecules using MS, it is clear that functional modification (e.g., chemical labeling) of natural biomolecules for the purposes of improved separation before MS analysis, enhanced ionization efficiency, controlled fragmentation behaviors to investigate specific structural features of analytes and accurate quantitative analysis is necessary along with continuous development of sample separation techniques, instrumentation, ion fragmentation methods and related data processing software [79]. Herein, a detailed overview of chemical labeling strategies for improved MS-based analysis of biomolecules is described.

1.2 Chemical Labeling Strategies for Improved Identification, Characterization and Quantification of Biomolecules Using Mass Spectrometry

Most of the chemical labeling strategies used for improved MS-based analysis of biomolecules can be classified into one or both of the categories discussed below. The first involves linking functional groups, covalently or non-covalently, to the targeted biomolecules to facilitate their MS-based identification and structural elucidation. The second requires stable isotope labeling through chemical or metabolic incorporation of stable isotopic elements (e.g., D, ^{13}C , ^{15}N and ^{18}O) to enable MS-based characterization

of tertiary/quaternary structures of large biomolecules, studies on the mechanisms of their gas phase ion fragmentations and most importantly, quantitative analysis.

1.2.1 Applications of Structural Labeling for Improved Identification and Structural Characterization

1.2.1.1 Ionization Efficiency

Since MS is an analytical tool to study gas phase ions, the ionization efficiency of analytes is closely related to MS sensitivity, limit of detection and limit of quantification. The chemical labeling methods for ESI-based analysis are primarily discussed here since ESI is the most widely employed ionization technique for both qualitative and quantitative mass spectrometry analysis. During ESI, the chemical properties of analytes play important roles in the processes of desolvation and charge acquisition; thus chemical labeling to facilitate desolvation (e.g., increasing the surface activity of analytes by modifying their hydrophobicity) and/or incorporation of fixed charges are the main directions to enhance ionization efficiency [62, 80].

For improved ionization efficiency of peptides, structural labeling to incorporate hydrophobic chemical structures (e.g., alkyl groups with long methylene chains) and/or fixed charges (mainly quaternary ammonium and sulfonium group) mainly targets the primary amine (N-terminus) and carboxylic (C-terminus) groups as well as side chains of specific amino acid residues. Acylation- and alkylation-based chemistries are commonly used for derivatization of peptide primary amine groups. For example, Mirzaei and Regnier developed an *N*-hydroxysuccinimide (NHS) ester-based labeling reagent containing a quaternary ammonium group linked to a straight alkyl chain with 8 carbons [81]. After acylation of primary amine groups in peptides under 500 Da, the

ionization efficiency increased (up to 500 fold) and a 10 fold enhancement of ESI response was generally observed for most of the peptides studied. Another NHS ester-based reagent, S,S'-dimethylthiobutanoylhydroxysuccinimide ester iodide (DMBNHS) containing a sulfonium group linked to an alkyl chain has been employed to derivatize phosphopeptides by Lu *et al.* [82]. A 2.5 fold increase in ionization efficiency in general was demonstrated and more ETD-friendly phosphopeptides with multiple charges (i.e., >+3) were observed. A method employing alkylation chemistry was also reported by Kulevich *et al.* [83]. Tryptic peptides from selected protein digests were dialkylated using aldehydes with varying length (i.e., 4, 6 and 8 carbons) through a simple one step alkylation reaction. Both ionization efficiency and sequence coverage of selected proteins were improved after combined analysis of alkylated and unlabeled tryptic peptides. Studies describing esterification of carboxylic groups [84], guanidation of lysine residues [85] and alkylation of cysteine residues [86] for improved ionization efficiency of peptides were also reported.

For lipids, chemical labeling strategies to improve ionization efficiency similar to that of peptides have also been developed, mainly through incorporating or uncovering a fixed charge after chemical labeling. A typical example is the application of the primary amine specific DMBNHS reagent containing sulfonium group to both phosphopeptides (as discussed in the last paragraph) and aminophospholipids for enhanced ESI response [24]. After a 30 min acylation reaction using deuterium labeled DMBNHS reagent at room temperature, the average fold changes in intensity of glycerophosphoethanolamine (PE) and glycerophosphoserine (PS) lipid ions in positive ionization mode ESI-MS were around 3 and 6 fold, respectively. Methods employing

incorporation of quaternary amine groups to fatty acids and diacylglycerols [87, 88], phosphonium group to hydroxyl group-containing lipids [89] and sulfate group to free cholesterol [90] to improve their ionization efficiency were also reported. Another method to uncover inherent charges in lipids through converting the zwitterionic lipids to anionic species was reported by Han *et al.* [91]. After a one-step *in situ* acylation reaction of primary amine groups in zwitterionic PE and lyso PE lipids using 9-fluorenylmethoxycarbonyl chloride, the detection sensitivity of the derivatized anionic lipids was significantly improved (at picomolar level) under negative mode ESI. Instead of covalent chemical labeling, non-covalent complexation has also been used to enhance the ionization efficiency of lipids. Pham and Julian reported an approx. 10 fold increase in detection sensitivity of PE species by non-covalent complexation with 18-crown-6 ether during positive ion mode ESI [92], possible due to the increased surface activity of ions complexed with 18-crown-6 ether [93].

In comparison to peptides and lipids, oligosaccharides are inherently difficult to ionize due to their hydrophilicity and lack of basic sites to be protonated. To improve the ionization efficiency of oligosaccharides, many methods have been developed to increase their hydrophobicity, mainly targeting the hydroxyl groups through permethylation and peracetylation reactions [94, 95]. However, the wider application of permethylation and peracetylation-based labeling strategies was limited by their time-consuming sample preparations and 'non-quantitative' labeling. Alternatively, hydrazone labeling methods targeting carbonyl groups in the open-ring aldehyde form of oligosaccharides is gaining popularity due to the absence of cleanup after labeling and quantitative labeling efficiency [96]. The effects of permanent charge and hydrophobicity

of various forms of hydrazide labeling reagents on ionization efficiency of derivatized oligosaccharides were also studied, suggesting that increased hydrophobicity enhanced the ESI response while the incorporated permanent charge decreased the MS abundance of derivatized oligosaccharides [97].

Similarly, incorporating hydrophobic groups or fixed charges into nucleobases, nucleotides, oligonucleotides [98-100] and amino acids [101] have been reported to enhance their ESI response for improved qualitative and quantitative analysis of nucleic acids and metabolites.

1.2.1.2 Structural Characterization of Peptides and Proteins

1.2.1.2.1 Sequence of Amino Acid Residues

The structures of proteins, including their primary structures (i.e., the sequence of amino acid residues), are closely related to their biological functions and therefore sequencing of proteins is necessary to further understand their functioning mechanisms [47]. To improve MS-based sequencing of peptides derived from proteins, the fragmentation behaviors of peptide ions have been modified through structural labeling with functional groups in order to simplify the MS/MS spectra or provide more abundant and/or diverse fragment ions. Most of the reported labeling approaches follows the principles including 1) modifying the charge (e.g., charge state, mobility and polarity) of gas phase peptide ions to change their fragmentation behaviors in CID or to enable ETD; 2) modifying the proton mobility of peptide ions in order to produce more abundant and/or diverse sequence-specific fragment ions after activation and 3) incorporating functional groups to enable fragmentation upon specific ion activation methods (e.g., PD and radical-directed disassociation (RDD)).

Incorporating fixed charges to peptides not only increases their ionization efficiency as discussed in Chapter 1, section 1.2.1.1, but also facilitates sequencing of peptides by resembling the directing influence of the positions of inherently charged basic amino acid residues on CID fragmentation of protonated peptides [82, 102] or increasing the abundance of ETD-friendly multiply charged (i.e., >+3) peptide cations [82, 103]. Methods employing solution phase labeling of quaternary ammonium [103, 104], phosphonium [105] and sulfonium [82] have been reported. Instead of performing a labeling reaction in solution phase, gas phase charge polarity inversion of peptide ions with the advantages of minimal sample preparation has been reported to improve sequence coverage by acquiring complementary CID fragment ions in both polarities [106] or enabling ETD fragmentation [107]. To modify the proton mobility of peptide ions, both solution phase [108] and gas phase modification [109] methods have been developed to either decrease the proton mobility of tryptic peptide anions or increase the proton mobility of tryptic peptide cations to produce more diverse sequence-specific fragment ions during CID-MS/MS analysis. For complementary sequence-specific fragmentation of peptide ions induced by other ion activation methods compared to that in CID, various forms of chromophore labeling reagents have been developed to enable or improve PD (mainly at 351 nm [110-112], 355 nm [113] and 10.6 μm [114]) of derivatized peptide ions. RDD has also been used to aid the sequencing of peptides incorporated with radical precursors containing ultraviolet (UV)-labile covalent bonds (e.g., carbon-iodine [115], carbon-sulfur [116] and carbon-oxygen bonds [117]) or weak bonds which undergo homolysis upon collisional activation [118].

Recently, two papers described gas phase synthesis of linear [119, 120] or branched [120] peptide ions with controlled sequences in a mass spectrometer. Without time-consuming condensed-phase synthesis and separation, gas phase ultraviolet photoexcitation or ion/ion reactions were employed to induce the formation of an amide bond in a peptide dimer complex ion followed by facile mass-based separation and MS/MS-based structural analysis of the products. Although the quantity of synthesized peptides in the gas phase is unlikely to be sufficient for additional solution phase modification, this type of method provides an approach to rapidly generate the library of peptide MS/MS data to facilitate sequencing of unknown peptides.

1.2.1.2.2 Post-Translational Modifications

After biosynthesis, proteins are often post-translationally modified in potentially hundreds of different ways [121]. Although PTMs occur at low stoichiometry and abundance, they perform more precise regulations of cellular functions compared to gene expression [122]. As a powerful analytical tool for structural elucidation, MS has been widely used for analysis of PTMs [64], however for certain PTMs, sample preparation including structural labeling for improved enrichment and favored gas phase fragmentation is necessary for their improved identification and localization [79]. Biotin tag labeling at sites of phosphorylation [123] and O-linked glycosylation [124] followed by affinity chromatography are typical examples of enrichment strategies achieved by structural labeling. For identification and localization of multiple PTMs (e.g., phosphorylation) in the same peptide, or very labile PTMs (e.g., glycosylation) during gas phase fragmentation, ETD [37] and RDD [116] have been proved to be advantageous compared to the conventional low energy CID fragmentation technique.

Therefore, labeling methods to enable ETD or RDD through increasing the percentage and abundance of highly charged (>3) peptide ions or incorporating UV-labile radical precursors have been developed [82, 125].

1.2.1.2.3 Tertiary and Quaternary Structures of Proteins

Preliminary structural labeling can also be applied for mass spectrometric analysis of protein tertiary (e.g., protein conformations) and quaternary (i.e., protein/protein or protein/ligand interactions) structures. The basic principle is that after changing the masses of the proteins via chemical labeling at the side chains of amino acid residues in a structure-dependent manner, structural information can be derived from mass spectrometry-based identification and relative quantification of peptides derived from the labeled proteins. For example, information on protein conformational changes can be derived from the changed surface residue accessibility characterized by 'bottom-up' mass spectrometric analysis of proteolytic peptides of the labeled proteins since surface residues exposed to solvent can more readily react with the labeling reagent while other residues buried in the proteins react slower or not at all [126]. Various covalent labeling reagents targeting side chains of specific amino acid residues have been developed for this purpose [127-131]. For instance, Zhou *et al.* developed the protein surface lysine accessibility mapping strategy using the fixed charge containing DMBNHS reagent combined with data-dependent multistage tandem mass spectrometry analysis [127]. By monitoring the changed lysine modification rates between native and oxidized proteins using the developed strategy, it was found that the functional domains within an important protein phosphatase, calcineurin became more accessible to the DMBNHS labeling upon H₂O₂ oxidation-induced conformational

perturbation and suggested the phenomenon as a novel mechanism explaining the inactivation of calcineurin caused by H₂O₂ oxidation [128]. Other reagents including iodoacetamide [129], vicinal dicarbonyl compounds [130], and diethylpyrocarbonate [131] have also been commonly used to map the accessibility of protein surface cysteine, arginine, and histidine residues, respectively, but to a lesser extent compared to lysine-specific reagents due to the wide range of available reagents targeting primary amine group and the high frequency of lysine residue in proteins. In addition, as a promising method to acquire broad sequence coverage of labeled proteins and with no need for enzymatic digestion as in the 'bottom-up' approach, a 'top-down' strategy probing conformational changes during denaturation of myoglobin and domain C of PARP-1 proteins by gas phase UVPD fragmentation of intact protein ions after lysine-specific labeling using S-methylacetimidate was reported by Cammarata *et al.* [132]. However, more efforts on the elucidation of gas phase UVPD fragmentation mechanisms and the development of diverse ion activation methods for intact protein ions are required for broader applications of the 'top-down' approach.

To characterize the interaction (e.g., distance and/or sites) of mutual interacting sites within proteins or between protein/protein and protein/ligand complexes, cross-linking reactions combined with mass spectrometric analysis can be employed [133]. Typically, a cross-linker reagent with reactive sites on two ends and a 'spacer' with fixed length in the middle is used to covalently link two nearby sites in a protein or between two components in a protein complex. Cross-linking reagents having two amine-specific reactive sites targeting lysine residue were again used most frequently due to the availability of reagents and the occurrence frequency of lysine in proteins as described

above. Photo-reactive cross-linkers containing diazirine, aryl azide and benzophenone as reactive sites were also used as non-specific cross-linking reagents [134]. Subsequent 'bottom-up' mass spectrometric analysis can provide identities of cross-linking sites and low resolution maximum distances between cross-linked sites [135]. Interestingly, employing the ion/ion reaction between ubiquitin protein cations and homobifunctional sulfo-N-hydroxysulfosuccinimide ester reagent anions in an ion trap reaction vessel, Webb *et al.* demonstrated the protein intra-molecular cross-linking reactions in gas phase and characterized the cross-linked structures based on product ions from CID experiments in a 'top-down' manner [136]. Although it is still not clear that whether the mass spectrometric analysis of gas phase cross-linked proteins ions can provide useful solution phase structural information, this method represents a creative direction toward high throughput protein interaction study with minimal time for sample preparation.

1.2.1.3 Structural Characterization of Lipids

1.2.1.3.1 Lipid Classes and Sum Compositions

For high throughput profiling of complex lipid mixtures or cellular lipidomes, it is meaningful to separate and collectively study lipids based on their classes or subclasses or sum compositions considering the similar physiochemical properties affecting related cellular events of lipids with the same class, subclass or sum composition [47]. However, many challenges exist due to the structural diversity and complexity of lipid mixtures within crude cellular extractions. For example, during shotgun lipid analysis with no LC separation, lipids of the same class but different subclasses may not be able to be resolved based on mass due to their isomeric

structures and resultant same exact mass (e.g., plasmalogen lipids containing one less site of unsaturation compared to alkyl-ether containing lipids, both with the same head group (e.g., $[\text{PC}_{(\text{P}-36:0)} + \text{H}]^+$ and $[\text{PC}_{(\text{O}-36:1)} + \text{H}]^+$ both have the elemental composition of $\text{C}_{44}\text{H}_{89}\text{NO}_7\text{P}$). Also, lipids in different classes may suffer from the same situation (e.g., $[\text{PE}_{(32:0)} + \text{H}]^+$ and $[\text{PC}_{(29:0)} + \text{H}]^+$ both have the elemental composition of $\text{C}_{37}\text{H}_{75}\text{NO}_8\text{P}$). To overcome this limitation, Phaner *et al.* developed a sequential structural labeling strategy for aminophospholipids (i.e., PE and PS lipids) and the O-alkenyl ether double bond of plasmalogen lipids, using a ‘fixed charge’ sulfonium ion-containing stable isotope-labeled-S,S-dimethylthiobutanoylhydroxysuccinimide ester reagent (DMBNHS), and iodine and methanol, respectively, to eliminate potential overlap of these lipids with other lipid classes or subclasses [24, 137]. Using the structural labeling strategy combined with high resolution/accurate mass MS and “targeted” MS/MS analysis, >600 molecular lipid species from 36 lipid classes and sub-classes have been identified from various colorectal cancer cell lines and their secreted exosomes, without need for extensive sample handling or chromatographic fractionation prior to analysis [24, 138]. Similarly, Han *et al.* noted that identification and further structural characterization of the interested lipids were potentially improved by shifting the m/z range of a labeled lipid class to a region with much less interference with other lipid classes after using the 9-fluorenylmethoxycarbonyl chloride reagent targeting at aminophospholipids including PE and lyso PE lipids [91].

1.2.1.3.2 Identities and Linkage Positions of Glycerol Backbone Substituents

Analysis of X-ray protein crystal structure data have suggested that the identities (e.g., length) and linkage positions of glycerol backbone substituents of

glycerophospholipids are likely to affect their binding affinity to nuclear receptor SF-1, which can be regulated by glycerophospholipid second messengers [139]. To further understand the functional roles of lipids in cellular events, a comprehensive characterization of lipid structure including subtle structural features is necessary [140]. Although MS-based identification of the length of the glycerol backbone substituents for most glycerolipids is straightforward and does not require structural labeling, the identification of other lipids is still challenging. For instance, glycerophosphocholine lipids, containing an endogenous fixed positive charge quaternary amine, ionize poorly in negative mode and yield generally limited structural information under positive ionization mode CID-MS/MS conditions [2]. Methods describing solution phase hydrolysis for analysis of resultant fatty acids [141] or addition of high concentration of salts to enable acquisition of glycerol backbone substituent-specific fragment ions at both positive [142] and negative polarities [143] have been reported. However, their wider applications are limited by the absence of molecular structure information or by low sensitivity. For this, Stutzman *et al.* converted the gas phase protonated PC lipid ions, $[PC+H]^+$ into demethylated PC anions, $[PC-CH_3]^-$ through non-covalent labeling of doubly deprotonated 1,4-phenylenedipropionic acid followed by CID-induced ion/ion reaction [144]. Subsequent CID analysis of the $[PC-CH_3]^-$ anions produced abundant fatty acid carboxylate anions indicating the length and unsaturation degree of glycerol backbone substituents.

Another more challenging task is to characterize the subtle structural features of glycerophospholipids (i.e. the linkage position (sn position) of their glycerol backbone substituents). Pham *et al.* have demonstrated the existence and differentiation of sn

positional isomers for six major glycerophospholipids classes through gas phase ozonolysis (i.e., addition of ozone to carbon-carbon double bonds) of product ions arising from CID of sodium adduct of glycerophospholipids [145]. After the CID/ozonolysis experiments, abundant and predictable product ions that are characteristic to the specific sn position of glycerol backbone substituents were observed.

1.2.1.3.3 Positions and Stereochemistry of Carbon-Carbon Double Bonds

Location and stereochemistry (i.e., *cis* or *trans*) of carbon-carbon double bonds (C=C) in lipids are also subtle structural features of lipids that can change their biochemical properties [146-148]. Differentiation of C=C bond positional isomers in lipids were traditionally conducted by separation through gas chromatography (GC) or HPLC followed by mass spectrometric or other detection methods [141]. However, direct determination of positions and stereochemistry of C=C bonds in underivatized lipids using MS is problematic since the C=C bond isomers of lipids give identical low energy CID-MS/MS spectra. Although methods employing high energy CID [15, 16] and MSⁿ [72, 73, 149] are available, low sensitivity and complicated spectra interpretation limit their broader applications. To facilitate the localization of C=C double bonds in lipids, structural labeling strategies have been developed to selectively induce more abundant fragmentation cleavages within their unsaturated aliphatic chains. Several methods exploiting selective gas phase ion/molecule reactions (e.g., covalent adduct chemical ionization [150], ozonolysis [145], Paternò-Büchi reactions [151]) targeting at C=C double bonds were demonstrated to modify the fragmentation behaviors of lipid ions and product abundant fragment ions indicating the position of C=C double bonds.

RDD has also been employed to induce C=C bond position-specific fragmentations occurring within the unsaturated aliphatic chains of lipid ions after introduction of lipid ions, which are covalently [152] or non-covalently [92, 153] linked to a UV-labile radical precursor, into the mass spectrometer via ESI followed by activation of UV photons to release the radicals. Finally, although still very challenging, MS-based differentiation of lipid isomers only differing in stereochemistry of C=C double bonds was demonstrated to be feasible by Pham *et al.* without prior separation [154]. Relative abundance of CID product ions of proton bound complex ions consisting of fatty acid methyl esters and iodoaniline were proved to be sensitive to the stereochemistry (i.e., *cis* or *trans*) of C=C double bonds.

1.2.1.4 Intra- and Inter-Molecular Interactions of Nucleic Acids

Although the role of MS in genome-wide sequencing analysis was superseded by other high-throughput methods in the late 1990s [155], structural labeling combined with mass spectrometric analysis is still advantageous as a rapid and sensitive method to characterize the intra- and inter-molecular interactions of nucleic acids, mainly using alkylating cross-linkers based on the same principles applied to probe protein intra- and inter-molecular interactions, discussed in Chapter 1, section 1.2.1.1.2 [3].

1.2.1.5 Structural Characterization of Oligosaccharides

In addition to enhancing the ionization efficiency, structural labeling of oligosaccharides is helpful in obtaining characteristic tandem mass spectra allowing identification of their sequence, branching and interglycosidic linkages [79]. Permethylation and peracetylation of the hydroxyl groups of oligosaccharides are traditionally used to modify the fragmentation behaviors as well as increase ionization

efficiency [4]. Labeling strategies enabling RDD and UVPD of oligosaccharides are gaining attention due to the ability to acquire complementary fragment ions indicating extra structural information compared to that from CID. For example, both 355 nm UVPD of chromophore-incorporated oligosaccharides [156] and photo-induced RDD of oligosaccharides labeled with iodoaniline [157] were reported to provide fragment ions distinguishing positional oligosaccharide isomers.

1.2.2 Applications of Stable Isotope Labeling for Improved Structural Characterization and Quantification

1.2.2.1 Structures of Large Biomolecules and Mechanisms of Gas Phase Biomolecular Ion Fragmentation

Stable isotope labeling is widely used for MS-based structural characterization of large biomolecules (i.e., proteins and their complexes) [158] and mechanistic studies of gas phase fragmentation of other smaller biomolecular ions (i.e., peptide [159-162], lipid [163], nucleic acid [164], oligosaccharide [165] and other small molecule metabolite ions [166]). After replacement of specific elements in selected regions of biomolecules with corresponding stable isotopes, the masses of stable isotope-labeled regions are changed while covalently and non-covalently connected structures and resultant gas phase ion fragmentation behaviors are kept the same or near identical. Thus, by comparative study of labeled and unlabeled analytes, the identity of ions derived from the stable isotope-labeled regions which are characterized by MS can be linked back to their spatial positions in the original biomolecules.

Hydrogen-deuterium exchange (HDX) MS is a typical example and a key technique employing stable isotope labeling to characterize the intactness of hydrogen

bonding networks of proteins and their complexes in solution [158]. The principle of this method is that when exposed to deuterium-labeled water (D_2O), amide bond hydrogens in the disordered or highly dynamic regions of proteins undergo rapid exchange with surrounded deuterium due to lack of stable hydrogen-bonding [158]. The 'bottom-up' mass spectrometric analysis workflows are typically used to analyze structure-dependent HDX patterns of proteolytic peptides from proteins under different experimental conditions for structural characterization [167]. However, attention needs to be given during selection of an appropriate ion activation method for MS/MS-based identification of residue-specific HDX patterns of peptides. Consistent with the mobile proton model explaining the CID fragmentation mechanisms of protonated peptides, it was demonstrated that intra-molecular migration of hydrogen and deuterium during the collision-induced vibrational activation process could lead to complete randomization (i.e., 'scrambling') of the HDX patterns [168]. Therefore, ion activation methods not involving the vibrational excitation (e.g., ETD [169] and ECD [170]) are more advantageous in acquiring residue-specific HDX patterns of peptides. Also, experimental procedures need to be optimized to minimize back exchange from deuterium to hydrogen during proteolysis and followed LC separation of deuterium-labeled proteins. Keeping the solution temperature close to 0 °C after HDX and minimizing the time for sample preparation can effectively preserve much of the HDX patterns [158]. Alternatively, the back exchange in proteolysis step can be avoided in 'top-down' analysis where the gas phase fragmentation of deuterium-labeled intact protein ions directly generates peptide ions for HDX pattern study and sequencing. The

'scrambling' processes in "top-down" analysis can also be minimized by using ECD [171] and ETD [172] instead of CID.

Understanding gas phase fragmentation mechanisms of biomolecular ions is essential for accurate interpretation of mass spectra data and structural elucidation. Direct comparison between fragmentation spectra of stable isotope-labeled and unlabeled biomolecules provides a straightforward approach to investigate fragmentation mechanisms. For this purpose, various stable isotopes (e.g., D, ^{18}O , ^{15}N and ^{13}C) have been incorporated into peptides [159-162], lipids [163], nucleic acids [164], oligosaccharides [165] and other small molecule metabolites through HDX or chemical synthesis.

1.2.2.2 Quantification of Biomolecules

Unlike quantitative analysis based on the Beer-Lambert law, there is no fixed response coefficient between an MS signal and the concentration of an individual analyte. Therefore, for accurate and absolute MS-based quantification, ratiometric measurement of simultaneously determined intensities of the analyte ions and their stable isotopic analogue ions as internal standards having the same or near identical MS signal responses is the ideal requirement [60]. For targeted analysis of a limited number of analytes, this approach, referred to as isotope dilution mass spectrometry (IDMS) is applicable with the advantage of providing absolute quantities of targeted biomolecules [90, 173-175]. However, during a typical quantitative '-omics' study, the requirement to quantify hundreds to thousands of individual analytes makes the preparation of the corresponding stable isotope-labeled standards impossible. Alternatively, metabolic labeling and chemical labeling can incorporate stable isotope

labels to biomolecules at large scale, enabling relative quantification of individual biomolecule in cells or tissues under various stimuli [4, 60, 71]. Details of isotope labeling strategies developed and their application for quantitative analysis of biomolecules are discussed below.

1.2.2.2.1 Stable Isotope-Labeled Analogue Internal Standards

For absolute quantification of targeted peptides using IDMS, most isotopically labeled internal standards can be easily synthesized using commercially available isotopically labeled amino acids and automated peptide synthesis [176]. For proteins, either their unique peptide sequences or the proteins themselves can be isotopically labeled through chemical or biological synthesis as internal standards. Currently, although still relatively expensive, isotope-labeled peptides are widely employed as surrogates for absolute quantification of proteins using MRM analysis [173, 177]. However, since those isotopically labeled peptides are usually spiked into the samples at a late stage of the sample preparation, systematic errors (e.g., sample loss and sample handling-induced modification of targeted proteins) prior to standard spiking can affect the accuracy of quantification if no correction is made [178, 179]. Alternatively, several methods using various types of isotopically labeled protein internal standards were developed to overcome this limitation. Carroll *et al.* used recombinant DNA techniques to construct an isotopically labeled protein containing 59 tryptic internal standard peptides for absolute quantification of 27 enzymes using IDMS [180]. Systematic errors arising from tryptic digestion were minimized since targeted proteins and the biologically synthesized protein standards were mixed before digestion. Methods describing biosynthesis of stable isotopic analogues of targeted proteins in

cells or cell-free systems were also reported and applied to considerably minimize sample handling-related errors in IDMS analysis by spiking these protein standards into samples at the earliest stage of sample handling (e.g., cell lysis or collection of biofluids) [178, 179, 181].

Due to the structural complexity of lipids, especially for glycerolipids and glycerophospholipids, synthesizing a large array of their stable isotopic analogues is very challenging [66]. To date, quantitative IDMS analysis of lipids using stable isotopic analogue internal standards mainly target biologically relevant 'simple' lipids (e.g., cholesterol [90], fatty acid [174] and ceramide [182]). For the similar reason related to lack of enough stable isotopic analogue standards, methods for quantitative IDMS analysis of oligosaccharides were less developed. For nucleic acids, IDMS analysis for quantification of DNA damage is continuously gaining popularity [3]. Due to the often low abundance and stoichiometry of DNA damage or modification, DNA is usually hydrolyzed to produce nucleobase monomers instead of the whole biopolymer as targets of MS analysis [3]. Correspondingly, stable isotopic analogues of the targeted modified nucleobase monomer can be spiked in before downstream sample preparation and analysis. For other small molecule metabolites, IDMS is now the gold standard for quantitative analysis [183].

1.2.2.2.2 Metabolic Labeling

Metabolic labeling for MS-based quantitative analysis of biomolecules is mainly achieved through replacing the monomers of biopolymers (e.g., proteins [60] and saccharides [184]) with corresponding stable isotopic analogues during biosynthesis. For MS-based quantitative proteomics, metabolic labeling can incorporate stable

isotope labels into proteins at the earliest stages (i.e., biosynthesis) to maximally avoid the sample handling-related errors [60]. Currently, the most widely applied metabolic labeling method for protein samples derived from cultured cells is stable isotope labeling with amino acid in cell culture (SILAC) developed by Ong *et al.*. Heavy stable isotope (i.e., ^{13}C and ^{15}N) labeled arginine and lysine added in the cell medium ensure that, after digestion of the extracted proteins, most of the tryptic peptides having arginine or lysine residues at their C-terminus will contain at least one stable isotope labeled amino acid residue [185]. By adding arginine and lysine incorporated with various numbers or identities of stable isotopes during cell culture to differentially label multiple sets of samples, intensities of isotopic clusters of the differentially labeled and pooled peptides can be detected through mass spectrometric analysis and used as surrogates for protein expression levels. More modified versions of the SILAC strategy were also developed to quantitatively study protein synthesis and degradation (i.e., pulsed SILAC) [186] or enable quantitative analysis of proteins between animals [187].

Mass spectrometry-based quantitative analysis of metabolically labeled oligosaccharides has also been demonstrated using murine embryonic stem cells cultured with and without addition of ^{15}N -labeled glutamine as the only nitrogen source of hexosamines [184]. One of the disadvantages for metabolic labeling strategies is that most of the methods are only applicable to cultured cells instead of samples from animals or human where the stable isotope incorporation during biosynthesis of analytes is unlikely. Another disadvantage is the possibility of overlapping peaks in the mass spectra of multiplexed (>3) metabolically labeled samples, which can compromise the accuracy of quantification [60]. High resolution MS ($m/\Delta m > 200,000$ at m/z 400)

combined with neutron-coded SILAC represents a promising quantitative strategy employing subtle mass differences of stable isotopes (e.g., 36 mDa between $^{13}\text{C}_6^{15}\text{N}_2$ -labeled lysine and D_8 -labeled lysine) to theoretically enable highly multiplexed quantitative analysis but has not been practically applied [25]. An alternative solution is chemical labeling as discussed below.

1.2.2.2.3 Chemical Labeling

In chemical labeling strategies for stable isotope incorporation and subsequent MS-based quantitative analysis, samples under different experimental conditions are separately derivatized by a set of stable isotope-encoded reagents so that the same labeled biomolecules in different samples become stable isotopic analogues. After pooling of separately derivatized samples, MS analysis can provide quantitative information based on ratiometric measurement of 1) the intensities of differentially labeled biomolecular ions in mass spectra if they have different m/z or 2) the intensities of reporter ions derived from differentially labeled and isobaric biomolecular ions in MS/MS or MS^3 spectra [60].

For quantitative analysis of peptides and proteins, chemical labeling methods employing MS-based quantification include isotope-coded affinity tags (ICAT) and dimethyl labeling [188, 189]. ICAT reagents target the thiol group-containing side chains of cysteine residue. A biotin group is also incorporated in each ICAT reagent to enable sample enrichment through affinity chromatography. Dimethyl labeling selectively reacts primary amine groups on the N-terminus and side chains of lysine residues with formaldehyde and its stable isotopic analogues followed by reduction using cyanoborohydride. This method is gaining its popularity due to the inexpensive reagents

and applicability to a broad quantity range of samples (sub-micrograms to milligrams) [189]. However, due to the incorporated deuterium in both reagents, these two methods suffer from the deuterium isotope effect-induced retention time shift during reverse phase LC [190]. The ability to perform highly multiplexed quantification is also limited to pools of at most three differentially labeled samples due to the increasing complexity of the mass spectra when combining multiple labeled samples together [60].

Alternatively, isobaric stable isotope-coded reagents employing MS/MS or MS³-based quantification can overcome these limitations by measuring the peak intensities of reporter ions in the low mass range of MS/MS or MS³ data where the spectra are relatively simple compared to MS data [60]. Retention time shifts during reverse phase LC separation can be avoided since isobarically labeled peptides co-elute precisely [60]. Tandem mass tags (TMTs) (up to 10 plex) [191] and isobaric tags for relative and absolute quantification (iTRAQ) (up to 8 plex) [192] are the two most popular methods for this purpose and both types of reagents are commercially available. Similar to dimethyl labeling, TMTs and iTRAQ reagents both target the primary amine groups of peptides. Even higher orders of multiplexed quantification (12 plex) have been demonstrated by a combination of ICAT, dimethyl labeling and iodoacetyl-TMT methods [193].

For lipids, iTRAQ and other NHS ester-based reagents were also developed for MS/MS-based quantification of primary amine-containing lipids. For example, Berry *et al.* have previously reported results from iTRAQ and isotope labelled 4-(dimethylamino)benzoic acid NHS ester derivatization of primary amino groups for the quantitative analysis of diacyl-, ether- and plasmalogen-PE lipids in complex biological

mixtures [194-196]. Nabetani *et al.* also recently applied the iTRAQ labeling strategy for the quantitative analysis of hydrolyzed ceramide lipids [197]. For quantitative analysis of oligosaccharides, a modified TMT reagent, stable isotope labeled carbonyl-reactive tandem mass tags (glyco-TMTs) was also developed and applied to study N-linked protein glycosylation profiles of the isogenic primary colorectal cancer cell line, SW480 and its malignant cell line, SW620 [198]. It should be noted that depending on the mixture complexity and prior chromatographic fraction that may be used, these current isobaric stable isotope tagging methods for quantification of biomolecules using low mass reporter ions may suffer from interference in the reporter ion abundances due to the presence of co-isolated and fragmented precursor ions present within the isolation window that is used prior to dissociation [199, 200]. MS³ dissociation [201], gas phase purification using proton transfer reaction [202] and ion mobility separation [203] have been proposed to minimize the described limitations for quantitative proteomic studies. A method employing neutral loss product ions of derivatized aminophospholipids for relative quantification after isobaric stable isotope labeling is also described in Chapter three to avoid the possible interference in low mass reporter ions-based quantification.

1.3 Aims of this Dissertation

The aims of this dissertation include:

1. Development of a novel gas-phase cross-linking reaction for saturated and unsaturated TG lipid ions using di-iodoaniline reagents and photo-induced radical chemistry in a modified ion trap mass spectrometer enabling UVPD experiments.

2. Characterization of the structures and formation mechanisms of cross-linked TG lipid ions and elucidation of the effects of various cross-linkers and TG lipid structures using multistage CID-MS/MS.
3. Characterization of CID and HCD fragmentation behaviors of S,S'-dimethylthiobutanoylhydroxysuccinimide ester iodide (DMBNHS) derivatized aminophospholipids.
4. Development of a novel strategy for characterization and multiplexed quantification of deuterium-coded DMBNHS derivatized aminophospholipids in complex biological samples using high resolution/accurate mass ESI-MS, CID-MS/MS, HCD-MS/MS and -MS³.
5. Development of a quantitative immuno LC-MS/MS method for parathyroid hormone (PTH) and its *in vivo* oxidation and truncation.
6. Characterization of novel post-translationally modified PTH in patient samples using the immuno LC-MS/MS workflow.
7. Quantitative proteomic analysis to study the drug action mechanism of a non-competitive proteasome inhibitor, TCH-013 using dimethyl labeling and two dimensional LC-MS/MS.

CHAPTER TWO

Photo-Induced Inter-Molecular Cross-Linking of Gas Phase Triacylglycerol Lipid Ions

2.1 Introduction

Plant derived oils have widespread use as renewable 'green' feedstock components in a diverse range of industrial applications, including food, cosmetics, pharmaceuticals, antioxidants, biofuels, surfactants, lubricants, and polymers. For example, the cross-linking of triglycerol (TG) lipids or their derivatives is a common process associated with the industrial scale synthesis of plant oil-based polymers [204], as well as being an unwanted reaction associated with long term storage [205] and high temperature cooking (e.g., frying) [206]. However, the physical and chemical properties of the polymeric products from these reactions are known to be affected by many factors, including the structures of the TG monomers (i.e., the length of the fatty acyl chains, the number and positions of unsaturation sites, and their stereochemistry) [207], the mechanism of the cross-linking reaction [208], and other experimental conditions. Thus, a detailed understanding of these factors, particularly those relating to the structure and intrinsic reactivity of the TG monomers under a given set of cross-linking conditions, may provide important insights for the improved manufacture of polymers with desired properties.

Traditionally, the cross-linking reactions of TG lipids or their derivatives are conducted in the solution phase, then the products are analyzed by Fourier transform

The results described in this chapter were published in: Nie, S., Pham, H.T., Blanksby, S.J. and Reid, G.E. "Photo-induced inter-molecular cross-linking of gas phase triacylglycerol lipid ions." *Eur. J. Mass Spectrom.* **2015**, 21, 287.

infrared spectroscopy, Fourier transform Raman spectroscopy [209], and/or by reverse-phase high-performance liquid chromatography [210] or gel permeation chromatography [211]. However, these methods are often limited in their ability to obtain detailed molecular information regarding the individual structural features of the TG lipids that may be present within a complex mixture, that may affect their cross-linking reactivity and the structure of their polymerized products. Thus, there remains a need for the development of alternative approaches that enable monitoring and characterization of the intrinsic intra- and/or inter-molecular interactions and chemical reactivity of individual lipids within a given mixture.

As discussed in chapter one, MS and MS/MS-based methods are increasingly being used to analyze the solution phase products of cross-linked biomolecular polymers [212], as well as to characterize the products of cross-linking reactions performed in the gas phase, using a variety of activation methods including collision induced dissociation (CID) [213] and ultraviolet photo-dissociation (UVPD) [214]. Interestingly, Muller *et al.* recently reported the formation of an inter-molecular cross-linking reaction within a non-covalent dimer of a diacylglycerol (DAG) anion and a neutral DAG molecule upon performing CID in negative ionization mode [215]. However, the S_N2 nucleophilic substituent mechanism associated with this reaction cannot readily be directly applied to the formation and analysis of cross-linked TG lipids, which may contain carbon-carbon (C=C) double bonds as the only reactive sites, and are usually observed in positive ionization mode.

Considering that the C=C bond of unsaturated TG lipids is one type of reactive site commonly involved in the solution phase radical polymerization of plant oils [216], it

is interesting to study whether similar reactions could be achieved in the gas phase, in which radical addition and recombination drive the cross-linking process. Radicals can be easily generated by UVPD of precursors containing carbon-iodine [115] or carbon-sulfur bonds [116], via the incorporation of weak bonds that easily undergo homolysis during CID [118, 217] and through CID-induced one-electron oxidative dissociation of metal ion/biomolecule complex ions [218, 219]. An example of the formation of a covalent linkage between a radical precursor and the site of unsaturation within a TG lipid via radical addition, using 266 nm UVPD, was recently reported by Pham *et al.* [153]. In that work, a non-covalent complex consisting of protonated 4-iodoaniline ion and a neutral unsaturated TG lipid was introduced into a modified ion trap mass spectrometer via electrospray ionization (ESI), then isolated and subjected to activation with 266 nm UV photons. This resulted in homolysis of the carbon-iodine bond and the formation of an aniliny radical that subsequently underwent radical addition to yield a covalent bond between the protonated aniline and the TG molecule. The presence of the radical within this product ion was then shown, using CID-MS³, to direct the dissociation toward novel analytically useful fragmentation pathways (e.g., to enable determination of the site(s) of unsaturation within the acyl chain(s)). In this chapter, it was demonstrated that using UVPD and multistage CID-MSⁿ experiments, similar reactions involving a protonated diiodoaniline ion non-covalently associated with two neutral saturated or unsaturated TG lipid molecules can occur, resulting in the formation of multiple cross-linked TG products.

2.2 Results and Discussion

2.2.1 Photo-Induced Dissociation of Protonated Diiodoaniline-TG Dimer Complex Ions

Diiodoaniline (diIA) was selected as a potential cross-linker for TG lipids for several reasons. First, the protonated amine group of diIA could be an effective ionizing adduct for a TG dimer since the detection of an ammonium cation complexed with a TG dimer after ESI has been reported [220]. Second, the phenyl ring of diIA is a chromophore, which increases the cross section for photon absorption. Finally, the biradical product that is generated upon cleavage of the two carbon-iodine bonds upon activation with UV photons has the potential to form covalent linkages by reaction at sites of unsaturation (as well as at other sites – see below) within the TG lipids [153]. To first establish the feasibility of using diIA as a photo-induced inter-molecular cross-linking reagent for TG lipids, sample solutions containing either mono-unsaturated TG_(14:0/16:1/14:0) or saturated TG_(14:0/16:0/14:0) with 3,4-diIA, 2,4-diIA or 3,5-diIA were introduced into the modified linear ion trap mass spectrometer via ESI. In the resultant mass spectra (data not shown), abundant ions were observed at m/z 1841 and 1845, respectively, with broad peak widths, that were found to correspond to the presence of [2TG_(14:0/16:1/14:0) + diIA + H]⁺ and [2TG_(14:0/16:0/14:0) + diIA + H]⁺ with calculated m/z values of 1843.3 and 1847.3, respectively. The broadened peak widths and shifted m/z values compared to the theoretical values for these non-covalent complexes can be explained as being due to dissociation occurring during resonance ejection [221, 222]. The phenomenon of mass shifts and broadened peak widths associated with the presence of non-covalently linked TG dimer complex precursor and product ions were observed

consistently in the experiments described herein, but did not negatively affect interpretation of the results. Figure 2.1A and 2.1B show the product ion spectra obtained following 266 nm UVPD-MS/MS spectra of the precursor ions of $[2\text{TG}_{(14:0/16:1/14:0)} + 3,4\text{-diIA} + \text{H}]^+$ (complex 1) and $[2\text{TG}_{(14:0/16:0/14:0)} + 3,4\text{-diIA} + \text{H}]^+$ (complex 2) containing 3,4-diIA, respectively, while Figure 2.1C shows the UVPD-MS/MS spectrum obtained from the $[2\text{TG}_{(14:0/16:1/14:0)} + 2,4\text{-diIA} + \text{H}]^+$ (complex 3) precursor ion containing 2,4-diIA. In each case, product ions corresponding to the sequential neutral losses of one and two iodine radicals were observed, as well as, additional products corresponding to the further losses of intact neutral TG molecules. The anilinyI biradical-containing product ions that were formed via the loss of two iodine radicals (i.e., m/z 1588.7 in Figure 2.1A, 1592.7 in Figure 2.1B and 1588.9 in Figure 2.1C) can then potentially undergo subsequent reactions via either radical addition or hydrogen abstraction. Radical addition at unsaturation site(s) within the unsaturated $\text{TG}_{(14:0/16:1/14:0)}$ containing dimers in Figure 2.1A and 2.1C would be analogous to chemistry previously reported by Pham *et al.* [153]. Hydrogen abstraction is at least thermodynamically feasible [223] at some sites along the fatty acyl chains and on the glycerol backbone of the TG molecules within both the unsaturated $\text{TG}_{(14:0/16:1/14:0)}$ and the saturated $\text{TG}_{(14:0/16:0/14:0)}$ dimers.

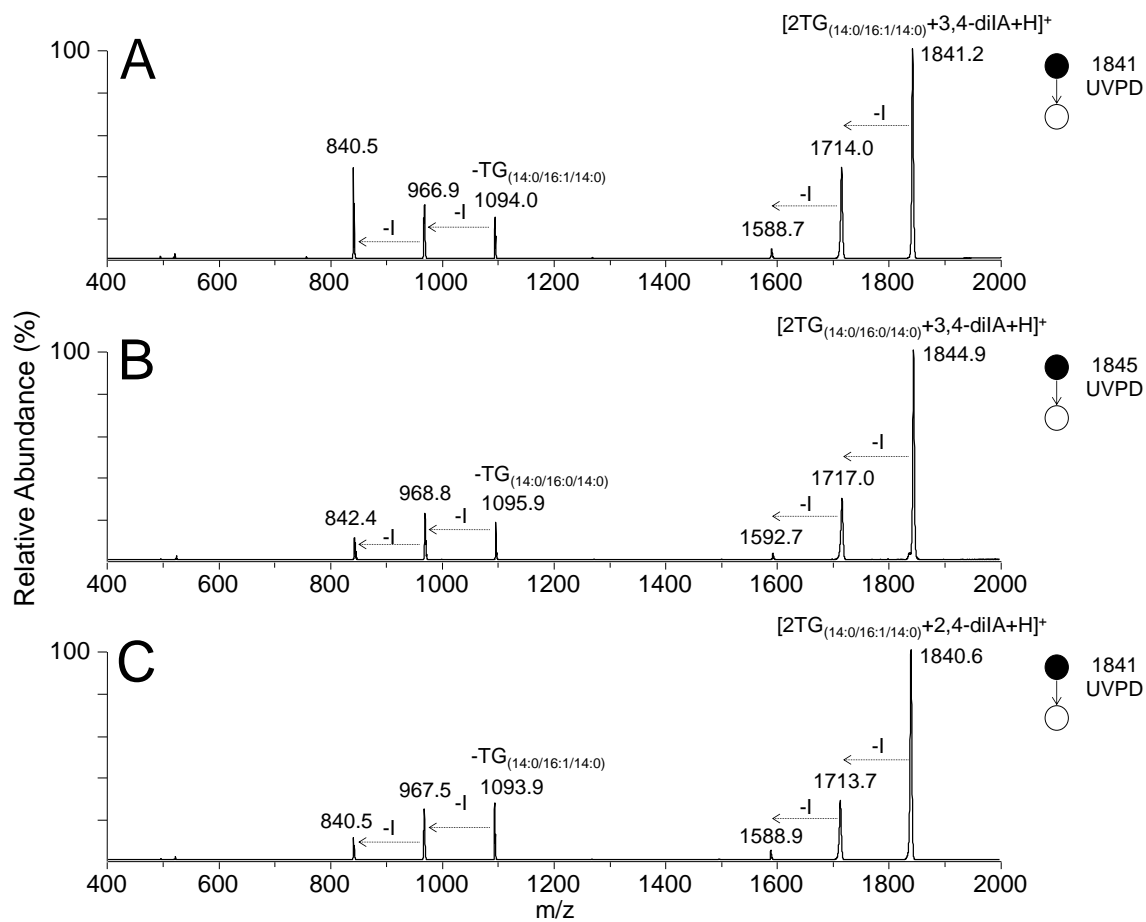


Figure 2.1 Ion trap 266 nm UVPD-MS/MS of mono-unsaturated and saturated TG homodimer complex ions with protonated diIA. (A) $2TG_{(14:0/16:1/14:0)} + 3,4\text{-diIA}$ (complex 1), (B) $2TG_{(14:0/16:0/14:0)} + 3,4\text{-diIA}$ (complex 2) and (C) $2TG_{(14:0/16:1/14:0)} + 2,4\text{-diIA}$ (complex 3). Note, that high mass ion complexes are fragile ions and as such exhibit an apparent mass-shift to lower m/z (see explanation provided in the text).

2.2.2 Proposed Mechanisms and Structures of Covalently Cross-linked TG Dimer Product Ions

Figure 2.2 shows proposed mechanisms for the initial photo-dissociation reaction and subsequent formation of cross-linked TGs as well as unlinked products from complex **1**. After homolysis of the carbon-iodine bonds, and formation of the protonated anilinyli biradical ion, H-abstraction at an aliphatic C-H bond followed by radical recombination may occur to yield the inter-molecular cross-linked product ion structure **1a**. Alternatively, radical addition to a C=C bond followed by radical recombination, or H-abstraction at an aliphatic C-H bond followed by radical recombination, would yield structures **1b** and **1c**, respectively. It should be noted that while H-abstraction may be possible from C-H bonds at a number of positions on each of the fatty acyl chains of the two saturated or unsaturated TG molecules in the complex ion, the thermodynamically preferred H-abstraction positions are expected to involve activated C-H bonds adjacent to the C=C, C=O and C-O bonds [223]. Cross-linking could also take place at sites remote to the site of the initial H-abstraction, after radical site migration. Thus, structures **1a** and **1c** should be considered representative of the many possible inter-molecular cross-linked structures that may result from the mechanisms illustrated in Figure 2.2.

Interestingly, a significant increase in the relative abundance of the 266 nm UVPD-MS/MS cross-linked TG dimer product ions, $[2TG + diIA - 2I + H]^+$ under the same experimental conditions was observed as a function of the number of C=C bonds within the TG lipids. For example, the % relative abundance of the product ions from complex **1**, and from $[TG_{(14:0/16:1/14:0)} + TG_{(16:0/18:1/16:0)} + 3,5-diIA - 2I + H]^+$ (data not

shown), both containing two C=C bonds, were found to be $5.6\% \pm 0.3$ ($n=3$) and $4.7\% \pm 0.1$, respectively, whereas the yield of $[\text{TG}_{(14:0/16:0/14:0)} + \text{TG}_{(16:0/18:1/16:0)} + 3,5\text{-diIA} - 2\text{I} + \text{H}]^+$ (complex **4**) containing one C=C bond and complex **2** containing no C=C bonds were only $3.2\% \pm 0.1$ and $1.9\% \pm 0.3$, respectively. This suggests that TG lipids containing a greater number of sites of unsaturation are more easily cross-linked with diiodoaniline in the gas phase.

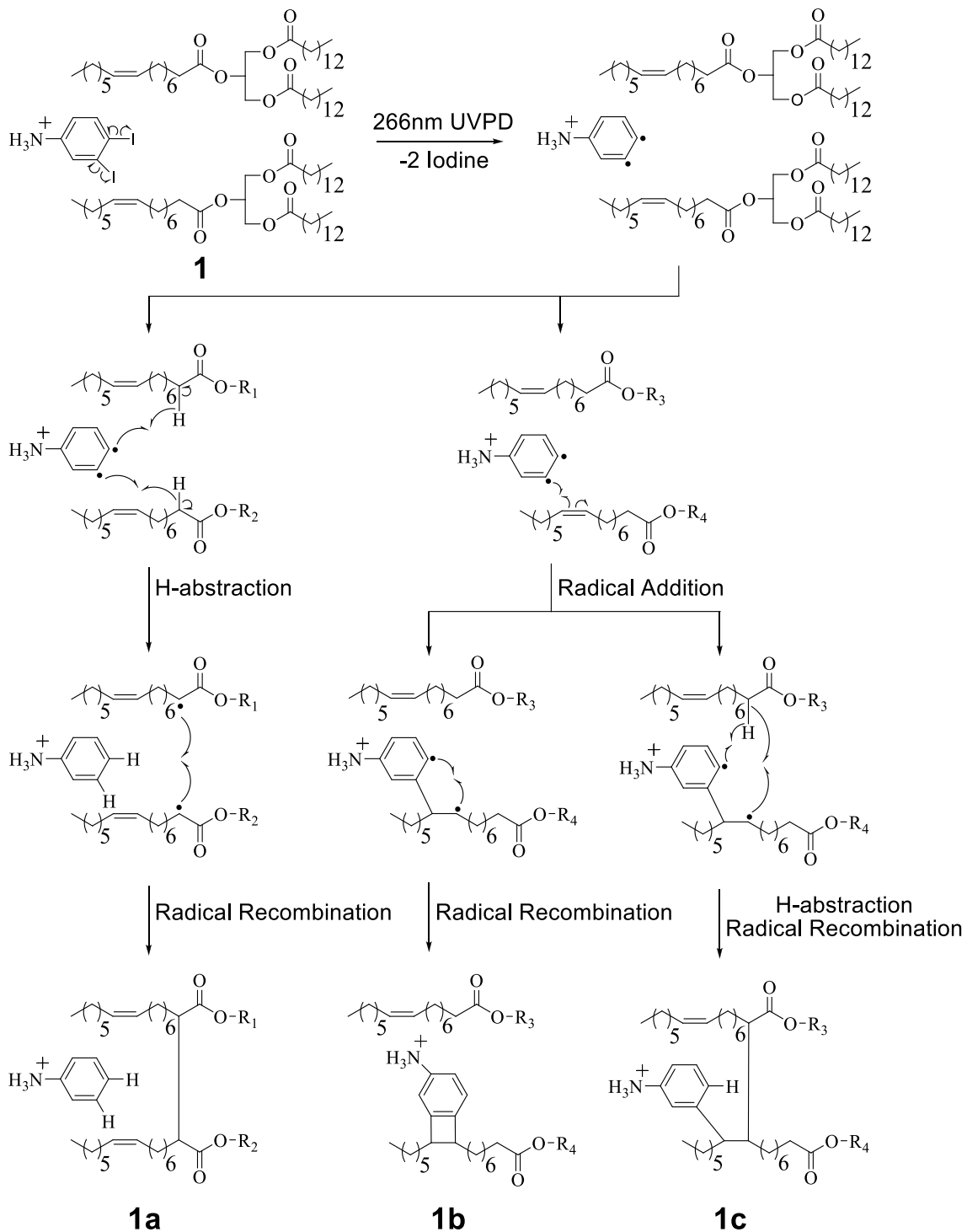


Figure 2.2 Proposed mechanisms for the photo-induced cross-linking reactions of TG dimer complex ions $[2TG_{(14:0/16:1/14:0)} + 3,4\text{-diIA} + H]^+$ (complex 1).

2.2.3 Proposed Fragmentation Mechanisms of TG Dimer Product Ion Structures **1a**, **1b** and **1c**

Initial evidence for the various cross-linking reaction product ion structures proposed in Figure 2.2 was provided by performing CID-MS³ of unsaturated [complex **1** - 2I]⁺ at m/z 1588.7 in Figure 2.1A, saturated [complex **2** - 2I]⁺ at m/z 1592.7 in Figure 2.1B and unsaturated [complex **3** - 2I]⁺ at m/z 1588.9 in Figure 2.1C. The resultant spectra are shown in Figure 2.3A, 2.3B and 2.3C, respectively. CID-MS/MS of unsaturated complex **1** and saturated complex **2** (data not shown) each resulted in the loss of a neutral TG_(14:0/16:1/14:0) or TG_(14:0/16:0/14:0) as the only dissociation pathway. Thus, the presence of additional products formed upon CID-MS³ of the three [2TG + diIA - 2I + H]⁺ UVPD-MS/MS product ions are suggestive of the formation of new covalent linkages within these products. Furthermore, the differences between the CID-MS³ spectra from the unsaturated complex **1** and saturated complex **2** must be due to the presence of the unsaturation site(s) in the TG_(14:0/16:1/14:0) dimer ion, and therefore can be assigned as arising from dissociation of structures **1b** or **1c**. These include m/z 1361.0 (loss of 14:0 fatty acid (FA)), 1132.8 (loss of two 14:0 FA), 1076.7 (loss of diacylglyceride_(14:0/14:0) (DG_(14:0/14:0))), 848.6 (loss of DG_(14:0/14:0) and 14:0 FA), 564.5 (loss of 2 DG_(14:0/14:0)) and 538.4 (loss of DG_(14:0/16:1) and DG_(14:0/14:0)), each formed via cleavage of covalent bonds within the TG dimer ion [224], and the increased abundance of m/z 840.5 in Figure 2.3A relative to m/z 842.4 in Figure 2.3B. Similarly, the differences between the CID-MS³ product ion spectra from the unsaturated [complex **1** - 2I]⁺ and [complex **3** - 2I]⁺ in Figure 2.3A and 2.3C must be due to the locations of the radical sites upon photo-dissociation of the protonated 3,4-diIA and 2,4-diIA adducts.

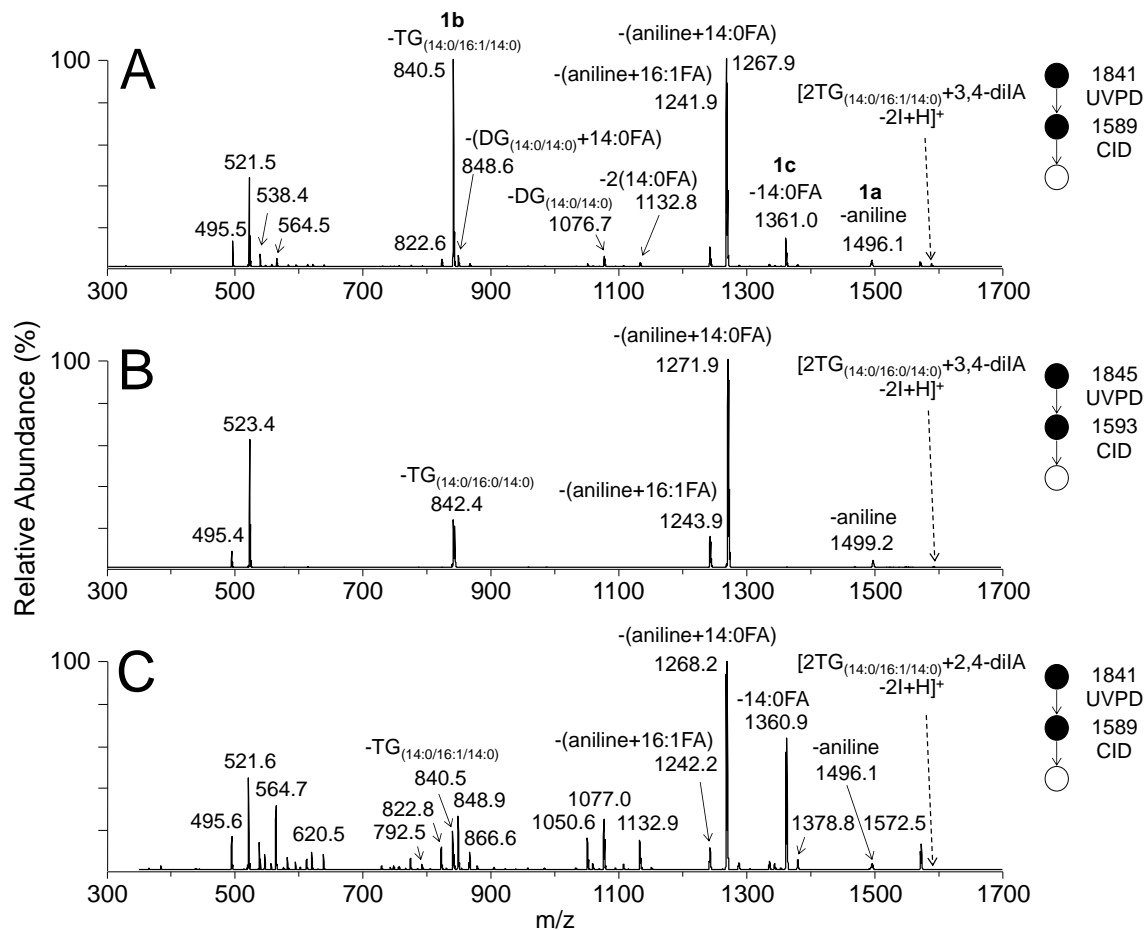


Figure 2.3 Ion trap CID-MS³ analysis of cross-linked mono-unsaturated and saturated TG homodimer complex ions with protonated 3,4-diIa or 2,4-diIa, formed by 266 nm UVPD-MS/MS. (A) [complex 1 - 2I]⁺ from Figure 2.1A, (B) [complex 2 - 2I]⁺ from Figure 2.1B, and (C) [complex 3 - 2I]⁺ from Figure 2.1C. The major product ions formed from proposed structures **1a**, **1b** and **1c** in Figure 2.2 are labeled in Figure 2.3A.

To obtain further direct evidence for the proposed 266 nm UVPD-MS/MS product ion structures **1a**, **1b** and **1c**, each of the major product ions observed in the CID-MS³ spectra shown in Figure 2.3 were then subjected to further dissociation. For example, the CID-MS⁴ spectra of m/z 1496.1 [complex **1** - 2I - aniline]⁺, m/z 840.5 [complex **1** - 2I - TG_(14:0/16:1/14:0)]⁺ and m/z 1361.0 [complex **1** - 2I - 14:0 FA]⁺ from Figure 2.3A, representing first generation products formed from proposed structures **1a**, **1b** and **1c**, respectively, are shown in Figure 2.4A, 2.4B and 2.4C.

It is reasonable to expect that structure **1a**, containing an inter-molecular cross-link directly between the two TG monomers, would undergo the facile loss of neutral aniline upon CID-MS³ activation. Thus, CID-MS⁴ of the [complex **1** - 2I - aniline]⁺ product was performed (Figure 2.4A), resulting in the dominant loss of a neutral 14:0 fatty acid at m/z 1267.9, that notably was also observed as the dominant product ion in the CID-MS³ spectra in Figure 2.3A. This ion subsequently underwent further dissociation (as determined by MS⁵, and by MS⁴ of the m/z 1267.9 in Figure 2.3A), to yield the products at m/z 495.5 and m/z 521.5 in Figure 2.4A (and in Figure 2.3A). The proposed structures of the m/z 1267.9 and m/z 495.5 ions, and mechanisms for their formation, are shown in Figure 2.5. The product ion at m/z 521.5, containing a 16:1 fatty acyl chain, would be formed by a mechanism similar to that for m/z 495.5, but involving an initial UVPD-MS/MS product ion cross-linked between 16:1 and 14:0 fatty acyl chains rather than the two 16:1 chains as shown in Figure 2.5. Notably, the spectrum obtained by CID-MS⁴ of the m/z 1499.2 and m/z 1496.1 product ions in Figures 2.3B and 2.3C (i.e., saturated [complex **2** - 2I - aniline]⁺ with 3,4-diIA and unsaturated [complex **3** - 2I - aniline]⁺ with 2,4-diIA) were both similar to that in Figure 2.4A (the

characteristic mass shifts due to the lack of double bonds in the product ions formed from the saturated TG dimer were used to help assign the compositions of the various product ions). This demonstrates that the presence of the double bond(s) and the location of the radical sites within the protonated diIA ion played no significant role in the formation of proposed structure **1a**.

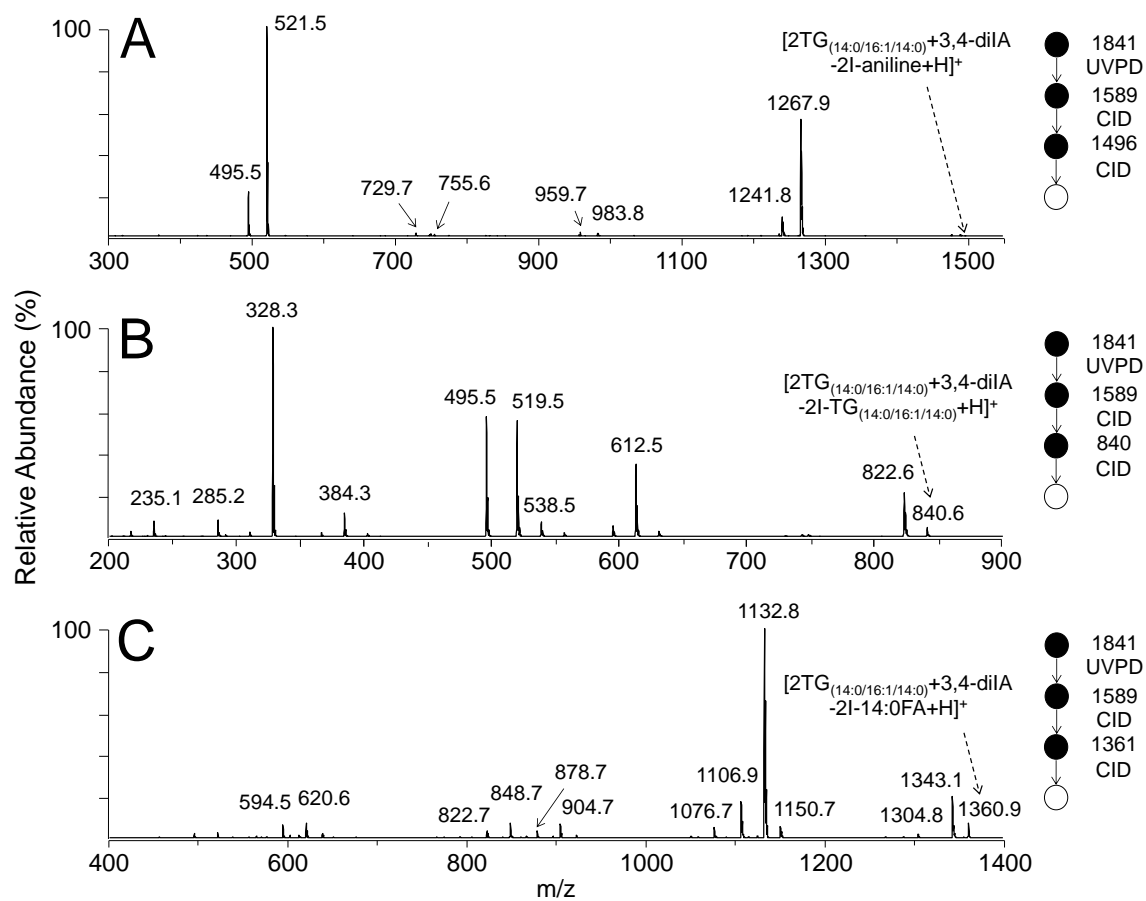


Figure 2.4 Ion trap CID-MS⁴ analysis of cross-linked mono-unsaturated TG homodimer complex ions from Figure 2.3A. (A) [complex 1 - 2I - aniline]⁺, (B) [complex 1 - 2I - TG_(14:0/16:1/14:0)]⁺, and (C) [complex 1 - 2I - 14:0 FA]⁺.

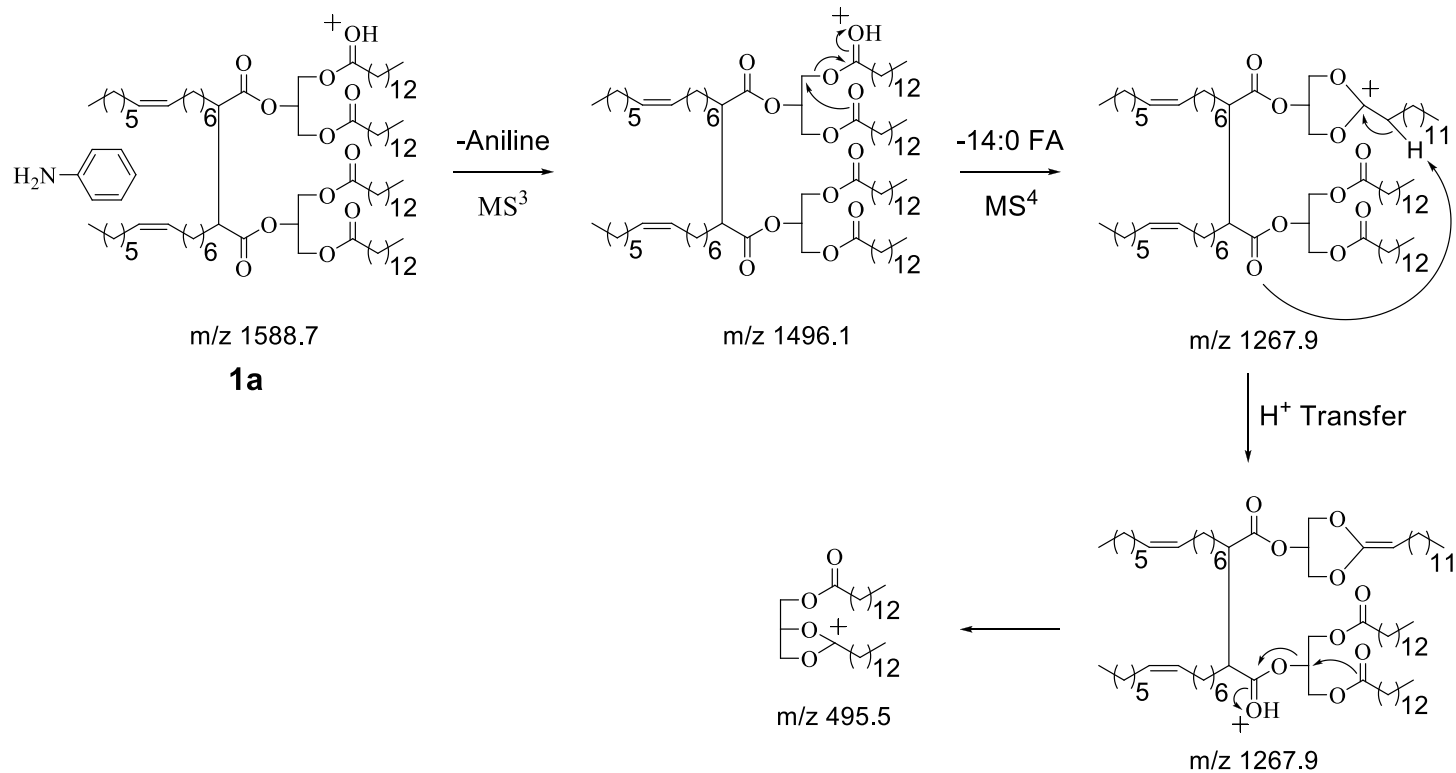


Figure 2.5 Proposed mechanisms for the CID-MS³ and -MS⁴ fragmentation reactions of [complex 1 - 2I]⁺ ions corresponding to structure **1a** in Figure 2.2.

Structure **1b**, containing an intra-molecular four-membered ring resulting from radical addition and radical recombination of the two phenyl radicals to a C=C double bond in one of the TG molecules, does not contain any covalent cross-links between the two TG molecules. Thus, it is expected that the major CID-MS³ fragmentation pathway for this structure would involve the loss of a neutral TG to yield the product ion at m/z 840.5 in Figure 2.3A. CID-MS⁴ of the [complex **1** - 2I - TG_(14:0/16:1/14:0)]⁺ product ion (Figure 2.4B) resulted in the formation of a dominant product at m/z 328.3 consistent with aniline covalently linked to a protonated 16:1 fatty acyl containing ketene product ion, as well as various other product ions consistent with structure **1b**. Proposed mechanisms and structures for formation of the various product ions shown in Figure 2.4B, are shown in Figure 2.6.

Further evidence for the presence of the non-cross-linked structure **1b** was obtained by examining the CID-MS³ dissociation of the UVPD-MS/MS product ion of unsaturated/saturated TG heterodimer complex **4** (Figure 2.7), where the major fragmentation pathways could involve the loss of either a neutral TG_(16:0/18:1/16:0) or TG_(14:0/16:0/14:0). However, primarily only the neutral TG_(14:0/16:0/14:0) loss was observed, indicative of the involvement of the C=C bond in the structure of the precursor .

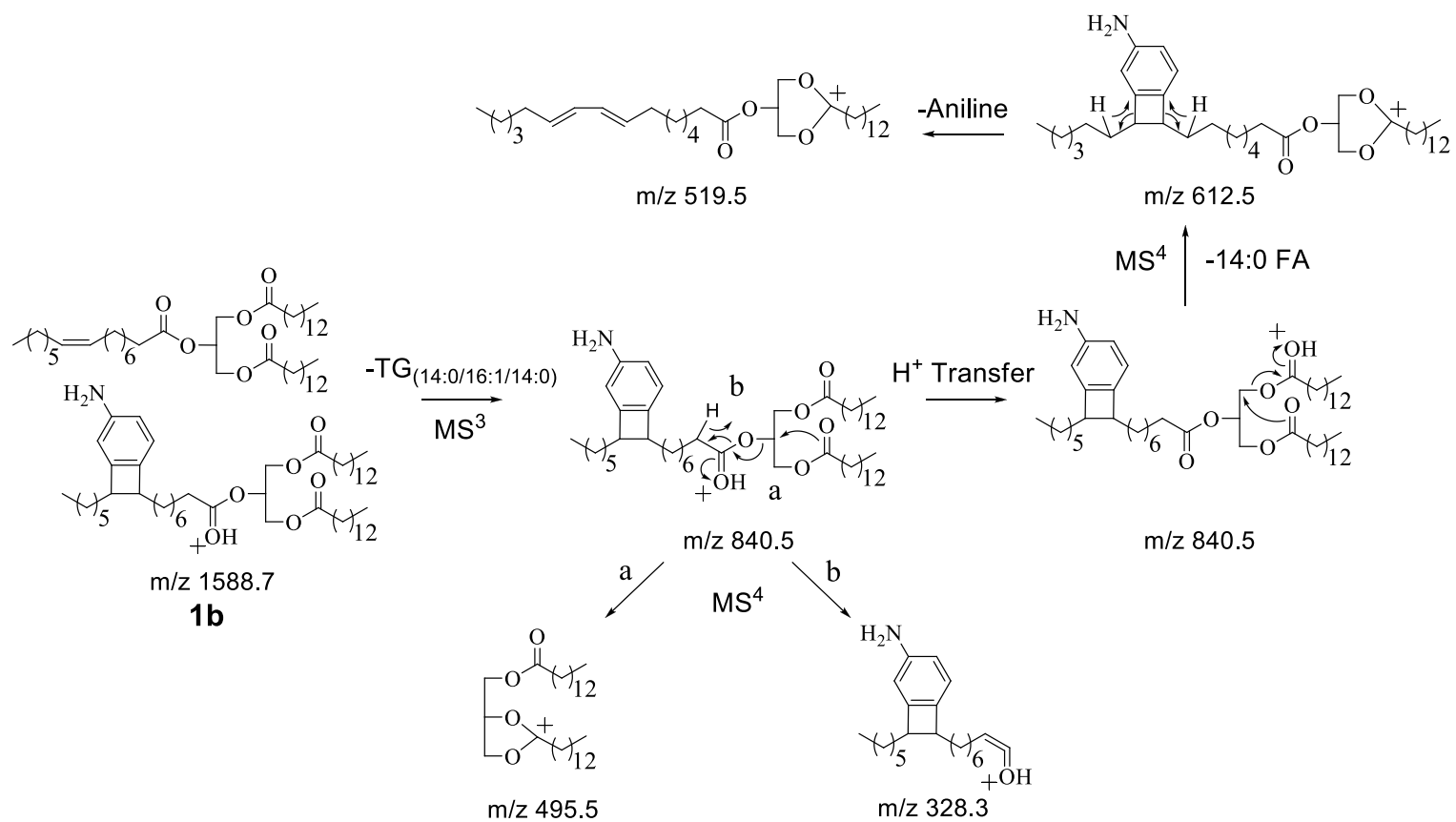


Figure 2.6 Proposed mechanisms for the CID-MS³ and -MS⁴ fragmentation reactions of [complex **1** - 2I]⁺ ions corresponding to structure **1b** in Figure 2.2.

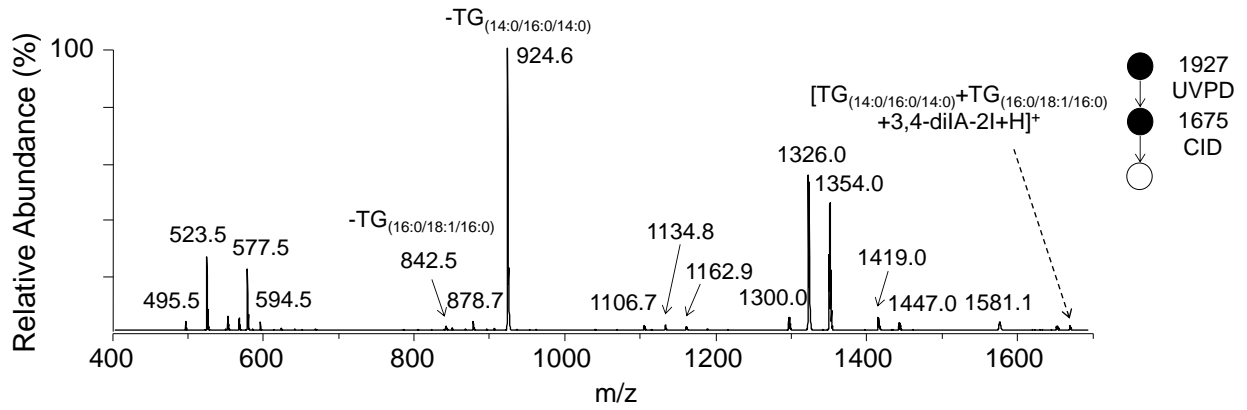


Figure 2.7 Ion trap CID-MS³ analysis of the cross-linked saturated/mono-unsaturated TG heterodimer complex ion [complex 4 - 2I]⁺, formed by 266 nm UVPD-MS/MS.

Evidence for structure **1c** was obtained by CID-MS⁴ of the [complex **1** - 2I - 14:0 FA]⁺ product ion at m/z 1361.0 from Figure 2.3A (Figure 2.4C), in which the dominant product observed at m/z 1132.8 corresponded to the neutral loss of a second 14:0 fatty acid molecule (as well as m/z 1106.9 corresponding to the loss of a 16:1 fatty acid), and various other products consistent with the presence of the anilinyll moiety covalently linked at the site of unsaturation in the 16:1 fatty acyl chain. Proposed structures and mechanisms for the formation of these ions are shown in Figure 2.8. Inter-molecular cross-linking between the two sites of unsaturation (i.e., via sequential radical addition reactions of the anilinyll biradical with the two separate C=C bonds within the 2TG_(14:0/16:1/14:0) homodimer) cannot be ruled out. However, the data obtained from control experiments involving the TG heterodimer complex **4** consisting of a saturated TG_(14:0/16:0/14:0) and a mono-unsaturated TG_(16:0/18:1/16:0) (whose CID-MS³ spectrum is shown in Figure 2.7) resulted in similar fragmentation behaviors, indicating that complexes with two versus only one C=C bond have similar cross-linked structures. In other words, cross-linking between two sites of C=C bond cannot be a dominant process.

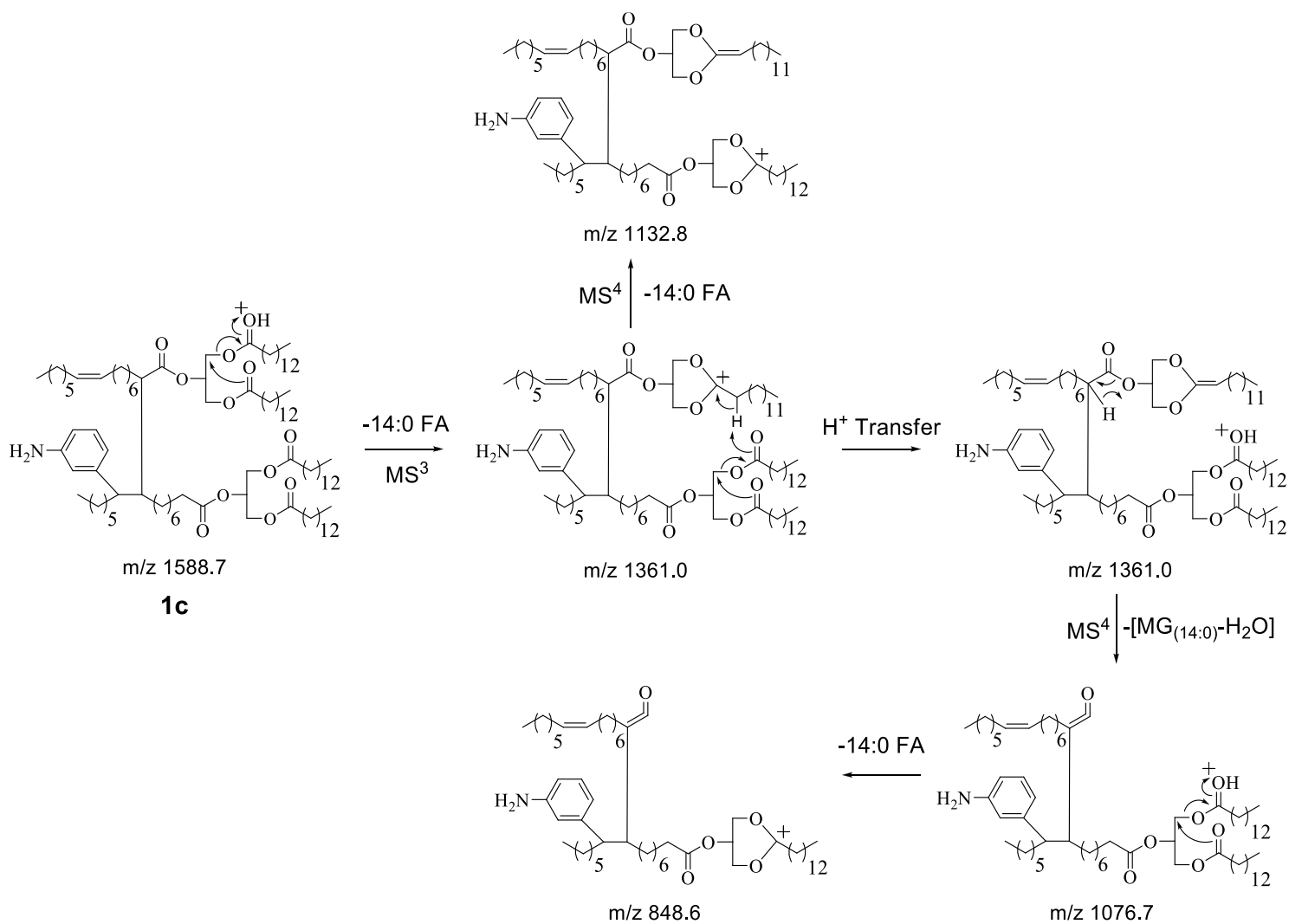


Figure 2.8 Proposed mechanisms for the CID-MS³ and -MS⁴ fragmentation reactions of [complex 1 - 2I]⁺ ions corresponding to structure **1c** in Figure 2.2. MG denotes monoacylglyceride.

2.2.4 Effects of Structures of the Cross-Linker and TG Lipids on the Formation of Cross-Linked TG Dimer Product Ions

Next, the effect of the structure of the cross-linker on the reactivity and formation of product ion structures of cross-linked TG dimer product ions was investigated by using 2,4-diIA versus 3,4-diIA as the cross-linker. No difference in the initial 266 nm UVPD-MS/MS reaction efficiency was observed as a function of the identity of the diiodoaniline adduct (e.g., compare the relative abundance of the $[2\text{TG}_{(14:0/16:1/14:0)} + \text{diIA} - 2\text{I} + \text{H}]^+$ product ions in Figures 2.1A and 2.1C). However, a significant decrease in the formation of the non-cross-linked product ion structure **1b** was observed when using 2,4-diIA, as evidenced by the low relative abundance of the ion at m/z 840.5 in Figures 2.1C and 2.3C corresponding to $[\text{complex } \mathbf{3} - 2\text{I} - \text{TG}_{(14:0/16:1/14:0)}]^+$ compared to Figures 2.1A and 2.3A. A reasonable explanation is that after UVPD-MS/MS, the 3,4-biradical can readily undergo radical addition and recombination with the C=C bond of the TG molecule to form a stable four-membered ring. Furthermore, the 3,4-biradical has aryne-character and thus may undergo concerted [2+2]-cycloaddition at sites of unsaturation [72, 225]. This mechanism would also result in product **1b** and may compete favorably with the desired cross-linking biradical reactions that yield product types **1a** and **1c**. In contrast, the yield of the characteristic product ions for structure **1c** were observed to significantly increase when using the 2,4-diIA adduct compared to 3,4-diIA. This observation is consistent with the thermochemistry of H-abstraction for the 2,4- and 3,4-biradicals based on the known bond energies of the benzyne archetype. That is, experimental measurements find *ortho*-benzyne to be some 16 kcal mol⁻¹ more stable than its *meta*-isomer which translates to an enhanced H-atom affinity in the latter of the

same magnitude [223, 226]. While the impact of the local ammonium moiety on the benzyne energetics is unknown, the stability trend is likely to be preserved and thus predicts that the 2,4-biradical formed from 2,4-diIA is more likely to initiate H-abstraction chemistries than its 3,4-isomer, consistent with the observations made here.

2.2.5 Solution Phase Cross-Linking of TG lipids

The reactivity of TG lipids toward cross linking reaction upon activation of 266 nm UV photon and addition of diiodoaniline cross linker in solution phase was also investigated. After irradiation of 266 nm UV photons to the sample solution containing TG_(14:0/16:1/14:0) and 3,5-diIA for 9 min, product ions at m/z 1495.9 corresponding to m/z of [2TG_(14:0/16:1/14:0) + 3,5-diIA – aniline - 2I + H]⁺ were observed in the MS analysis in Figure 2.9A. In Figure 2.9B, further CID-MS/MS analysis of the product ions at m/z 1495.9 from Figure 2.9A produced similar fragmentation patterns compared to that of the major cross-linked product ions at m/z 1496 from structure **1a** in Figure 2.4A. The observed similarity suggested that same cross-linked TG lipids were synthesized in both gas phase and solution phase. Compared to Figure 2.1A, the missing product ions of [2TG_(14:0/16:1/14:0) + 3,5-diIA – aniline - 2I + H]⁺ in Figure 2.9A was possibly due to the fact that the required irradiation time (~minutes) of solution phase TG cross-linking reactions in order to observe abundant product ions was much longer than that in gas phase (<= 30 ms). Thus most of the [2TG_(14:0/16:1/14:0) + 3,5-diIA - 2I + H]⁺ ions were activated by UV photons and further fragmented to loss an aniline.

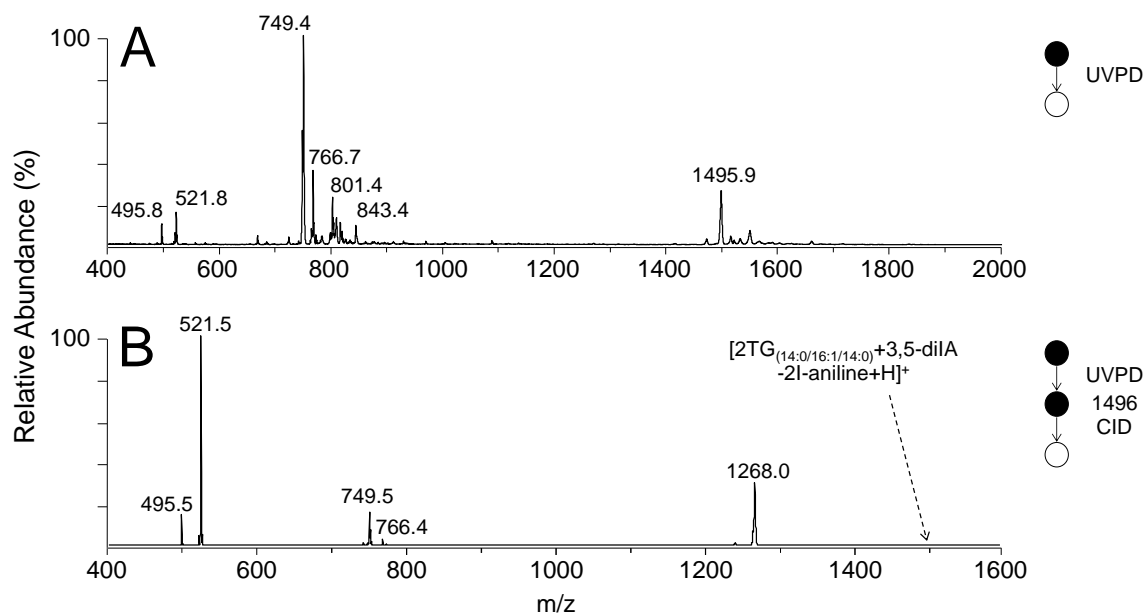


Figure 2.9 Ion trap MS and MS/MS analysis of products in solution phase intermolecular cross-linking reactions of TG lipids. (A) MS analysis of products in the solution containing TG_(14:0/16:1/14:0) and 3,5-diiodoaniline after 9 min of irradiation with 266 nm UV photons; (B) CID-MS/MS analysis of the product ions at m/z 1496 from Figure 2.9A.

2.3 Conclusions

The inter-molecular gas phase cross-linking of TG lipid dimers has been demonstrated using anilinyll biradical ions formed via 266 nm UVPD-MS/MS of protonated diiodoaniline adducts. Using multistage CID-MS³, -MS⁴ and -MS⁵, cross-linking was shown to occur via sequential combinations of H-abstraction, radical addition and recombination reactions. The efficiency of the UVPD reactions, and the competition between the various inter-molecular cross-linking and non-cross-linking reaction pathways, were shown to be dependent on the number of unsaturation sites present within the TG lipids, as well as on the locations of the biradical sites within the protonated aniline adduct ion. The reactivity of cross linking reactions in the gas phase were observed to be identical to those obtained upon photo irradiation of the TG lipids in the presence of 3,5-diiodoaniline in solution. Importantly, while there are many possible inter-molecular cross-linked structures that may result due to the large number of sites at which H-abstraction can occur (and in which the aniline adduct may or may not be covalently incorporated), this type of novel gas phase cross-linking reaction provides a method to covalently link two molecules without the requirement of any specific functional group. Thus, the same approach could be applied to perform gas phase cross-linking within a wide range of biomolecular classes.

CHAPTER THREE

Characterization and Multiplexed Quantification of Derivatized Aminophospholipids

3.1 Introduction

Glycerophosphoethanolamine (PE) and glycerophosphoserine (PS) lipids are subclasses of glycerophospholipids containing a primary amine functional group attached to the terminal end of the phosphoglycerol backbone. Under normal physiological conditions in eukaryotic cells, anionic PE and PS lipids reside predominantly or exclusively in the inner leaflet of the plasma membrane, respectively, where they play important roles in regulating various biological processes including intra- and inter-cellular signaling, phagocytic recognition, apoptotic cell clearance, cell division, angiogenesis and vascular remodeling [227-230]. Abnormalities in the metabolic regulation of aminophospholipid compositions and distributions therefore have established roles in human diseases including cancer, diabetes, obesity and neurodegeneration [231-235].

Significant advances in lipidomics over the past ten years have largely been driven by developments in mass spectrometry instrumentation and associated methods for the comprehensive identification, structural characterization and quantification of the array of structurally diverse lipid classes and molecular lipid species that may be present within a cell, tissue or body fluid (e.g., plasma) sample of interest [66]. To date however, most of the developed quantification strategies have required the separate

The results described in this chapter were published in: Nie, S., Phaner, C.J., Liu, S., Peake, D., Kiyonami, R., Huang, Y. and Reid, G.E. Characterization and multiplexed quantification of derivatized aminophospholipids. *Int. J. Mass Spectrom.* **2015**, doi:10.1016/j.ijms.2015.07.002.

analysis of each sample, with appropriate technical replicates and corrections based on the inclusion of internal standards, in order to be able to draw any conclusions regarding the biological significance of changes observed between the samples. This is a particular challenge for certain lipid classes, e.g., PS lipids that are observed as only minor components of eukaryotic membranes. Improved sensitivity for the positive ionization mode MS detection of low abundant aminophospholipids has been demonstrated using various chemical labeling methods (i.e., incorporation of fixed charge and/or hydrophobic groups) [24, 91, 92].

For mass spectrometry-based absolute quantification of molecular lipid concentrations, isotopically labeled internal standards that are chemically identical to the lipid molecule of interest are required. However, this is often impractical due to the limited number of lipid internal standards that are commercially available, and the estimated thousands of possible lipid structures that may be present. Alternatively, albeit with its own potential limitations, a single internal standard for a lipid class can be used [23]. Thus, many groups chose to report quantification results using relative, rather than absolute, methods which require internal standards only for normalization of differences in technical variances between the samples [24, 138, 236-238].

An emerging method for improving the accuracy of mass spectrometry-based relative quantification of lipids involves the use of isobaric mass stable isotope labeling derivatization reagents, coupled with MS/MS analysis, analogous to those used in contemporary quantitative proteomics e.g., iTRAQ or TMTs as described in Chapter one, section 1.2.1.3.3 [239]. For example, primary amine specific iTRAQ and isotope-labeled 4-(dimethylamino)benzoic acid NHS ester derivatization have been employed for

quantification of aminophospholipids [194-196] and hydrolyzed ceramide lipids [197]. Quantitative information can be readily obtained by ratiometric measurement of the abundances of isotopically encoded low mass reporter ions from each sample, upon MS/MS of their isobaric mass precursor ions. Using these methods, run-to-run or even scan-to-scan variance in lipid ion abundances can be avoided since different samples are ionized and mass analyzed simultaneously after separate derivatization and mixing. However, special attentions need to be paid to avoid the interference in the intensities of low mass reporter ions caused by the presence of co-isolated and fragmented precursor ions present within the isolation window that is used prior to dissociation. For example, diacyl-PE or -PS lipids have only a Δm of 0.0363 Da compared to ether-PE or -PS lipids which contain the same degree of unsaturation but with one more carbon on their acyl, alkyl or alkenyl chains. Although MS³ dissociation, gas phase purification using proton transfer reaction and ion mobility separation methods have been developed to overcome the similar limitation for quantitative proteomic studies, they are not necessarily applicable to lipid analysis due to the decreased sensitivity [201] or the need for multiply charged precursor ions [202] or specific instrumentation [203]. Moreover, structural information on the acyl, alkyl or alkenyl chain compositions of aminophospholipid ions cannot be acquired in positive ionization mode using current isotope tagging methods, which compromises the throughput of analysis if structural characterization of lipid molecular species is desired.

Lu *et al.* have previously reported the development and application of an isobaric mass stable isotopic labeled derivatization strategy using d₆-‘heavy’ and d₆-‘light’ variants of the DMBNHS reagent described above, coupled with high

resolution/accurate mass MS/MS for the simultaneous differential quantitative analysis of phosphopeptides [82]. Using these reagents, the potential problem of reporter ion overlap from co-isolated and co-fragmented precursors is reduced or eliminated, as quantitative information is obtained by measurement of the intensity ratios of pairs of isotopically encoded high m/z neutral loss 'reporter' ions formed by the loss of $S(CD_3)_2$ and $S(CH_3)_2$, rather than low m/z products. In this chapter, after first evaluating the gas phase fragmentation behavior of DMBNHS derivatized diacyl-, alkyl ether- and plasmalogen-aminophospholipids using different positive ionization mode collisional activation conditions, a method employing d_6 -heavy and d_6 -light DMBNHS derivatization for the simultaneous 'two-plexed' quantification and structural characterization of aminophospholipids from within complex, crude lipid extracts has been developed and its initial application was reported.

3.2 Results and Discussion

3.2.1 Characterization of the Gas Phase Fragmentation Reactions of DMBNHS Derivatized Aminophospholipids

In order to develop an optimized strategy for the identification, structural characterization and multiplexed quantification of DMBNHS derivatized diacyl-, alkyl ether- and plasmalogen-aminophospholipids, their gas phase fragmentation behavior using different collisional activation methods (linear ion trap CID and quadrupole-based HCD) was first evaluated.

3.2.1.1 Diacyl-Aminophospholipids

A hybrid quadrupole-Orbitrap-linear ion trap mass spectrometer was used to study the fragmentation of DMBNHS derivatized diacyl-PE and -PS lipids under linear

ion trap CID and quadrupole-based HCD ion activation conditions. Representative examples of the HCD-MS/MS fragmentation of DMBNHS derivatized PE_(18:0/18:1) and PS_(16:0/18:1) lipids are shown in Figure 3.1A and 3.1B, respectively. Proposed mechanisms for the observed fragmentation reactions are shown in Figure 3.2. Alternative mechanisms involving S_N2 nucleophilic attack by one of the acyl chain carbonyl groups onto the glycerol sn-3 position are also possible, similar to that previously demonstrated for the fragmentation of protonated PC lipids [35]. Further experiments using deuterium labeled lipids would be required to determine the actual mechanism that is responsible. However, both mechanisms yield product ion structures with the same elemental compositions, so the specific mechanism that is responsible does not negatively affect their assignment. In both spectra, a characteristic ‘reporter’ neutral loss of dimethylsulfide (S(CH₃)₂, 62 Da) was observed as the initial fragmentation channel, similar to that previously described for other DMBNHS derivatized primary amine-containing biomolecules [82, 127]. The product ions at m/z 605 in Figure 3.1A and m/z 577 in Figure 3.1B both correspond to the sequential loss of an additional 209 Da (total neutral loss of 271 Da) or 253 Da (total neutral loss of 315 Da) from the initial [M-S(CH₃)₂]⁺ product ions. These ions are analogous to the neutral losses of 141 Da and 185 Da observed from non-derivatized protonated PE and PS lipids, and were accompanied by complementary ‘reporter’ protonated product ions at m/z 210 and 254 [2]. The observation of these low m/z ‘reporter’ ions is most likely due to the higher proton affinity of the phosphoethanolaminohydrofuran containing structures in these products compared to the phosphoethanolamine or phosphoserine containing structures formed from the non-derivatized lipids. The decreased relative

abundance of the m/z 254 product ion in the spectrum from the derivatized PS lipid compared to m/z 210 for the PE lipid, and the corresponding increase in its complementary m/z 605 neutral loss product, is likely due to its decreased proton affinity resulting from the presence of the carboxylic acid group. Linear ion trap CID-MS/MS spectra from the DMBNHS derivatized diacyl PE_(18:0/18:0) and PS_(16:0/18:1) lipids were also acquired (data now shown). The exclusive neutral loss of S(CH₃)₂ (62 Da) was observed as the only product for both the PE_(18:0/18:0) and PS_(16:0/18:1) lipids. CID-MS³ of these neutral loss product ions (data not shown) resulted in the formation of secondary products and relative abundances similar to those seen in Figure 3.1A and 3.1B, thereby confirming the sequential nature of the fragmentation reactions proposed in Figure 3.2.

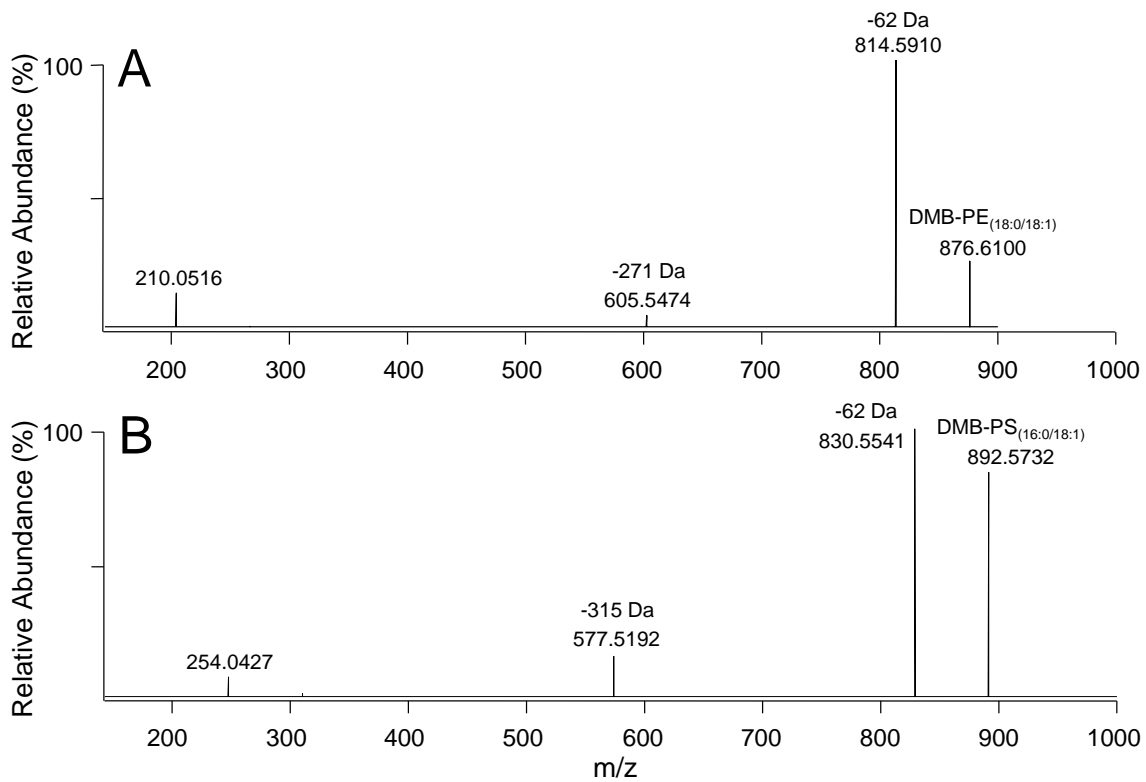


Figure 3.1 HCD-MS/MS analysis of DMBNHS derivatized (A) PE_(18:0/18:1) and (B) PS_(16:0/18:1).

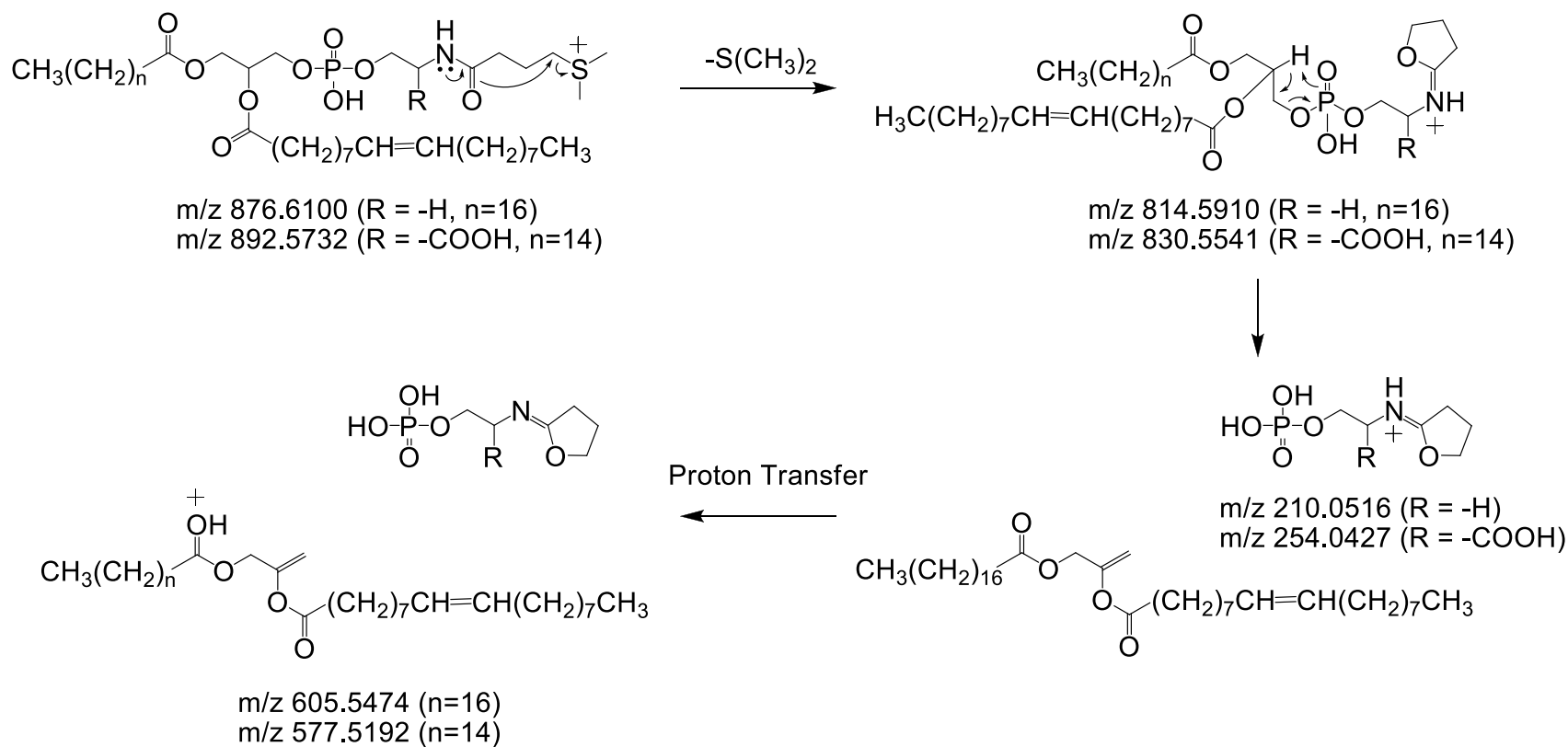


Figure 3.2 Proposed CID-MS/MS fragmentation mechanisms for DMBNHS derivatized PE_(18:0/18:1) and PS_(16:0/18:1).

HCD-MS³ of the S(CH₃)₂ neutral loss product ions formed by linear ion trap CID of the DMBNHS derivatized PE_(18:0/18:1) (Figure. 3.3A) and PS_(16:0/18:1) (Figure. 3.3B) lipids also yielded the expected secondary product ions at m/z 210 and the neutral loss of 271 Da for the PE lipid, and m/z 254 and the neutral loss of 315 Da for the PS lipid. The accurate mass values obtained for these products under Orbitrap detection conditions provided further confidence for the composition of the structures proposed in Figure 3.2. A series of molecular structure-specific fragment ions indicative of the identity of the sn-substituents on the glycerol backbone were also observed in these spectra, similar to that recently reported by Almeida *et al.* [23]. For example, in Figure 3.3A four product ions were observed at m/z 267.2668, 339.2876, 265.2512 and 341.3033, formed by further dissociation of m/z 605 and corresponding to protonated and neutral losses of sn-1 18:0 and sn-2 18:1 ketene chains. Proposed mechanisms for the formation of these ions are shown in Figure 3.4, analogous to those previously described by Hsu and Turk for CID-MS/MS of protonated and lithiated aminophospholipid ions [240, 241]. Similar fragmentation channels allowing assignment of the sn-1 16:0 and sn-2 18:1 chains were also observed for the DMBNHS derivatized PS_(16:0/18:1) lipid (m/z 239.2372, 339.2897, 265.2528 and 313.2739 in Figure 3.3B). Finally, the product ion observed at m/z 156.0656 in Figure 3.3B corresponds to the neutral loss of H₃PO₄ from the m/z 254.0426 product ion. The equivalent product ion from the DMBNHS derivatized PE_(18:0/18:1) lipid in Figure 3.3A was not observed due to the low mass cut off of m/z 150 used in these experiments.

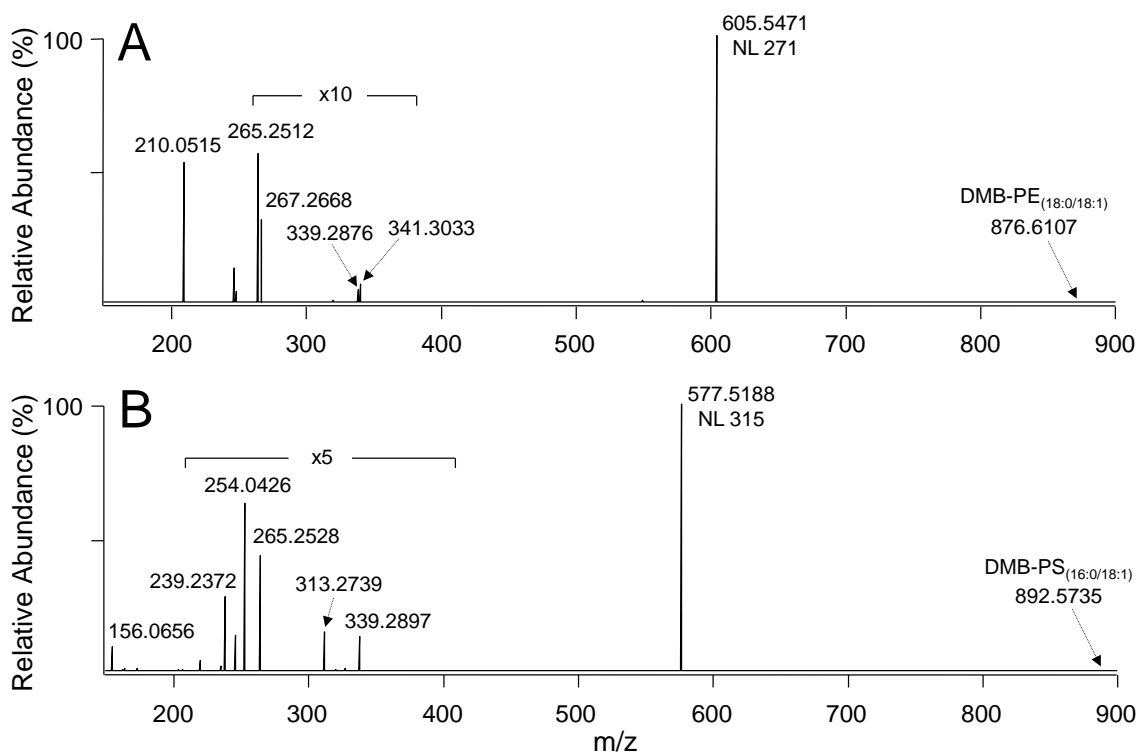


Figure 3.3 HCD-MS³ analysis of the S(CH₃)₂ neutral loss (NL) product ions formed by linear ion trap CID-MS/MS of the DMBNHS derivatized (A) PE_(18:0/18:1) and (B) PS_(16:0/18:1).

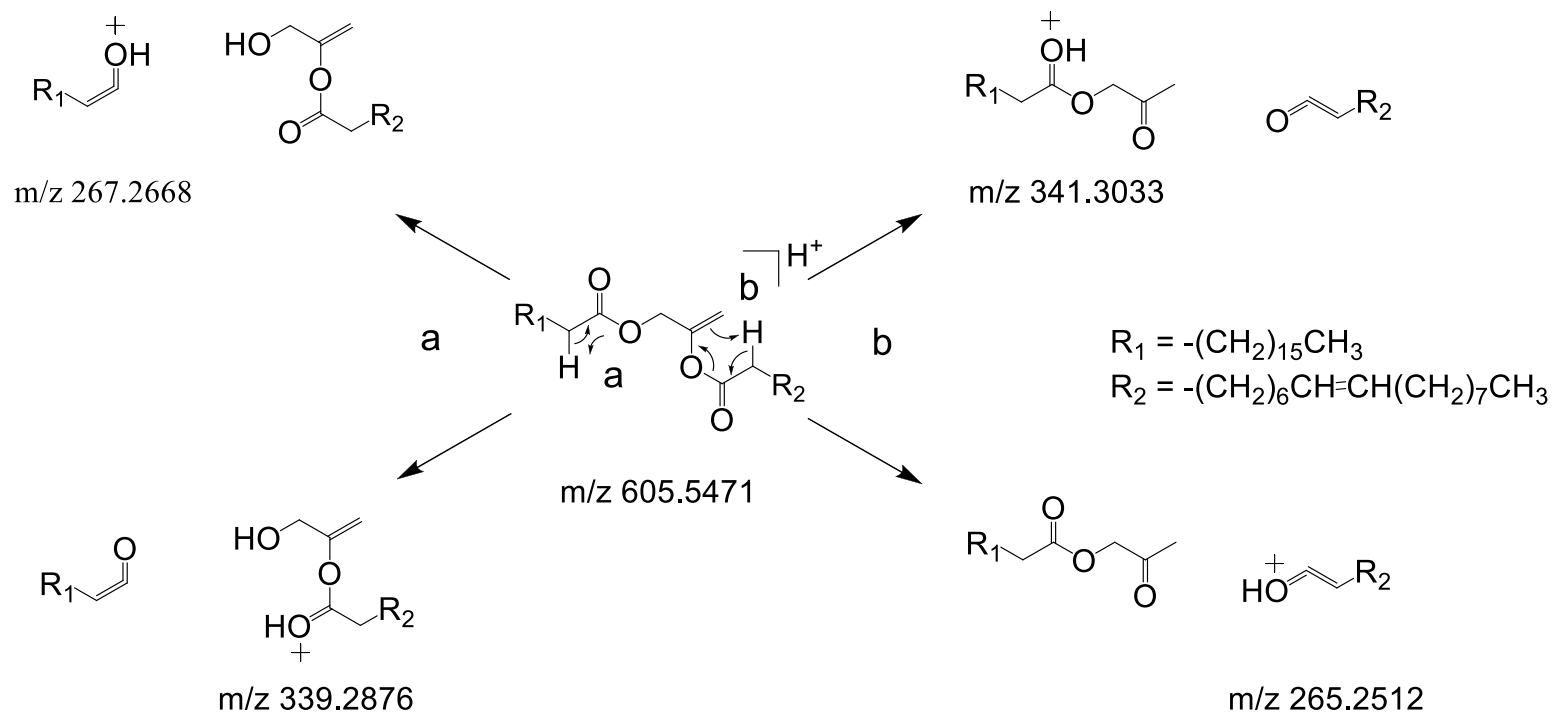


Figure 3.4 Proposed HCD-MS³ fragmentation mechanisms for DMBNHS derivatized PE_(18:0/18:1) after the neutral loss of 271 Da.

3.2.1.2 Alkyl Ether-Aminophospholipids

Alkyl ether-containing PE and PS lipid standards are not commercially available. Thus, an abundant PE_(O-34:1) lipid found in a crude lipid extract of SW620 colorectal cancer cells was used here (after initially confirming its identity and structure by exact mass ESI-MS and negative ion mode HCD-MS/MS) to study the fragmentation of DMBNHS derivatized ether-PE lipids. Linear ion trap CID-MS/MS of the DMBNHS derivatized PE_(O-34:1) yielded the neutral loss of S(CH₃)₂ (m/z 772.5836) as the dominant fragmentation channel (Figure 3.5), while HCD-MS³ fragmentation of this neutral loss ion yielded the neutral loss of 271 Da (m/z 563.5369) and a product ion at m/z 210.0516 (shown in the inset to Figure 3.5), similar to that described above for the diacyl PE lipid ions. An additional product ion at m/z 265.2513, corresponding to a protonated ketene 18:1, in the HCD-MS³ spectrum, and formed by the mechanisms described in Figure 3.4, allowed assignment of the molecular lipid structure of this lipid as PE_(O-16:0_18:1). These data indicate that the presence of the alkyl-ether linkage does not significantly alter the fragmentation behavior compared to their diacyl-linked counterparts. As alkyl ether-PS lipids are not commercially available, and were not observed as abundant 'pure' species in crude cellular lipid extracts from SW620 cells, the fragmentation of their DMBNHS derivatized ions was not examined. However, based on the data described above, it is expected that the fragmentation behavior of this sub-class of PS lipid would be similar to that of the DMBNHS derivatized diacyl-PS and alkyl ether-PE species.

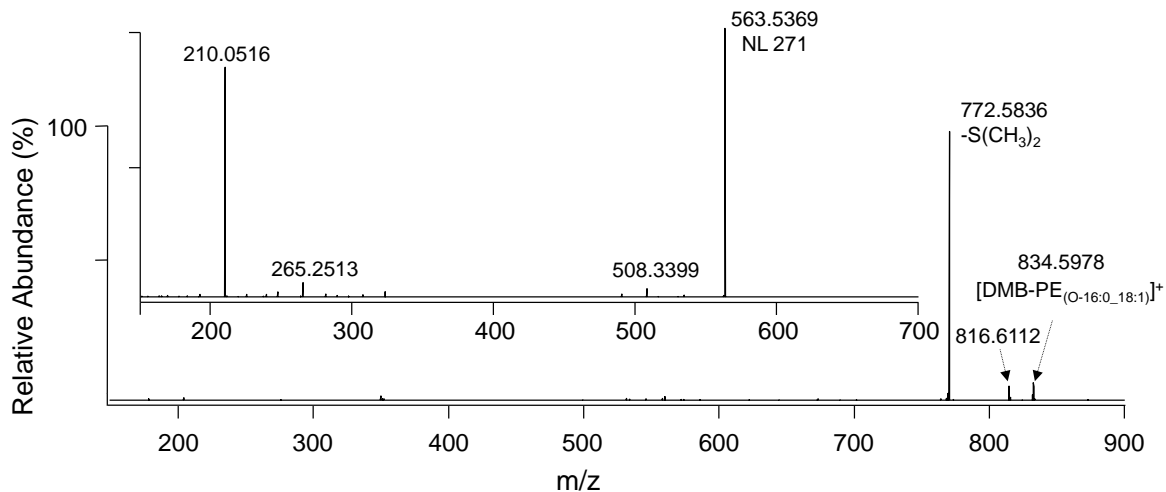


Figure 3.5 CID-MS/MS analysis of a DMBNHS derivatized monoalkyl-ether PE lipid $PE_{(O-16:0_18:1)}$ from a crude lipid extract of SW620 colorectal cancer cells. The inset shows the HCD-MS³ spectrum of the $S(CH_3)_2$ neutral loss (NL) product ion.

3.2.1.3 Plasmalogen-Aminophospholipids

Fhaner *et al.* have previously reported the HCD-MS/MS fragmentation behavior of plasmalogen-PE lipids following sequential DMBNHS derivatization of the amine head group and iodine/methanol derivatization of the plasmalogen *O*-alkenyl-ether double bond [137]. From this prior study, the neutral loss of dimethylsulfide was observed as the primary fragmentation pathway, similar to that described above for the DMBNHS derivatized diacyl- and alkyl ether- PE lipids. In contrast to these lipid subclasses however, this product then underwent further dissociation to yield a dominant product corresponding to neutral loss of a characteristic $\text{RCICH}(\text{OCH}_3)$ alkene (i.e., the derivatized plasmalogen *O*-alkenyl chain), that directly enables assignment of the molecular lipid identity. Albeit lower in abundance relative to the above mentioned fragmentation channel, the initial neutral loss product ion also underwent further dissociation (following the loss of methanol) to yield the PE headgroup specific ion at m/z 210 and its complementary neutral loss product, identical to those described above for the DMBNHS derivatized diacyl- and alkyl ether- PE species.

Systematic examination of the fragmentation behavior of DMBNHS and iodine/methanol derivatized plasmalogen PS lipids could not be performed here as plasmalogen PS lipid standards are not commercially available, and are not observed as abundant 'pure' species in crude cellular lipid extracts from SW620 cells. However, similar fragmentation behavior is expected to that described above for plasmalogen-PE lipids, given that the differences in head group structures do not play a significant role in the observed fragmentation reactions.

3.2.2 Characterization and Quantification of Isobaric Stable Isotope Containing DMBNHS Derivatized Aminophospholipid Standards

Lu *et al.* have previously reported the application of d_6 -‘heavy’ and d_6 -‘light’ DMBNHS reagents as an isobaric stable isotope-labeled derivatization strategy for the enhanced electrospray ionization and simultaneous (multiplexed) quantitative analysis of primary amine-containing phosphopeptides [82]. Here, using sequential amine specific d_6 -heavy/light DMBNHS and plasmalogen O-alkenyl-ether specific iodine/methanol derivatization, and the unique gas phase fragmentation behaviors discussed above, a ‘targeted’ high resolution/accurate mass ESI-MS and -MS/MS method for simultaneous (multiplexed) aminophospholipid quantification at the sum composition or molecular lipid levels [66], and further molecular lipid structural characterization, was developed. This method was first evaluated by derivatization of a diacyl-PE_(14:0/14:0) lipid standard with either d_6 -heavy or d_6 -light DMBNHS reagents, then mixing them together at a 1:1 ratio. Following ESI-MS, isolation of the isobaric mass precursor ions and linear ion trap CID-MS/MS, the exclusive formation of a pair of product ions differing by 6 Da were observed, corresponding to the neutral losses of S(CD₃)₂ and S(CH₃)₂ (m/z 704.4823 and 710.5194) from the ‘heavy’ and ‘light’ labeled lipids (Figure 3.6A). After correction for the isotope purity of the d_6 -heavy/light DMBNHS reagents (99% and 83%, respectively), the intensities of these ‘reporter’ ions can be directly used for sum composition level relative quantification of the concentrations of the lipids between the two samples. A linear dynamic range of quantitation was observed across more than 3 orders of magnitude ($R^2 = 0.99$) for this measurement, by monitoring the intensity ratio’s of the CID-MS/MS S(CD₃)₂ and S(CH₃)₂ neutral loss

reporter ions from d_6 -heavy derivatized $PE_{(14:0/14:0)}$ at concentrations ranging from 0.0025 μM to 5 μM , against 0.5 μM d_6 -light derivatized $PE_{(14:0/14:0)}$ (data not shown). Further structural characterization at the molecular lipid level was then performed by HCD- MS^3 of the heavy and light labeled neutral loss product ions (shown in the inset to Figure 3.6A for the m/z 704.4823 $[M-S(\text{CD}_3)_2]^+$ product ion). Similar to the HCD- MS^3 data in Figure 3.3A and proposed fragmentation mechanisms in Figure 3.2 and 3.4, MS^3 dissociation of this ion resulted in the secondary formation of m/z 210.0508 and the neutral loss of 209 Da (m/z 495.4365), that underwent further dissociation to yield characteristic product ions at m/z 211.2038 and 285.2399, indicative of the presence of the 14:0 acyl chains in this lipid. Albeit not required here as only a single molecular lipid species was present, the abundances of these characteristic molecular structure specific products ions formed by MS^3 of the heavy and light labeled neutral loss product ions may be used to provide quantitative information regarding the relative abundances of any individual molecular lipid species that may be present within a mixture of isobaric mass molecular lipid species. Similar CID- MS/MS and HCD- MS^3 fragmentation behavior was also observed for a 1:1 mixture of diacyl- $PS_{(14:0/14:0)}$ lipid standards derivatized with d_6 -heavy and d_6 -light DMBNHS reagents (data not shown).

Figure 3.6B shows the HCD- MS/MS spectrum acquired from a 1:1 mixture of a d_6 -heavy and d_6 -light DMBNHS and iodine/methanol derivatized plasmalogen lipid, $PE_{(P-18:0/22:6)}$. Abundant pairs of product ions differing by 6 Da were observed in this spectrum, including the DMBNHS derivatization specific 'heavy' and 'light' neutral losses of $S(\text{CD}_3)_2$ and $S(\text{CH}_3)_2$ at m/z 1002.5018 and 1008.5388, along with the subsequent losses of CH_3OH from these ions at m/z 970.4760 and 976.5130, and the

DMBNHS derivatized PE head group specific pair of low m/z 'reporter' ions at 210.0515 and 216.0891. However, via the fragmentation pathways previously reported [137], formation of a pair of isotopically encoded product ions at m/z 594.3157 and m/z 600.3530, via neutral loss of the derivatized plasmalogen *O*-alkenyl chain, directly enabled simultaneous quantification and structural characterization at the molecular lipid level.

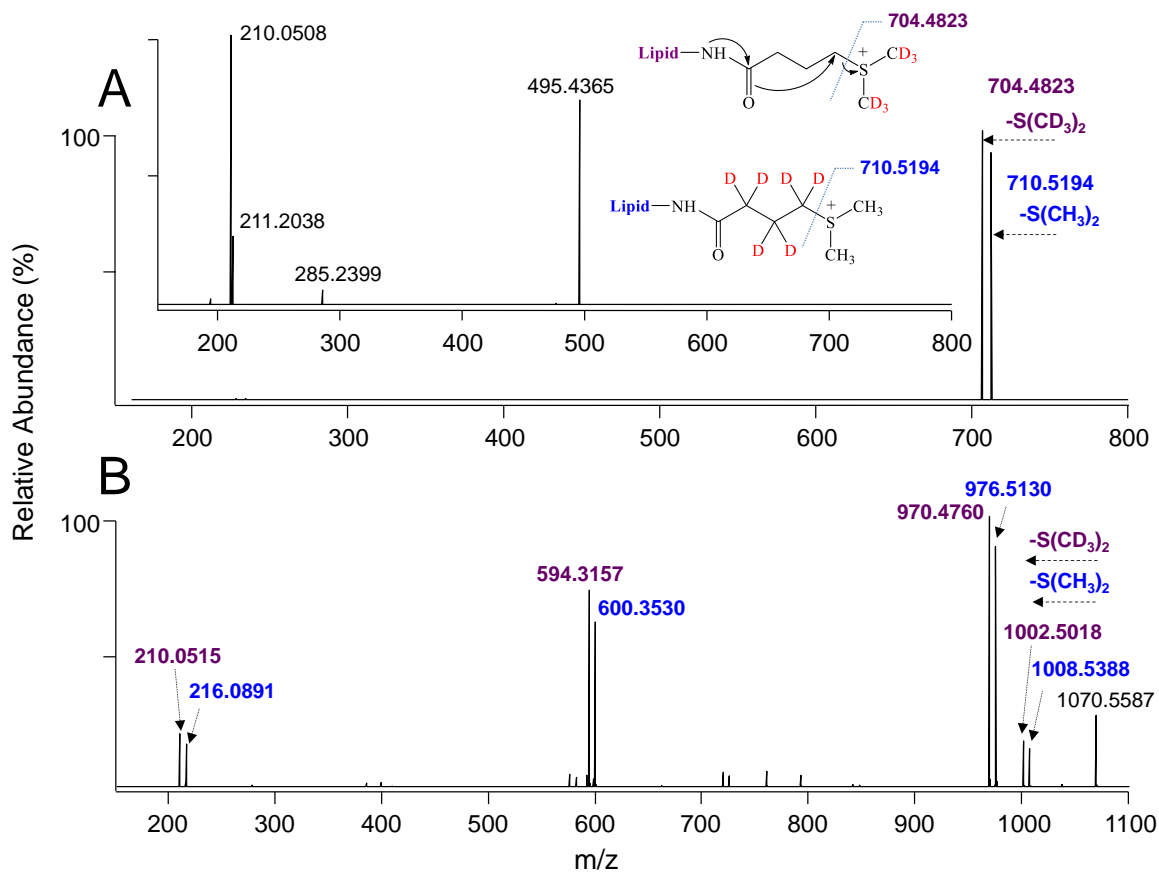


Figure 3.6 CID-MS/MS, HCD-MS³ and HCD-MS/MS of a 1:1 mixture of d₆-heavy/light DMBNHS and iodine/methanol derivatized PE lipids. (A) CID-MS/MS of pooled d₆-heavy/light DMBNHS derivatized PE_(14:0/14:0). The inset shows the HCD-MS³ spectrum of the S(CD₃)₂ neutral loss product ion from the d₆-heavy DMBNHS derivatized lipid as well as the structures and initial fragmentation sites for the d₆-heavy/light DMBNHS derivatized lipid species (B) HCD-MS/MS of pooled d₆-heavy/light DMBNHS and iodine/methanol derivatized PE_(P-18:0/22:6).

3.2.3 Multiplexed Quantification of Selected Aminophospholipid Ion Abundance Changes Between a Metastatic Colorectal Cancer Cell Line, SW620 and its AlkyGlycerone Phosphate Synthase (AGPS) siRNA Knockdown

To demonstrate the ‘proof of principle’ utility of the d_6 -heavy/light DMBNHS and iodine/methanol derivatization strategy coupled with high resolution/accurate mass ESI-MS and ‘targeted’ HCD-MS/MS for multiplexed quantification/characterization of aminophospholipids within complex lipid mixtures, a 1:1 mixture of crude lipid extracts (normalized to protein concentration) from a metastatic colorectal cancer cell line, SW620 and its alkyglycerone phosphate synthase (AGPS) silencing RNA (siRNA) knockdown, was analyzed. AGPS is the rate limiting enzyme involved in the biosynthesis of cellular ether lipids. Phaner *et al.* have previously found that the levels of several ether-containing lipid sub classes (both alkyl-ether and plasmalogens) are significantly enriched in the SW620 cell line compared to its isogenic primary colorectal cancer cell line, SW480 [24]. Thus, siRNA knockdown of these lipids by AGPS is expected to be useful for subsequent functional studies to elucidate the role of ether-lipid metabolism in malignancy and metastatic progression.

Figure 3.7 shows the full scan ESI mass spectrum obtained from the 1:1 crude lipid extract mixture of d_6 -heavy/light DMBNHS and iodine/methanol derivatized SW620 cells and its AGPS knockdown, with insets showing selected expanded m/z regions of the mass spectrum. After database searching of the high resolution/accurate mass values, 125 total PE and PS lipid ions were assigned at the sum composition level. Then, a non-redundant inclusion list of 101 m/z values (multiple PE and PS lipids were observed with the same nominal mass but different exact mass values), was submitted

for HCD-MS/MS. As described above, sum composition level relative quantification was then achieved by manual comparison of the peak intensities of paired neutral loss reporter ions from the HCD-MS/MS spectra, (i.e., the $[M - S(CD_3)_2]^+$ and $[M - S(CH_3)_2]^+$ product ions from the d_6 -heavy/light DMBNHS derivatized lipid ions, after correction for deuterium isotope purities. For the derivatized plasmalogen-aminophospholipids, further detailed structural characterization and quantification at the molecular lipid level was performed by analysis of the paired stable isotope containing O-alkenyl chain specific cleavage product ions observed within the HCD-MS/MS spectra.

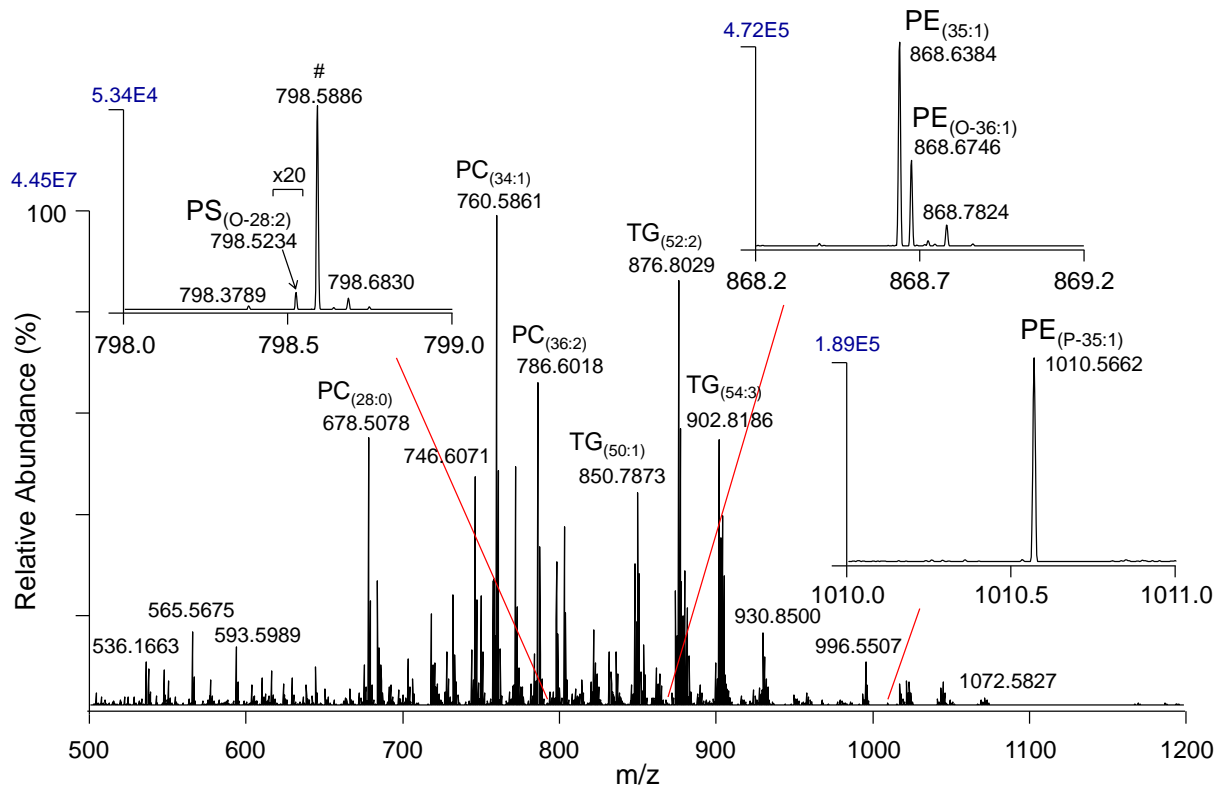


Figure 3.7 Ultra-high resolution/accurate mass ESI-MS of a 1:1 mixture (normalized to protein concentration) of isobaric d_6 -heavy/light DMBNHS and iodine/methanol derivatized crude lipid extracts from a metastatic colorectal cancer cell line, SW620 and its alkylglycerone phosphate synthase (AGPS) siRNA knockdown. The insets show expanded m/z regions containing the lipids $PE_{(35:1)}$ and $PE_{(O-36:1)}$, $PS_{(O-28:2)}$, and $PE_{(P-35:1)}$. The ion labeled with a # corresponds to a diisooctyl phthalate contaminant ion.

An example of the advantages of this approach for the sum composition level quantification of co-isolated and fragmented nominal mass lipids is shown in Figure 3.8, for HCD-MS/MS of the d_6 -heavy/light DMBNHS derivatized diacyl- $PE_{(35:1)}$ and alkyl ether- $PE_{(O-36:1)}$ ($\Delta m/z = 0.0362$ Da) lipids observed at m/z 868.6 in the inset on the top right of Figure 3.7. In this spectrum, the isotopically encoded product ions at m/z 210.0529 and 216.0907 (analogous to the low mass 'reporter ions' observed using TMTs or iTRAQ labeling strategies for multiplexed peptide quantification) are common to both the diacyl- and alkyl ether-linked PE species, so cannot be used for the quantitation of the individual lipid species. However, measurement of the abundances of the $S(CD_3)_2$ and $S(CH_3)_2$ neutral loss product ions (m/z 800.5821 and 806.6191 for the $PE_{(35:1)}$ lipid and m/z 800.6166 and 806.6528 for the $PE_{(O-36:1)}$ lipid in the inset to Figure 3.8) readily overcome this limitation. After correction for the isotope purity of the d_6 -heavy/light DMBNHS reagents, along with secondary correction of interference from any $M+1$ or $M+2$ ion overlap (e.g., where lipid ions having consecutive degree of unsaturation are present at lower m/z values), the intensity ratio between the APGS knockdown and control SW620 cells was found to be 0.56 for the $PE_{(35:1)}$ lipid and 0.28 for the $PE_{(O-36:1)}$ lipid.

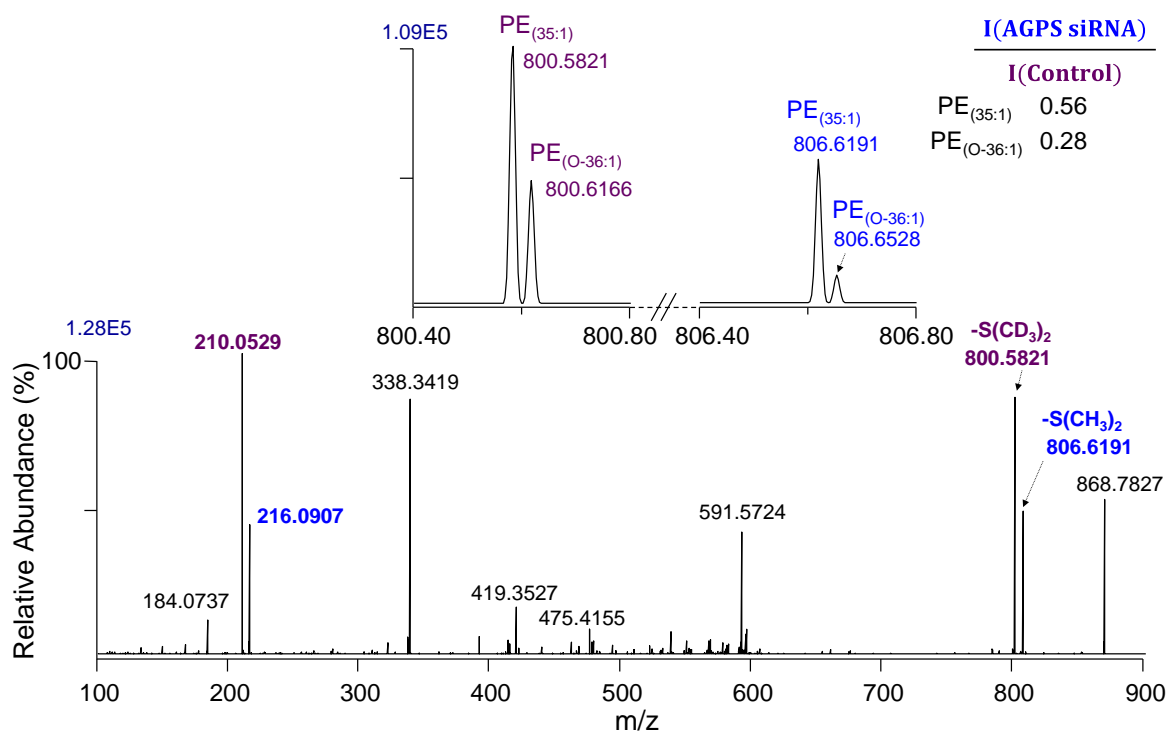


Figure 3.8 HCD-MS/MS of the isobaric d_6 -heavy/light DMBNHS derivatized PE_(35:1) and PE_(O-36:1) lipids from Figure 3.7. The inset shows expanded m/z regions of the spectrum containing the characteristic S(CH₃)₂/S(CD₃)₂ neutral loss product ions.

An example of HCD-MS/MS quantitation of d_6 -heavy/light DMBNHS derivatized alkyl ether-PS lipid (i.e., $PS_{(O-28:2)}$ at m/z 798.5234 in the inset on the left of Figure 3.7) is shown in Figure 3.9. Despite being present at very low abundance, the intensity ratio of the $S(CD_3)_2$ (control) and $S(CH_3)_2$ (knockdown) neutral loss reporter ions was determined with good signal-to-noise as 0.70, after correction for isotopic purity and interferences. In this example, the low mass d_6 -heavy/light DMBNHS derivatized PS specific reporter ions at m/z 254 and 260 were not observed due to the low abundance of the precursor ions. The identity of the other product ions in Figure 3.9 are mostly unknown, but presumably originate from the very abundant co-isolated species present at the same nominal m/z value as the $PS_{(O-28:2)}$ lipid (e.g., m/z 391.2847 corresponds to a monomeric protonated adduct of diisooctyl phthalate formed from the diisooctyl phthalate dimer ammonium adduct precursor ion at m/z 798.5886 in the inset of Figure 3.7). However, these ions clearly do not negatively affect the quantitation based on neutral loss of $S(CD_3)_2$ and $S(CH_3)_2$.

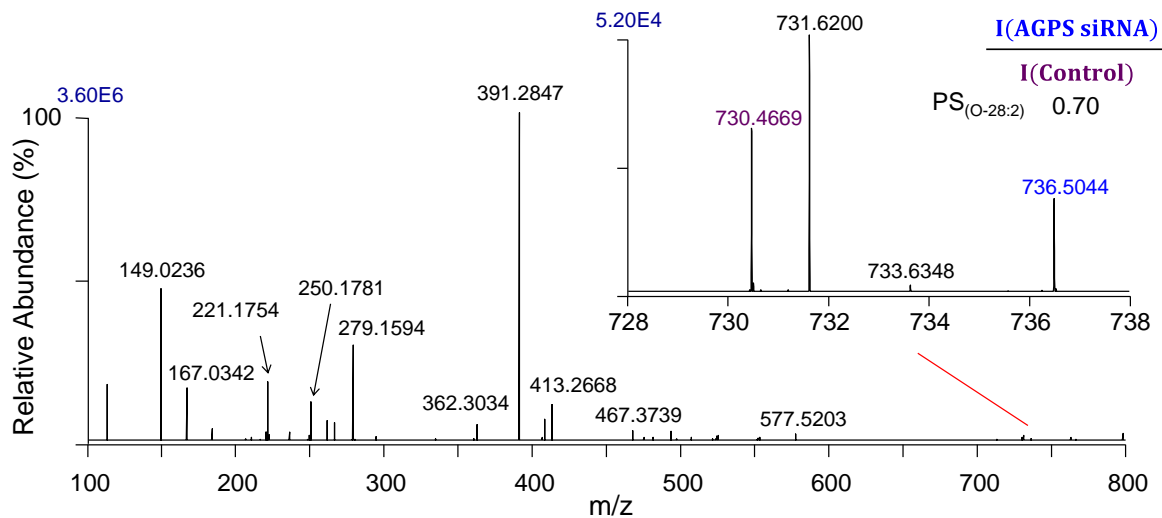


Figure 3.9 HCD-MS/MS of the isobaric d₆-heavy/light DMBNHS derivatized PS_(O-28:2) lipid from Figure 3.7. The inset shows an expanded m/z region of the spectrum containing the characteristic S(CH₃)₂/S(CD₃)₂ neutral loss product ions.

Finally, an example of secondary multiplexed quantification and molecular lipid structural characterization of a mixture of isomeric plasmalogen-PE lipids was demonstrated by HCD-MS/MS of the m/z 1010.5662 ion (i.e., d_6 -heavy/light DMBNHS and iodine/methanol derivatized $PE_{(P-35:1)}$) shown in the inset on the bottom right of Figure 3.7 (see Figure 3.10). Ratiometric measurement of the $-(S(CD_3)_2+CH_3OH)$ and $-(S(CH_3)_2+CH_3OH)$ neutral loss reporter ions at m/z 910.4837 and 916.5211, as well as the low mass reporter ions at m/z 210.0530 and 216.0907, yielded SW620 APGS knockdown/control ratios at the sum composition level for this lipid of 0.49 and 0.53, respectively. However, these ratios do not allow differences in abundance to be separately determined between the knockdown and control SW620 cell samples, for isomeric lipids that may be present (i.e., different combinations of acyl/O-alkenyl chain lengths) within the sum composition of $PE_{(P-35:1)}$ lipid. However, as described above in Figure 3.6B, HCD-MS/MS of d_6 -heavy/light DMBNHS and iodine/methanol derivatized plasmalogen lipids yields pairs of isotopically encoded product ions via neutral loss of the derivatized plasmalogen O-alkenyl chains, directly enabling simultaneous quantification and structural characterization at the molecular lipid level. In the inset to Figure 3.10, four pairs of these characteristic product ions were observed, corresponding to the presence of $PE_{(P-19:0_{16}:1)}$, $PE_{(P-18:0_{17}:1)}$, $PE_{(P-17:0_{18}:1)}$ and $PE_{(P-16:0_{19}:1)}$ lipids. Three of these odd-numbered carbon chain length containing molecular plasmalogen-PE lipid species have been identified previously from an underivatized lipid extract of SW620 cells, by HCD-MS/MS in negative ion mode [14]. After corrections, the intensity ratios between the siRNA knockdown and control samples for these molecular lipid species was determined to be 0.34, 0.34, 0.51 and 0.39. These different

ratios suggested that silencing of the RNA responsible for expression of AGPS may affect plasmalogen-PE lipids to a different extent depending on the identities of their acyl/alkenyl chains.

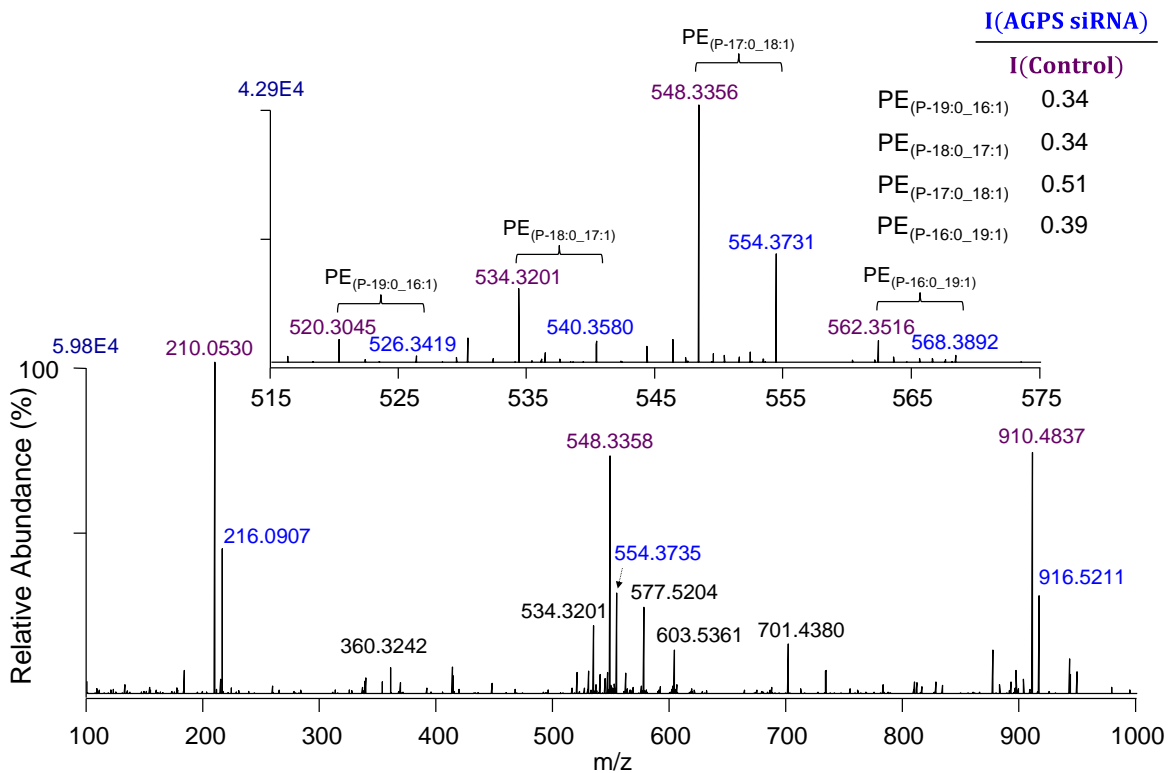


Figure 3.10 HCD-MS/MS of the isobaric d_6 -heavy/light DMBNHS and iodine/methanol derivatized PE_(P-35:1) lipid from Figure 3.7. The inset shows an expanded m/z region of the spectrum containing the characteristic O-alkenyl-chain neutral loss product ions.

3.3 Conclusions

The gas phase fragmentation behavior of DMBNHS derivatized diacyl- and alkyl ether-PE and -PS aminophospholipids, as well as sequential isotope-labeled DMBNHS and iodine/methanol derivatized plasmalogen-PE aminophospholipids, have been studied using linear ion trap CID-MS/MS and -MS³, HCD-MS/MS and CID-MS/MS with HCD-MS³. Importantly, the multiplexed quantification of derivatized PE and PS lipids within complex biological mixtures using d₆-heavy and d₆-light DMBNHS isobaric mass stable isotope labeling, and high resolution/accurate mass ESI-MS and targeted HCD-MS/MS, eliminates the possibility of interference from co-isolated and fragmented precursor ions with the same nominal mass values, that is inherent to quantification methods based on detection using low m/z reporter ions. With the additional benefits of obtaining molecular lipid level quantification and structural characterization of plasmalogen aminophospholipids from the MS/MS spectra, or by MS³ of the initial neutral loss product ions for diacyl- and alkyl ether-linked PE and PS lipids, this method is expected to be an effective lipidomics workflow for the comprehensive quantitative analysis of aminophospholipids within crude biological lipid extracts.

CHAPTER FOUR

Experimental Methods for Chapters Two and Three

4.1 Materials

Methanol (CH₃OH), chloroform (CHCl₃) and ACS grade isopropyl alcohol (IPA) were purchased from Macron Chemicals (Center Valley, PA). 99% formic acid (FA) was from Spectrum Scientific (Irvine, CA). 3,5-diiodoaniline (diIA), 2,4-diIA and 3,4-diIA were purchased from Spectra Group Limited, Inc. (Millbury, OH). 3-iodoaniline (IA) was purchased from Santa Cruz Biotechnology, Inc. (Dallas, TX). Aniline and Pd(OH)₂ on carbon (20 wt. %) were from Sigma-Aldrich (St. Louis, MO). Synthetic lipid standards were from Avanti Polar Lipids, Inc. (Alabaster, AL). Iodine, N,N-dimethylformamide (DMF) and triethylamine (TEA) were from Jade Scientific (Westland, MI). Acetonitrile (CH₃CN) was purchased from EMD Chemicals (San Diego, CA). Ammonium formate was obtained from Alfa Aesar (Ward Hill, MA). Ammonium bicarbonate was from J.T. Baker (Phillipsburg, NJ). SW620 colorectal cancer cells were purchased from the American Type Culture Collection (ATCC) (Manassas, VA). siGENOME SMARTpool siRNA was obtained from Thermo Fisher Scientific (Waltham, MA).

4.2 siRNA Knockdown of Alkyglycerone Phosphate Synthase (AGPS) in SW620

Colorectal Cancer Cells and Lipid Extraction

Alkyglycerone phosphate synthase (AGPS) knockdown of SW620 colorectal cancer cells and followed lipid extraction were performed by Cassie J. Fhaner in Reid Lab at Michigan State University (East Lansing, MI). Electroporation with an Amaxa Nucleofector II Device (Lonza, Basel, Switzerland) and siGENOME SMARTpool siRNA were employed for the knockdown experiments. Control siGENOME SMART-pool

siRNA was used for control experiments. Transfected cells were seeded in 6-well plates (5×10^5 cells / well) and cultured with RPMI 1640 growth medium with 10% FBS and 1% penicillin/streptomycin, for four days. Cells were harvested by scraping and then immediately extracted using a monophasic lipid extraction protocol as previously described [238].

4.3 Derivatization of Lipid Standards and Crude Lipid Extracts

4.3.1 Synthesis of Saturated TG Lipids from Unsaturated TG Lipid Standards

Pd(OH)₂ on carbon (1 mg) was added to 500 μ L of a 1 mM solution of mono-unsaturated TG_(14:0/16:1/14:0) in 4 : 2 : 1 (v/v/v) IPA/CH₃OH/CHCl₃ and the mixture was stirred for 24 hours under H₂ at room temperature. After filtration, a solution of saturated TG_(14:0/16:0/14:0) was obtained. The purity of the resultant saturated TG_(14:0/16:0/14:0) was determined as 99% by MS analysis of its ammonium adduct ion.

4.3.2 Photo-Induced Solution Phase Cross-linking of TG Lipid Standards

Sample solution containing 5 mM TG lipids, 5 mM 3,5-diiodoaniline and 10% formic acid in 4 : 2 : 1 (v/v/v) IPA/CH₃OH/CHCl₃ were prepared and then irradiated in a short NMR tube (inner diameter = 4 mm) using a flash-lamp pumped Nd:YAG laser (Continuum, Santa Clara, CA) with a beam diameter of 3 mm, UV photons of 266 nm, a frequency of 15 Hz and a pulse energy of 7 mJ. After reacting for 9 min, 5 μ L of sample solution was diluted 200 fold in 4 : 2 : 1 (v/v/v) IPA/CH₃OH/CHCl₃ for mass spectrometric analysis as described in Chapter 4, section 4.4.3 without photo-activation.

4.3.3 Derivatization of Aminophospholipids Using d₆-Heavy/light DMBNHS and Iodine/Methanol Methods

S,S'-Dimethylthiobutanoylhydroxysuccinimide ester iodide (DMBNHS) and isobaric mass stable isotope containing d₆-'heavy' and d₆-'light' DMBNHS reagents were synthesized as previously described [82]. The deuterium isotope purities of the d₆-heavy/light DMBNHS reagents were determined to be 99% and 83%, respectively. For characterization of gas phase CID- or HCD-MS/MS and -MSⁿ fragmentation behaviors, the standard aminophospholipids PE_(14:0/14:0), PE_(18:0/18:0), PE_(18:0/18:1), PE_(18:1/18:1), PE_(18:1/20:4), PE_(22:6/22:6), PS_(14:0/14:0) and PS_(18:0/18:1) were derivatized with DMBNHS as previously described [24, 127, 137, 138]. DMBNHS derivatized monoalkyl-ether PE_(O-16:0/18:1) lipid was obtained from a crude lipid extract of the control SW620 colorectal cancer cells. For characterization of CID-MS/MS, HCD-MS³ and HCD-MS/MS quantitation performance, mixtures of standard lipids PE_(14:0/14:0), PS_(14:0/14:0) and PE_(P-18:0/22:6) were derivatized separately with d₆-heavy and d₆-light DMBNHS, followed by further derivatization of the plasmalogen lipid with iodine/methanol as previously described [137], then combined at a 1:1 ratio. For determination of the linear dynamic range of lipid quantification, DMBNHS derivatized PE_(14:0/14:0) (0.0005 μM to 5 μM) was mixed with 0.5 μM d₆-light DMBNHS derivatized PE_(14:0/14:0). Aminophospholipids within the crude lipid extracts from control and AGPS siRNA knockdown experiments were derivatized separately with d₆-heavy and d₆-light DMBNHS reagents, respectively, followed by derivatization of plasmalogen lipids with iodine/methanol, as previously described. Samples were then combined in a 1:1 ratio based on their normalized protein

concentrations. All samples were resuspended in 4 : 2 : 1 (v/v/v) IPA/CH₃OH/CHCl₃ containing 20 mM ammonium formate immediately prior to mass spectrometry analysis.

4.4 Mass Spectrometry

4.4.1 Photo-Induced Gas Phase Cross-linking MS/MS and CID-MSⁿ Structural Analysis of TG Dimer Complex Ions

Solutions of 100 μM of each TG lipid, 100 μM diiodoaniline in 4:2:1 (v:v:v) IPA/CH₃OH/CHCl₃ containing 0.1% formic acid were prepared then loaded into individual wells of a Whatman multichem 96-well plate (Sigma Aldrich, St. Louis, MO) and sealed with Teflon Ultra Thin Sealing Tape (Analytical Sales and Services, Prompton Plains, NJ). The samples were then introduced into an Thermo Scientific LTQ linear ion trap mass spectrometer (San Jose, CA) using an Advion Triversa Nanomate nano-electrospray ionization (nESI) source (Advion Ithaca, NY) with a spray voltage of 1.4 kV and a gas pressure of 0.3 psi. For MS/MS experiments, an isolation window of 30 m/z was used to provide sufficient signal for isolation of the non-covalent protonated diiodoaniline-TG dimer complex ions. For UVPD-MS/MS, the mass spectrometer was modified to enable usage of a flash-lamp pumped Nd:YAG laser (Continuum, Santa Clara, CA) with a beam diameter of 3 mm, UV photons of 266 nm, a frequency of 15 Hz and a pulse energy of 7 mJ. Laser pulses were introduced into the ion trap through a quartz window installed on the back plate of the mass spectrometer. Synchronization between the laser pulses and the beginning of the activation step of a typical MSⁿ experiment was achieved by feeding an amplified transistor-transistor logic (TTL) trigger signal from the mass spectrometer (± 3.2 V) to the laser (± 5.0 V) via a pulse/function generator (Hewlett-Packard, Palo Alto, CA). The laser was triggered from the Diagnostic

menu within the Tune Plus window of the Xcalibur software (Thermo Fisher Scientific, San Jose, CA). CID-MS³, -MS⁴ and -MS⁵ were performed to analyze the products from the UVPD-MS/MS experiments. Automated Gain Control (AGC) target numbers were optimized to maximize the signal to noise ratio of the spectra without lowering the resolution. Both electron multiplier voltages were set at -1350 V. Spectra shown are the average of at least 100 scans.

4.4.2 ESI-MS, -MS/MS and -MS³ Analysis of Derivatized Aminophospholipid Standards

Derivatized standard lipid samples were introduced for mass spectrometry analysis via the Advion Triversa Nanomate nESI source operating under the same conditions as described in Chapter 4, section 4.4.1. Samples were analyzed in positive ionization mode using a Thermo Scientific LTQ Orbitrap Velos mass spectrometer equipped with a linear ion trap and a HCD multipole collision cell (San Jose, CA). The inlet temperature, S-lens values and mass resolving power were set at 100 °C, 50 % and 100,000, respectively. Linear ion trap CID-MS/MS spectra were acquired using an isolation window of m/z 3, a q -value of 0.17 and an activation time of 10 ms, while HCD-MS³ spectra were collected with activation times of 0.1 ms and a low mass cut off of m/z 150. The HCD normalized collision energy (NCE) was optimized for each product ion of interest.

4.4.3 ESI-MS and -MS/MS Analysis of Derivatized Crude Lipid Extracts from Combined Control and AGPS siRNA Knockdown of the SW620 Colorectal Cancer Cells

Derivatized crude lipid extracts from the combined control and AGPS siRNA knockdown SW620 colorectal cancer cells were introduced into a Thermo Scientific Q Exactive High Field Orbitrap mass spectrometer equipped with a HCD cell, using the Advion Triversa Nanomate nESI source operating under the same conditions as described in Chapter 4, section 4.4.1. The inlet temperature, S-lens value and mass resolving power were set at 200 °C, 55 % and 240,000 (for MS scans) and 120,000 (for HCD-MS/MS scans), respectively. For MS scans, a maximum injection time of 50 ms and an AGC target of 1×10^6 was used. For HCD-MS/MS scans, an isolation window of m/z 1, a maximum injection time of 1000 ms, an AGC target of 1×10^5 and a HCD NCE of 15% were employed. Throughout this dissertation, the shorthand notation used for lipid classification and structural representation is that proposed by Liebisch *et al.* as an extension of the accepted International Lipid Classification and Nomenclature Committee nomenclature [242]. Initial assignment of derivatized PE and PS lipid ions, at the sum composition level (i.e., identity of the head group and fatty acyl/alkyl/alkenyl linkages, and the total carbon-carbon double bonds), was achieved from the ESI-MS accurate mass data by searching against a user-defined database of lipid species using the Lipid Mass Spectrum Analysis (LIMSA v.1.0) software [243], with automated peak finding and correction of ^{13}C isotope effects, as previously described [138]. Then, a non-redundant inclusion list of 101 m/z values (from 125 total PE and PS lipids) was submitted for HCD-MS/MS. 6 scans were acquired for each m/z value in the inclusion

list, with a total acquisition time of 8.5 minutes. Quantification at sum composition levels was achieved from the HCD-MS/MS spectra by manual comparison of the peak intensities of paired neutral loss reporter ions, (i.e., $[M - S(CD_3)_2]^+$ and $[M - S(CH_3)_2]^+$) from the d_6 -heavy/light DMBNHS derivatized lipid ions, after correction for deuterium isotope purities. For the derivatized plasmalogen-aminophospholipids, further detailed structural characterization and secondary quantification at the molecular lipid level was performed by analysis of the paired stable isotope containing characteristic product ions observed within the HCD-MS/MS spectra.

CHAPTER FIVE

Quantitative Immuno LC-MS/MS of Parathyroid Hormone and Its *In Vivo* Heterogeneous Post-Translational Protein Modifications: Oxidation and Truncation

5.1 Introduction

Parathyroid hormone is a protein produced in parathyroid glands and consists of 84 amino acids (PTH 1-84) in its full length active form [244]. The full length PTH 1-84 plays a critical role in the regulation of circulating calcium in plasma whose changing concentration is closely related to many physiological and pathological processes, including cell signaling, bone metabolism and reduction of the glomerular filtration rate [245, 246]. In response to decreased concentration of circulating calcium, more PTH is secreted into the circulatory system to stimulate the calcium reabsorption in kidney and calcium resorption from bones into blood [247]. Excessive secretion of PTH can result from abnormalities in the regulation system, which was defined as hyperparathyroidism [246].

Studies have reported that PTH 1-84 can be post-translationally modified to various truncated PTH variants through metabolic processes. A summary of previously reported fragments of PTH is presented in Figure 5.1A [248-250]. In fact, the major forms of the circulating PTH in human plasma are the amino (N)-terminally truncated fragments of full length PTH 1-84 (e.g., PTH 7-84) [248]. However, these fragments have no biologically active N-terminal residues to interact with type 1 PTH/PTH related protein (PTHrP) receptor and therefore do not regulate calcium levels in the same way as intact PTH 1-84 [251, 252]. Recent data have suggested that N-terminally truncated

PTH may have biological functions opposite to that of PTH 1-84 through interaction with a not yet cloned receptor [248, 253]. Other truncated forms including mid-molecular fragments having neither the N- or carboxyl (C)-terminal of PTH 1-84 have also been reported [249].

Two methionine (M) residues at positions 8 and 18 of PTH 1-84 are possible sites of oxidation when subjected to oxidative stress [254]. It has been reported that methionine oxidation of PTH 1-84 results in greatly reduced potency in stimulating the production of cyclic adenosine monophosphate (cAMP) through interaction with type 1 PTH/PTHrP receptor [255, 256]. Interestingly, a recent study in patients with late-stage renal disease and on dialysis reported that only 7%-34% of PTH in patient plasmas was free of oxidation [257]. In patients with renal impairment and parathyroid cancer, phosphorylation of serine (S) at residue 17 of PTH 1-84 was also identified and quantified with a large concentration range of 32-767 pg/mL [247].

Accurate quantification of the biologically active forms of PTH is a prerequisite to the successful diagnosis and appropriate treatment of hyperparathyroidism. Several generations of immunoassays have been developed for the measurement of PTH 1-84 in serum or plasma samples [258]. Current generation PTH assays use a 'sandwich type' antibody pair targeting at the C- and N-terminal of PTH 1-84 for capture and detection, respectively [259, 260]. However, due to the micro-heterogeneity within the PTH proteins (e.g., the structural similarity between PTH 1-84, 7-84 and their oxidized variants) and the cross reactivity of immunoassays, accurate measurement of PTH 1-84 is still problematic [257, 261, 262].

An alternate PTH assay or analysis strategy combining immuno-affinity enrichment with liquid chromatography-tandem mass spectrometry (LC-MS/MS) has been recently introduced as a possible reference level method to accurately quantify the full length PTH 1-84 and its post-translationally modified forms [247]. Generally, PTH proteins are first enriched using antibody, then digested and finally analyzed by LC-MS/MS. The method developed by Kumar *et al.* employed a ^{15}N -labeled PTH 1-84 as internal standard before digestion to correct errors from sample loss and targeted the PTH 1-13 peptide as a surrogate for full length PTH 1-84 while Lopez *et al.* spiked isotope-labeled PTH 1-13, 7-13 as well as 34-44 internal standards in processed patient samples before LC-MS/MS analysis, for quantitative analysis of both full length PTH 1-84 and truncated PTH 7-84 and 34-84 [249, 263]. A method for more comprehensive quantitative analysis of circulating PTH including full length, truncated and oxidized forms was previously developed in the Reid lab at Michigan State University [264]. The oxidation profile of PTH 1-84 and 7-84 during H_2O_2 oxidation was studied first to investigate the major oxidized variants of PTH that should be targeted for quantitative analysis. HPLC purification and 'top-down' mass spectrometric analysis of the oxidized products of PTH showed that PTH 1-84 and 7-84 with methionine sulfoxide at residue 8 and/or 18 were the major products. Therefore, a dual-internal standard approach employing ^{15}N -labeled PTH 1-84 and 7-84 as well as $^{13}\text{C}_6^{15}\text{N}_1$ -labeled lysine-containing PTH 1-13, 7-13 and 14-20 with methionine sulfoxide at residue 8 or 18 was applied to quantify PTH 1-84, 7-84 and their oxidized variants. The linear dynamic range was 5-2000 pg/mL and no significant biases in relative recovery yield among different oxidized variants of PTH 1-84 or 7-84 was observed. The recovery yield of the developed

immuno LC-MS/MS method was 66%. Interestingly, after analysis of three sets of patient samples processed separately, the methionine oxidation percentage of PTH was significantly higher (up to 80%) in most of the patient samples stored at -80 °C for more than a week compared to a different set of samples stored at the same condition for at most two days as shown in Figure 5.2. The dramatic difference related to sample handling suggested the high possibility of *ex vivo* oxidation. However, no further experiments were performed to quantitatively evaluate and correct the possible storage condition-related *ex vivo* oxidation in that study. Considering the not fully understood biological activities and possible clinical significance of post-translationally modified PTH, a method capable of identifying and accurately quantifying full length, truncated and oxidized PTH as well as differentiating *in vivo* and *ex vivo* oxidation should be the aim of assay development. In fact, clinical studies have suggested that ratio of PTH 1-84 over PTH 7-84 may be used to differentiate hyperparathyroid bone turnover and adynamic bone disease [260, 265, 266]. In this chapter, based on the preliminary method developed in the Reid lab at Michigan State University, an quantitative immuno LC-MS/MS method with optimized sample preparation procedures, high resolution/accurate mass HCD-MS/MS and near full sequence coverage was developed and applied to accurately quantify intact PTH 1-84, truncated PTH 7-84 and their oxidized variants after correction of possible *ex vivo* oxidation and truncation.

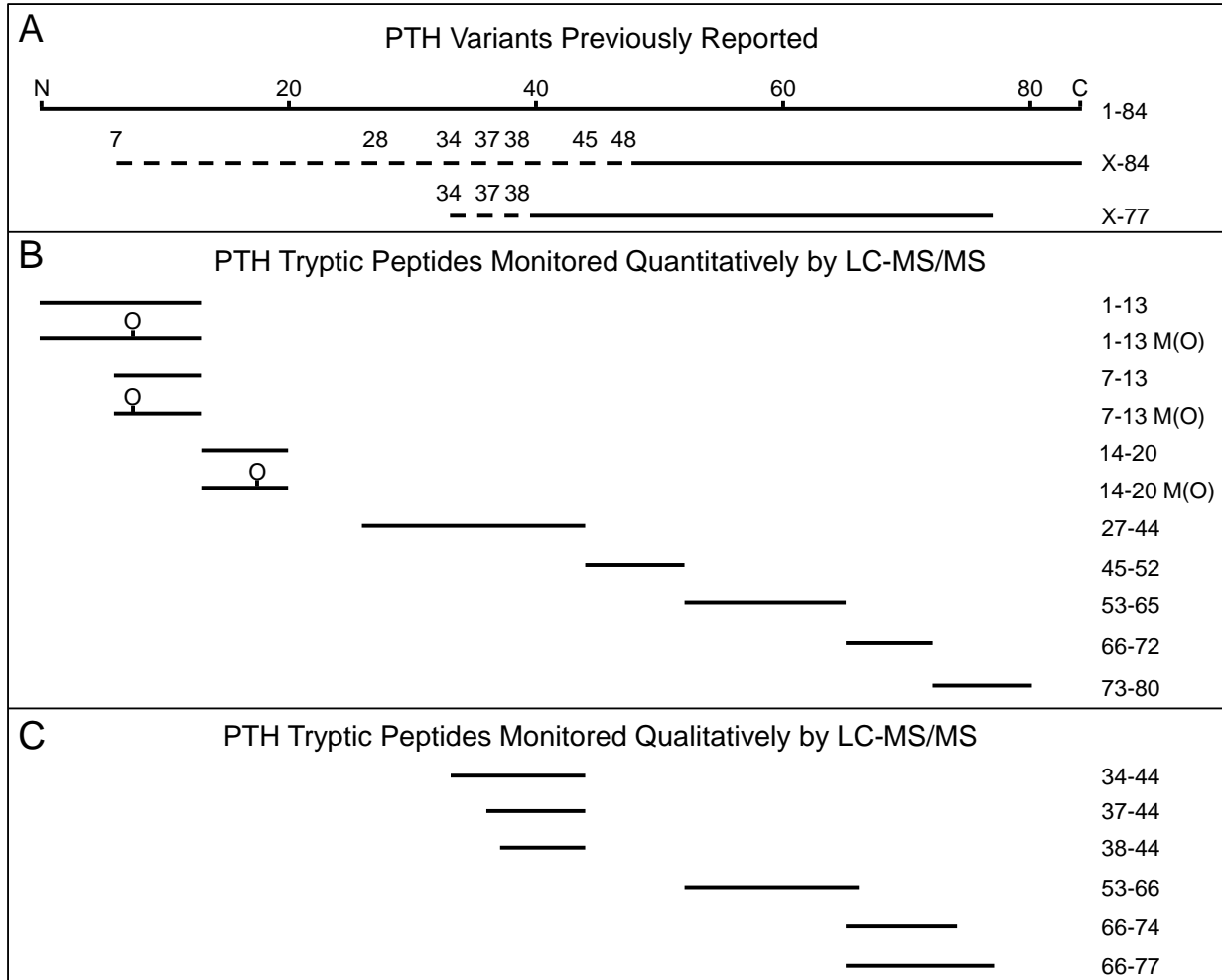


Figure 5.1 Summary of (A) previously identified full length PTH 1-84, N-terminally truncated PTH X-84 (X=7, 28, 34, 37, 38, 45 and 48) and mid-molecular fragment PTH X-77 (X= 34, 37 and 38) [248-250]; (B) full length, oxidized and truncated PTH protein-unique tryptic peptides monitored quantitatively during LC-MS/MS in this study; (C) truncated PTH protein-unique tryptic peptides monitored qualitatively during LC-MS/MS in this study. The dashed lines represent the variable lengths of truncated forms of PTH.

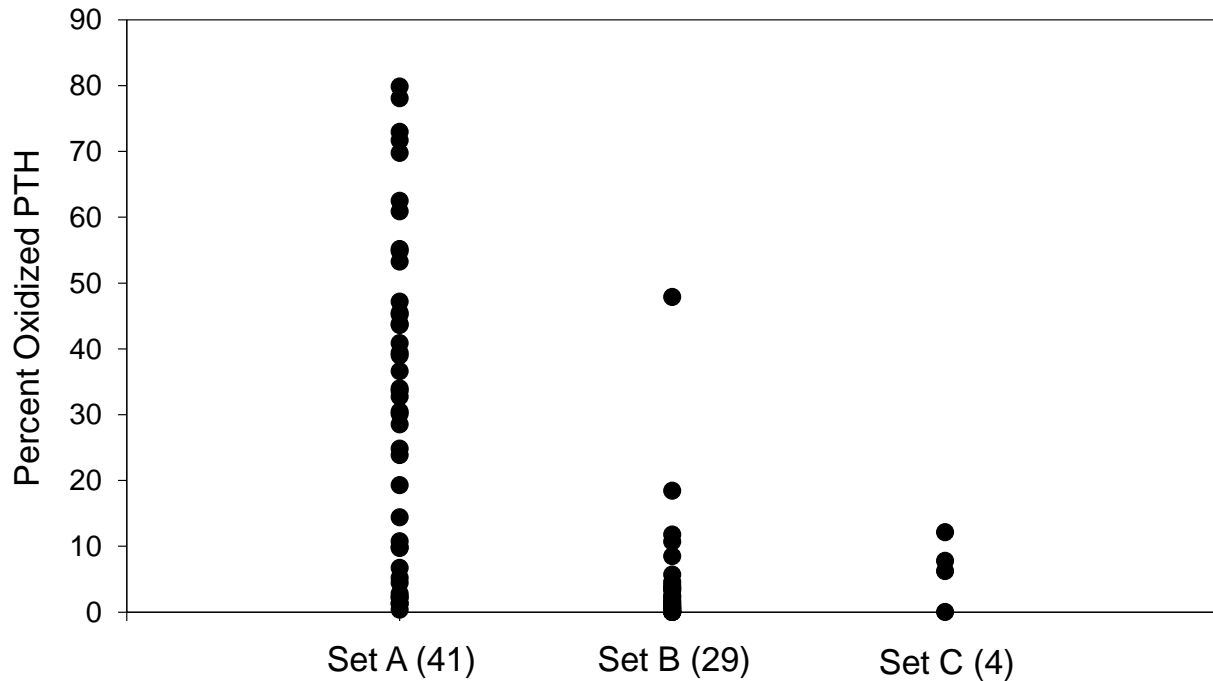


Figure 5.2 Oxidation percentages of PTH in different sets of patient samples [264]. The percentage of oxidation was calculated by taking the sum concentration of PTH 1-13 M(O), PTH 7-13 M(O) and PTH 14-20 M(O) divided by the sum concentration of all full length, truncated and oxidized tryptic peptides quantified. There were 41 blood samples in set A collected from site 1 and stored at least a week before sample analysis, and 29 samples in set B and 4 samples in set C collected from site 2 and stored at most 2 days before sample analysis.

5.2 Results and Discussion

5.2.1 Quantitative Immuno LC-MS/MS Workflow with Optimized Sample Preparation, High Resolution/Accurate Mass HCD-MS/MS and Near Full Sequence Coverage

A brief summary of the designed workflow for quantitative immuno LC-MS/MS analysis of PTH 1-84, 7-84 and their oxidized variants is presented in Figure 5.3. ^{15}N -labeled PTH 1-84 and 7-84 protein internal standards were spiked in patient plasma immediately after blood draw and centrifugation for quantitative analysis of PTH 1-84 and 7-84 as well as correction of possible *ex vivo* oxidation and truncation and sample loss. Also, all patient plasma samples were stored at $-80\text{ }^{\circ}\text{C}$ at most 2 days before analysis to further minimize the possibility of *ex vivo* modification. Then, a C-terminal antibody (against PTH 39-84) conjugated on paramagnetic particles (pmp) was selected to unbiasedly enrich all targeted analytes. After immuno-affinity enrichment and elution, tryptic digestion was performed to convert PTH proteins into peptides toward which LC-MS/MS analysis has higher sensitivity [247]. In Figure 5.1B, tryptic peptides providing near full sequence coverage of PTH 1-84, 7-84 and their oxidized variants as candidate monitored peptides quantitatively representing various forms of PTH proteins in this study are listed. Tryptic peptides representing other truncated PTH proteins with previously reported truncation sites at residue 34, 37, 38 and 77 as well as new truncation sites discovered in this study at residue 66 and 74 were also monitored qualitatively and listed in Figure 5.1C [249, 250]. Sequences of PTH tryptic peptides which are not unique to PTH 1-84 or 7-84 in human proteome were excluded. For quantification of oxidized PTH peptides, $^{13}\text{C}_6^{15}\text{N}_1\text{Leu}$ -labeled PTH 1-13 M(O), 7-13 M(O)

and 14-20 M(O) were added to samples following tryptic digestion. Finally, LC coupled with high resolution/accurate mass MS and HCD-MS/MS experiments were performed to identify and quantify the targeted PTH peptides. HCD-MS/MS transitions (Table 5.1) for targeted peptides were selected for optimal sensitivity based on HCD-MS/MS spectra of ^{15}N -labeled PTH peptides and $^{13}\text{C}_6^{15}\text{N}_1\text{Leu}$ -labeled oxidized PTH peptides with optimized charge states of precursor ions and HCD normalized collision energy (NCE) as shown in Figure 5.4. ^{15}N -labeled PTH 1-13 and $^{13}\text{C}_6^{15}\text{N}_1\text{Leu}$ -labeled PTH 1-13 M(O) gave only one dominant fragment ion (Figure 5.4A and B) while other isotope-labeled PTH 7-13, 7-13 M(O), 14-20 and 14-20 M(O) provided at least two major product ions (Figure 5.4C-F) for validation of the quantitative results based on intensities of multiple fragment ions from the same peptide.

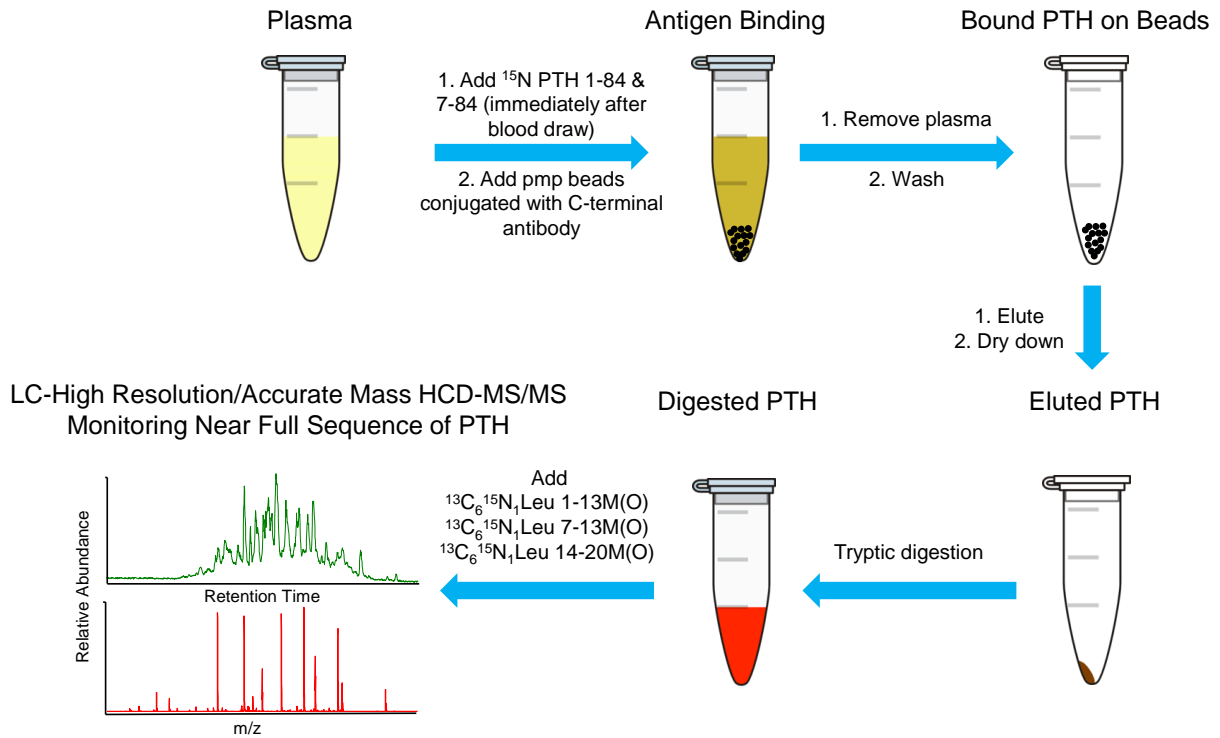


Figure 5.3 Quantitative immuno LC-MS/MS workflow with optimized sample preparation, high resolution/accurate mass HCD-MS/MS and near full sequence coverage. Pmp indicates paramagnetic particles.

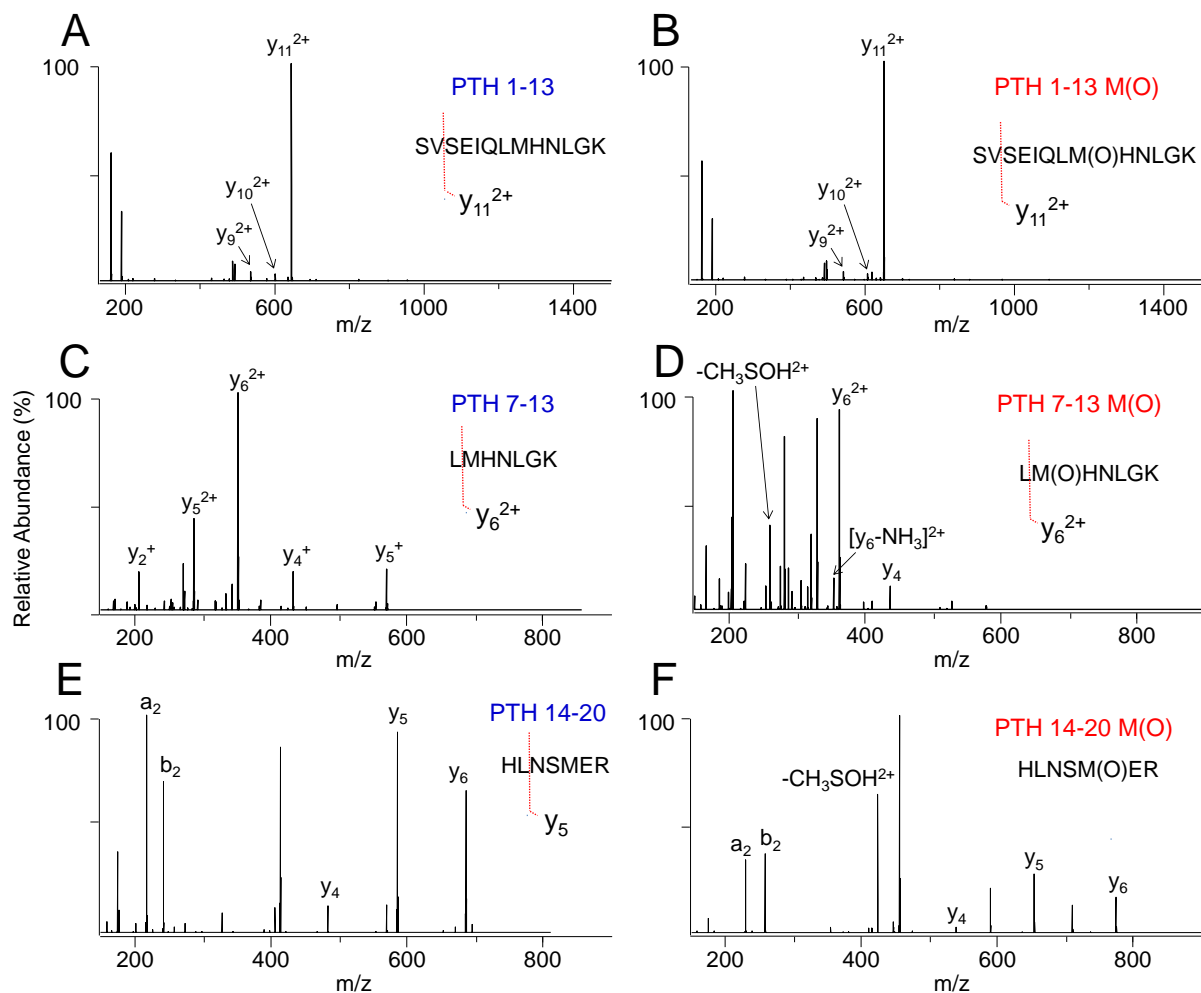


Figure 5.4 HCD-MS/MS spectra of (A) ^{15}N -labeled PTH 1-13 ($z = +3$); (B) $^{13}\text{C}_6^{15}\text{N}_1\text{Leu}$ -labeled PTH 1-13 M(O) ($z = +3$); (C) ^{15}N -labeled PTH 7-13 ($z = +3$); (D) $^{13}\text{C}_6^{15}\text{N}_1\text{Leu}$ -labeled PTH 7-13 M(O) ($z = +3$); (E) ^{15}N -labeled PTH 14-20 ($z = +2$); (F) $^{13}\text{C}_6^{15}\text{N}_1\text{Leu}$ -labeled PTH 14-20 M(O) ($z = +2$) with optimized charge states of precursor ions and HCD normalized collision energy (NCE) for sensitivity.

PTH Peptide Precursor Ion	PTH Peptide Sequence	Inclusion List Window (Retention Time)	Precursor Ion m/z			Optimized HCD NCE (%)	Monitored Most Abundant MS/MS Fragment Ion m/z		
			Native	¹⁵ N	¹³ C ₆ ¹⁵ N ₁ Leu		Native	¹⁵ N	¹³ C ₆ ¹⁵ N ₁ Leu
PTH 1-13 [M+3H] ³⁺	SVSEIQLMHNLGK	(12.0-13.0min) 12.5 min	485.9260	491.9080	NA	16	y ₁₁ ²⁺ 635.3346	y ₁₁ ²⁺ 643.3106	NA
PTH 1-13M(O) [M+3H] ³⁺	SVSEIQLM(O)HNLGK	(10.4-11.4min) 10.9 min	491.2576	497.2396	493.5968	16	y ₁₁ ²⁺ 643.3320	y ₁₁ ²⁺ 651.3080	y ₁₁ ²⁺ 646.8404
PTH 7-13 [M+3H] ³⁺	LMHNLGK	(8.0-9.0min) 8.5 min	271.4868	275.1424	NA	15	y ₆ ²⁺ 350.1840	y ₆ ²⁺ 355.1690	NA
PTH 7-13M(O) [M+3H] ³⁺	LM(O)HNLGK	(7.0-8.1min) 7.5 min	276.8184	280.4741	279.1575	20	y ₆ ²⁺ 358.1814	y ₆ ²⁺ 363.1664	y ₆ ²⁺ 358.1814
PTH 14-20 [M+2H] ²⁺	HLNSMER	(7.0-8.1min) 7.6 min	443.7139	450.1944	NA	27	y ₅ ⁺ 636.2770	y ₅ ⁺ 645.2500	NA
PTH 14-20M(O) [M+2H] ²⁺	HLNSM(O)ER	(6.0-7.0min) 6.5 min	451.7114	458.1919	455.2201	24	-CH ₃ SOH ²⁺ 419.7119	-CH ₃ SOH ²⁺ 426.1924	-CH ₃ SOH ²⁺ 423.2203
PTH 27-44 [M+4H] ⁴⁺	KLQDVHNFVALGAPL APR	(14.1-17.0min) 15.5min	487.2797	493.7602	NA	11	b ₁₃ ²⁺ 697.3830	b ₁₃ ²⁺ 706.3560	NA
PTH 45-52 [M+3H] ³⁺	DAGSQRPR	(4.0-11.5min) 5.5min	296.1545	301.1395	NA	10	y ₆ ²⁺ 350.6961	y ₆ ²⁺ 357.1766	NA
PTH 53-65 [M+4H] ⁴⁺	KKEDNVLVESHEK	(4.0-11.5min) 10.2min	389.4585	394.1942	NA	23	y ₅ ⁺ 629.2889	y ₅ ⁺ 637.2649	NA
PTH 66-72 [M+2H] ²⁺	SLGEADK	(4.0-11.5min) 9.2min	360.1821	364.1701	NA	17	y ₅ ⁺ 519.2409	y ₅ ⁺ 525.2229	NA
PTH 73-80 [M+2H] ²⁺	ADVNVLTk	(11.5-12.8min) 12.3min	430.2478	435.2328	NA	20	y ₆ ⁺ 673.4243	y ₆ ⁺ 681.4003	NA

Table 5.1 HCD-MS/MS precursor/fragment ion transitions, optimized HCD normalized collision energy (NCE) and retention times for quantitatively monitored PTH peptides.

High resolution/accurate mass HCD-MS/MS was employed to avoid possible interference from artefact ions given the complex background signals from patient samples. An example illustrating the advantage of using high resolution/accurate mass HCD-MS/MS to resolve monitored fragment ions of PTH peptides in a patient sample from artefact ions is shown in Figure 5.5. At a mass resolving power of 17,500, an artefact ion at m/z 643.3396 was found to overlap with the monitored HCD-MS/MS fragment ion (y_{11}^{2+} at m/z 643.3303) of PTH 1-13 M(O) (inset to Figure 5.5) and subtly shifted the retention time of the extracted ion current chromatogram (XIC) peak of the fragment ion (Figure 5.5A) compared that of ^{15}N -labeled PTH 1-13 M(O) (Figure 5.5B) and $^{13}\text{C}_6^{15}\text{N}_1\text{Leu}$ -labeled PTH 1-13 M(O) (Figure 5.5C). Since no other HCD-MS/MS transitions were available to be used to avoid the interference and also maintain a comparable sensitivity as shown in Figure 5.4B, HCD-MS/MS at ultrahigh resolution of 140,000 was therefore required to completely resolve the monitored fragment ion of PTH 1-13 M(O) from the artefact ions.

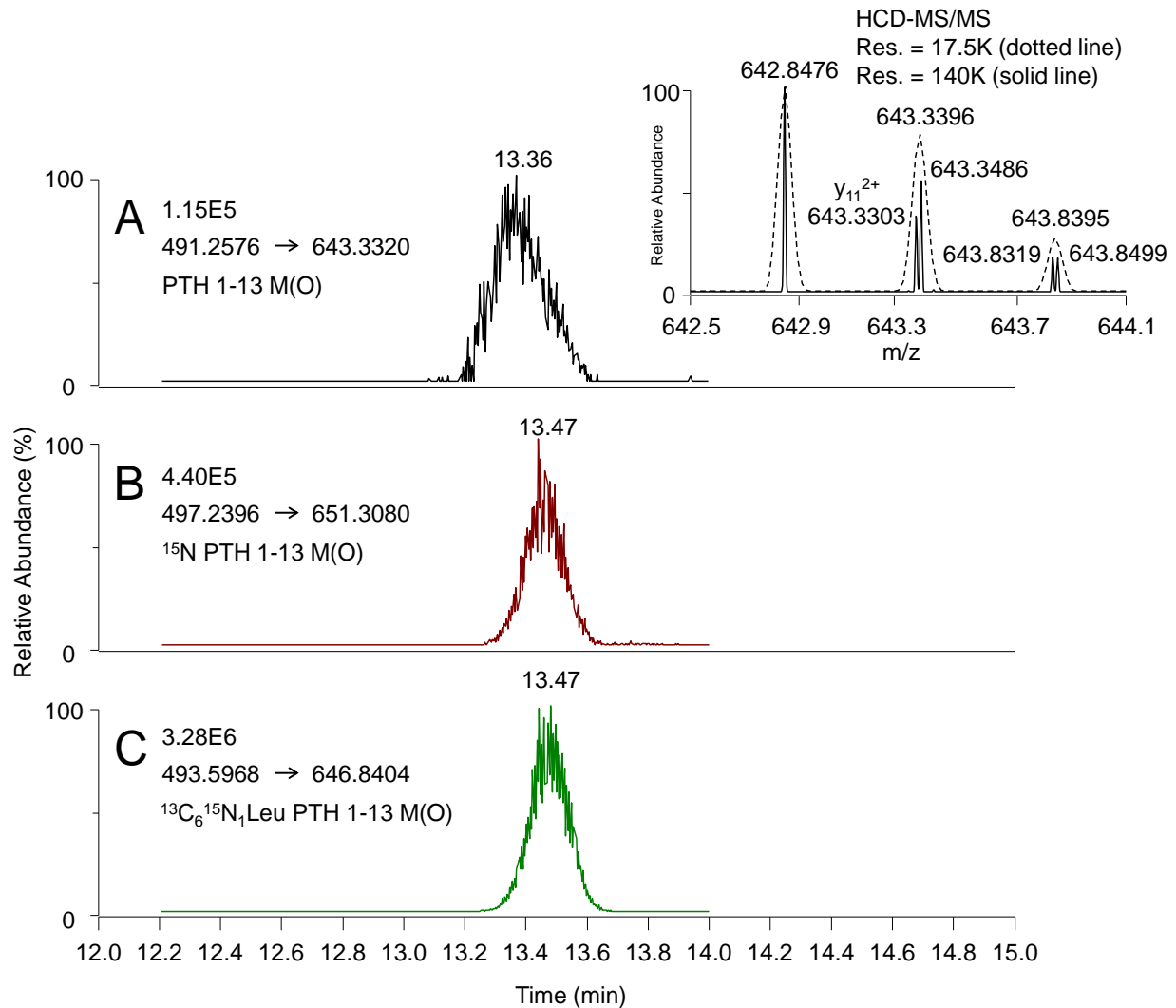


Figure 5.5 Resolving monitored fragment ions from artefact ions with isobaric m/z in a patient sample using high resolution/accurate mass HCD-MS/MS (A) extracted ion current (XIC) chromatogram of y_{11}^{2+} (m/z 643.3320) from PTH 1-13 M(O) (m/z 491.2576); (B) XIC chromatogram of y_{11}^{2+} (m/z 651.3080) from ¹⁵N-labeled PTH 1-13 M(O) (m/z 497.2396); (C) XIC chromatogram of y_{11}^{2+} (m/z 646.8404) from ¹³C₆¹⁵N₁Leu-labeled PTH 1-13 M(O) (m/z 493.5968). Resolution for Figure 5.5A-C was at 17,500 (at $m/\Delta m = 200$). The inset shows expanded m/z region of the HCD-MS/MS of PTH 1-13 M(O) averaged across the XIC peak in Figure 5.5A at resolution of 17,500 (dotted line) and 140,000 (solid line)

5.2.2 Quantitative Analysis of *In Vivo* Full Length, Oxidized and Truncated PTH Tryptic Peptides in Patient Samples

The practical performance of the quantitative immuno LC-MS/MS method using conditions described above was tested using a series of patient samples. An example of LC-MS and LC-MS/MS raw data for the various forms of monitored PTH 1-13 in a patient sample is shown in Figure 5.6A and Figure 5.6B-F, which include the unlabeled and ¹⁵N-labeled PTH 1-13 (Figure 5.6B and C) as well as unlabeled, ¹⁵N-labeled and ¹³C₆¹⁵N₁Leu-labelled PTH 1-13 M(O) (Figure 5.6D to F). LC-MS/MS raw data for the various forms of monitored PTH 7-13 and 14-20 are shown in Figure 5.6G-P. During the concentration calculation, to correct the effects from incomplete stable isotope incorporation in the stable isotope-labeled internal standards, the intensity of the isotopic cluster of representative fragment ion instead of that of the monoisotopic peak was used to represent the amount of the corresponding peptide. For each unoxidized peptide, the concentration ($C_{\text{non_ox}}$) was calculated using the equation (1),

$$C_{\text{non_ox}} = \frac{I_{\text{non_ox}}}{I_{^{15}\text{N_non_ox}}} \frac{C_{^{15}\text{N}}}{V} \quad (1)$$

where $I_{\text{non_ox}}$ and $I_{^{15}\text{N_non_ox}}$ are intensities of isotopic cluster of the representative product ion of the unoxidized PTH peptide and unoxidized ¹⁵N-labeled PTH peptide internal standard. $C_{^{15}\text{N}}$ is concentration of ¹⁵N-labeled PTH 1-84 or 7-84 internal standard spiked in plasma and V is the volume of original plasma solution. Possible *ex vivo* truncation and sample loss were already corrected by using the fragment ion intensities of ¹⁵N-labeled peptides as digest of ¹⁵N-labeled PTH 1-84 spiked in immediately after blood draw and centrifugation for plasma. Concentrations of *in vivo* oxidized PTH peptides (C_{ox}) were determined using the equation (2),

$$C_{\text{ox}} = \frac{I_{\text{ox}} - \frac{I_{^{15}\text{N}_{\text{ox}}}}{I_{^{15}\text{N}_{\text{non_ox}}}} I_{\text{non_ox}}}{I_{^{13}\text{C}^{15}\text{N}}} \frac{C_{^{13}\text{C}^{15}\text{N}}}{V} \frac{1}{y_{\text{recovery}}} \quad (2)$$

where I_{ox} , $I_{^{15}\text{N}_{\text{ox}}}$, $I_{^{13}\text{C}^{15}\text{N}}$ are the intensities of isotopic cluster of the representative product ion of the oxidized PTH peptide, oxidized ^{15}N -labeled PTH peptide internal standard and $^{13}\text{C}_6^{15}\text{N}_1\text{Leu}$ -labeled oxidized PTH peptide internal standard. $C_{^{13}\text{C}^{15}\text{N}}$ is concentration of $^{13}\text{C}_6^{15}\text{N}_1\text{Leu}$ -labeled oxidized PTH peptide internal standard spiked in sample before LC-MS/MS analysis and y_{recovery} is the recovery yield (66%) of the immuno LC-MS/MS method [264]. In equation (2), possible *ex vivo* oxidation can be corrected by the oxidation percentage of ^{15}N -labelled PTH peptide internal standards.

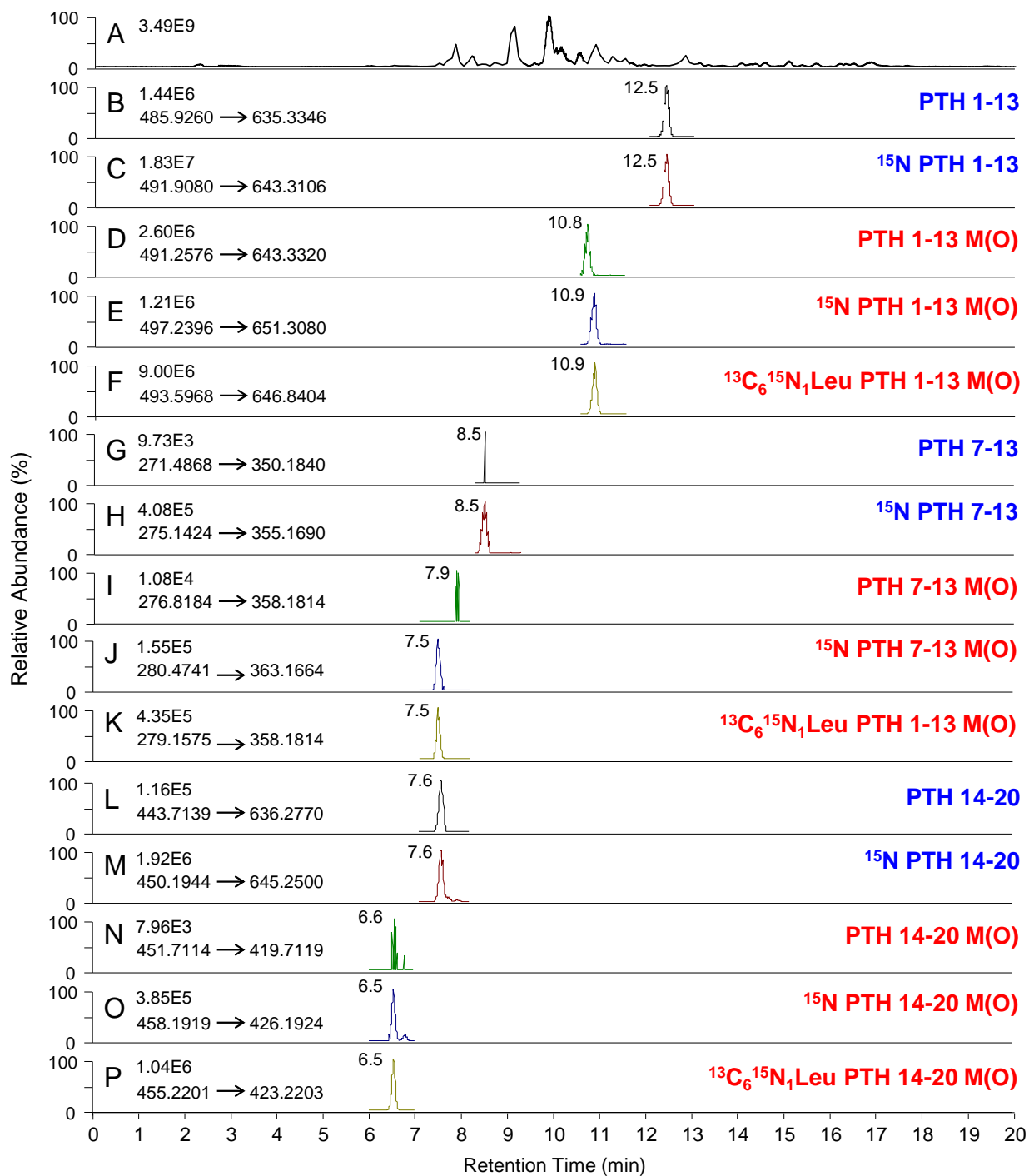


Figure 5.6 Extracted ion current (XIC) chromatograms from a patient sample for (A) base peak in MS data and for monitored HCD-MS/MS fragment ions of (B) PTH 1-13, (C) ^{15}N -labeled PTH 1-13, (D) PTH 1-13 M(O), (E) ^{15}N -labeled PTH 1-13 M(O), (F) $^{13}\text{C}_6^{15}\text{N}_1\text{Leu}$ -labeled PTH 1-13 M(O), (G) PTH 7-13, (H) ^{15}N -labeled PTH 7-13, (I) PTH 7-13 M(O), (J) ^{15}N -labeled PTH 7-13 M(O), (K) $^{13}\text{C}_6^{15}\text{N}_1\text{Leu}$ -labeled PTH 1-13 M(O), (L) PTH 14-20, (M) ^{15}N -labeled PTH 14-20, (N) PTH 14-20 M(O), (O) ^{15}N -labeled PTH 14-20 M(O), (P) $^{13}\text{C}_6^{15}\text{N}_1\text{Leu}$ -labeled PTH 14-20 M(O).

¹⁵N-labeled PTH 7-13, (I) PTH 7-13 M(O), (G) ¹⁵N-labeled PTH 7-13 M(O), (K) ¹³C₆¹⁵N₁Leu-labeled PTH 7-13 M(O), (L) PTH 14-20, (M) ¹⁵N-labeled PTH 14-20, (N) PTH 14-20 M(O), (O) ¹⁵N-labeled PTH 14-20 M(O) and (P) ¹³C₆¹⁵N₁Leu-labeled PTH 14-20 M(O) as listed in Table 5.1.

By employing the quantitative immuno LC-MS/MS strategy described above, the resultant concentrations of PTH peptides in five samples from patients with high concentration of circulating PTH 1-84 (500 to 1500 pg/mL) previously measured by PTH immunoassay were shown in Table 5.2. PTH 1-13 M(O) and 1-13 represent forms of PTH 1-84 with and without oxidation within residue 1-13 while PTH 7-13 M(O) and 7-13 represent forms of PTH 7-84 with and without oxidation within residue 7-13. PTH 14-20 M(O) and 14-20 represent forms of residue 14-84 containing-PTH (i.e., PTH 1-84 and 7-84) with and without oxidation within residue 14-20. ¹⁵N-labeled PTH 7-84 internal standard was not spiked in these five samples since the PTH 7-13 and 7-13 M(O) were not detected in preliminary experiments. The result is consistent with previous studies using other immuno LC-MS/MS methods [249, 267]. Surprisingly, it was found that no *in vivo* oxidized PTH peptides existed in the patient samples after correction for the *ex vivo* oxidation. High concentrations of PTH 1-13 were detected as expected. The generally higher concentrations of PTH 14-20 compared to that of PTH 1-13 (except in patient 1) indicated other possible truncation sites between residue 1 and 13 of PTH 1-84 except residue 7. Truncations at residues 4 and 10 have been suggested by D'Amour *et al.* [248]. However, no PTH X-13 peptides (X=2-12 except 7) were detected within these 5 patient samples, partially due to the decreasing ionization efficiency of shortening peptides if any truncation exists between residue 7 and 13. The concentrations of PTH tryptic peptides from the mid-molecular and C-terminal region of PTH 1-84 were also monitored. Despite that their measured concentration (up to 20 ng/mL) is out of the determined linear range of the method (5-2000 pg/mL as previously described [264]), the high concentration was consistent with the widely agreed knowledge that major

forms of the circulating PTH are N-terminally truncated fragments of PTH 1-84 [11]. The much lower concentrations of PTH 27-44 and 73-80 compared to that of PTH 45-52, 53-65 and 66-72 were also consistent with the identified PTH 34-44, 37-44, 38-44 and 66-77 with high abundance (Figure 5.7A-D). ¹⁵N-labeled PTH 34-44, 37-44, 38-44 and 66-77 were not observed in the five patient samples which confirmed that those identified non-isotope-labeled truncated PTH peptides were produced *in vivo* instead of *ex vivo*.

Concentration of PTH Tryptic Peptides in Patient Plasma (pg/mL)											
	PTH 1-13	PTH 1-13 M(O)	PTH 7-13	PTH7-13 M(O)	PTH14-20	PTH14-20 M(O)	PTH 27-44	PTH 45-52	PTH 53-65	PTH 66-72	PTH 73-80
Patient 1	432	0	ND	ND	382	0	1018	18853	20335	12787	3763
Patient 2	211	0	ND	ND	250	0	309	3228	3334	2515	736
Patient 3	196	0	ND	ND	292	0	486	7788	7272	5097	1405
Patient 4	283	0	ND	ND	391	0	811	18731	21758	19483	4245
Patient 5	682	0	ND	ND	923	0	1438	15798	18620	13540	3971

Table 5.2 Concentration of full length, oxidized and truncated PTH tryptic peptides in patient plasma determined by quantitative immuno LC-MS/MS with near full sequence coverage. Concentrations of oxidized PTH peptides were corrected to remove *ex vivo* oxidation. ND indicates that the peptide was not detectable.

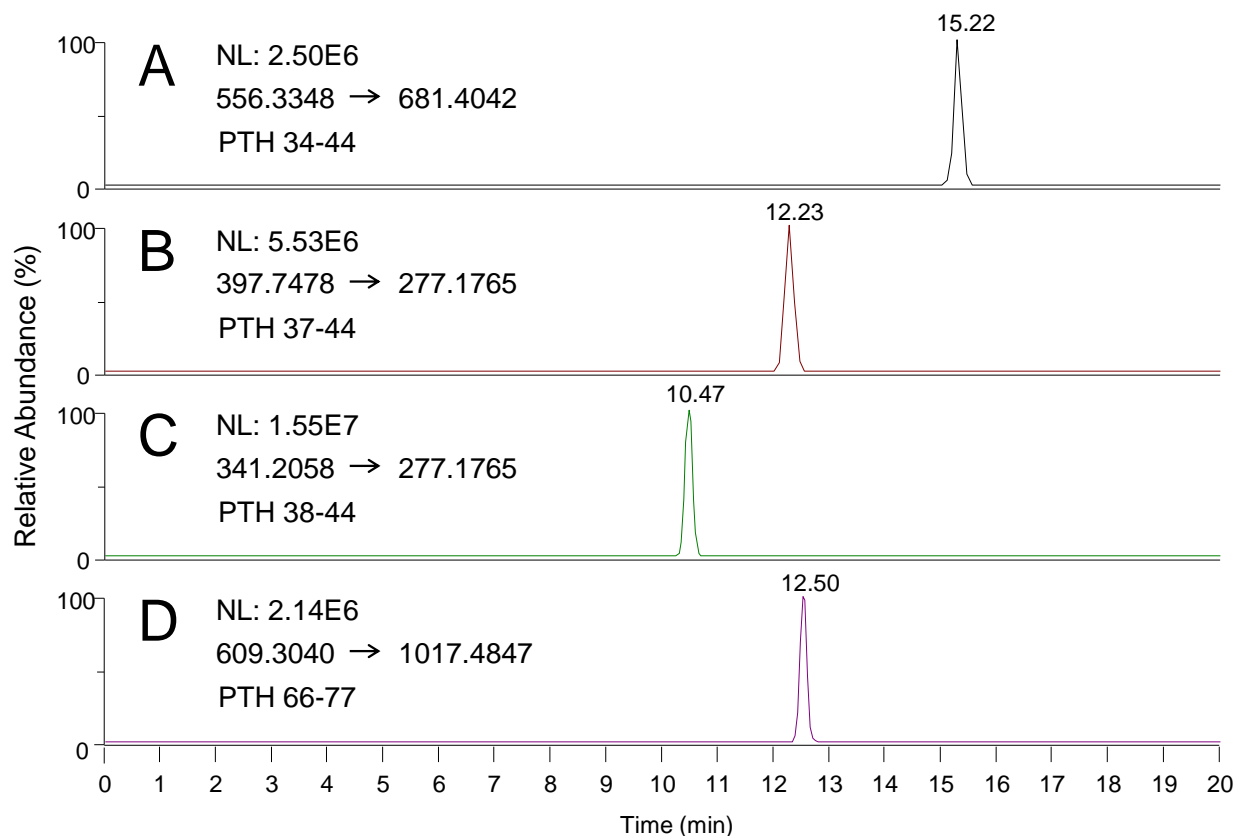


Figure 5.7 Extracted ion current (XIC) chromatograms of representative HCD-MS/MS fragment ions from truncated PTH peptides in a patient sample (A) XIC chromatogram of y_7^+ (m/z 681.4042) from PTH 34-44 (m/z 556.3348); (B) XIC chromatogram of y_5^{2+} (m/z 277.1765) from PTH 37-44 (m/z 397.7478); (C) XIC chromatogram of y_5^{2+} (m/z 277.1765) from PTH 38-44 (m/z 341.2058); (D) XIC chromatogram of y_{10}^+ (m/z 1017.4847) from PTH 66-77 (m/z 609.3040).

5.2.3 Identification of Novel Truncation Sites of PTH Proteins

Novel truncation sites at residue 66 and 74 of PTH 1-84 were also discovered and evidenced by HCD-MS/MS analysis of PTH-specific peptides including PTH 53-66 (KKEDNVLVESHEKS) and PTH 66-74 (SLGEADKAD) (Figure 5.8A and B) found in patient samples. Absence of ¹⁵N-labeled PTH 53-66 and 66-74 in patient samples confirmed that the truncation at residue 66 and 74 occurred *in vivo*. Phosphorylation at serine 17 of PTH 1-84 was not identified in these patient samples.

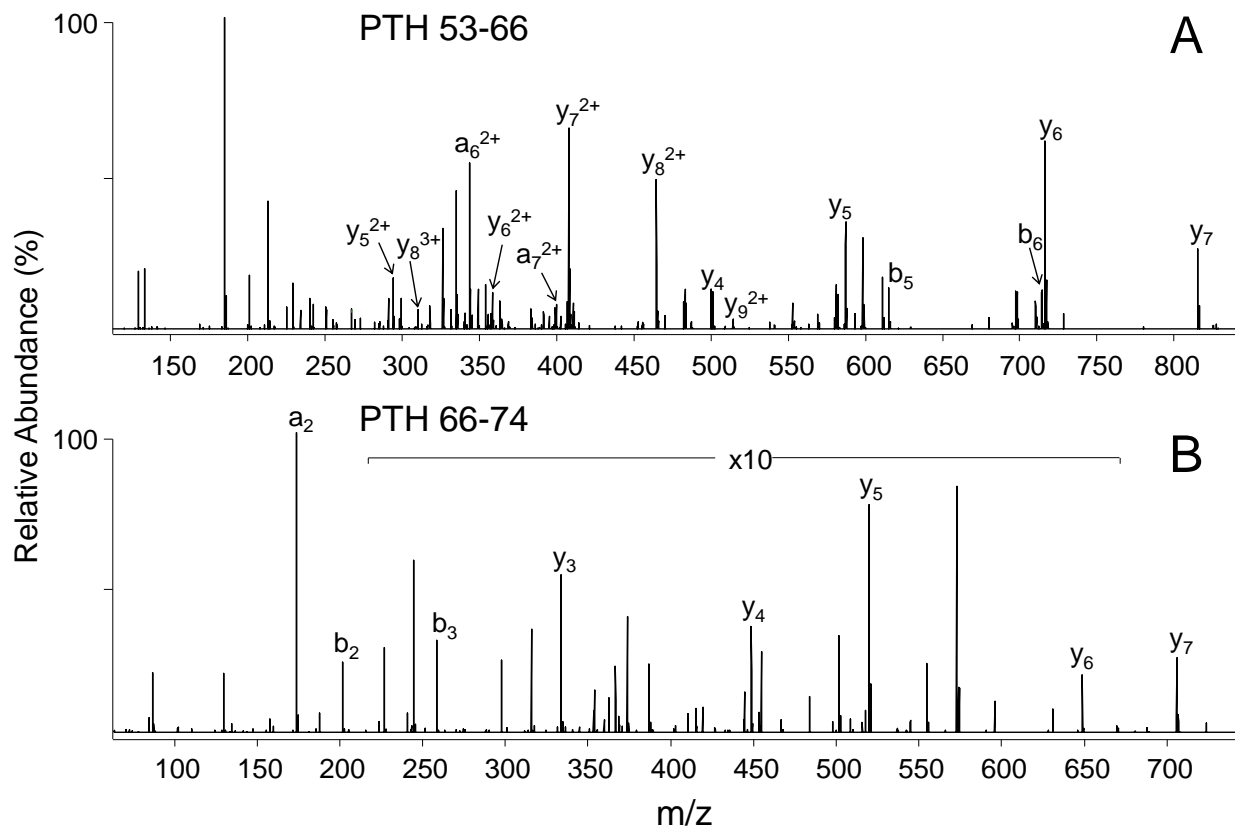


Figure 5.8 Identification of novel truncation sites of PTH by LC-HCD-MS/MS analysis of (A) PTH 53-66 ($z = +4$) and (B) PTH 66-74 ($z = +2$) from a representative patient sample.

5.3 Conclusions

An immuno LC-MS/MS method enabling simultaneous identification and quantification of *in vivo* full length, truncated and oxidized PTH was developed. Different heavy isotope-labeled PTH protein and oxidized peptide internal standards were employed for accurate quantitative analysis of various forms of PTH after correction of possible *ex vivo* post-translational modification (i.e., oxidation and truncation) occurring during sample handling. Transitions with near full sequence coverage were coupled with high resolution/accurate mass tandem mass spectrometry to avoid possible interference from complex background signals in patient samples and unambiguously quantify the targeted PTH peptides. After analysis of five patient samples using the developed method, no *in vivo* oxidation was detected after correction for *ex vivo* oxidation. Also, no notable quantities of N-terminally truncated PTH 7-84 was detected as previously reported. The inconsistent concentration of PTH 1-13 and 14-20 in patient samples indicated the existence of other previously unidentified truncated PTH except PTH 7-84. Novel *in vivo* truncation site at residue 66 and 77 of PTH 1-84 were also identified. It is expected that more post-translationally modified forms, mainly truncated forms of PTH will be discovered, identified and quantified in future study of PTH using immuno mass spectrometric methods for the purpose of studying their not fully understood biological activities and possible clinical utilities.

CHAPTER SIX

Quantitative Proteomic Analysis Using Dimethyl Labeling and Two Dimensional LC-MS/MS to Study the Mechanism of Action of the Non-Competitive Proteasome Inhibitor, TCH-013

6.1 Introduction

The 26S proteasome, consisting of a 20S catalytic core particle and 19S regulatory particle is the central protease responsible for maintaining cellular homeostasis through the ubiquitin-proteasome pathway [268]. Inhibition of this pathway using Bortezomib has emerged as a rational strategy for the chemotherapeutic treatment of multiple myeloma (MM), a cancer of plasma cells located within bone marrow [269]. Through covalent binding to the catalytic sites at N-terminal threonine of several 20S β -subunits of the 26S proteasome, Bortezomib competitively blocks the ubiquitin-proteasome pathway of protein degradation [270]. Via competitive inhibition, Bortezomib is effective in inducing death of cells (e.g., multiple myeloma cells) where the 26S proteasome is constantly under a high burden to degrade rapidly produced toxic misfolded proteins [271], however, >97% of patients become resistant or intolerant to treatment in the first few years, after which survival is typically less than a year [272]. Bortezomib resistance is, in part, due to the overexpressed mutated forms of catalytic subdomains of 26S proteasome at the original drug binding sites which inhibit the effectiveness of protein/Bortezomib binding [273, 274].

Alternatively, drugs enabling non-competitive inhibition of proteasomes have been suggested to overcome treatment resistance and can present lower toxicities [275-277]. Both peptide- and small molecules-based non-competitive proteasome inhibitors have been reported [275-280]. For example, a proline- and arginine-rich

peptide named PR-39 can inhibit degradation of specific proteins including I κ B after binding to the non-catalytic α -subunit of 20S proteasome and changing the structure of the proteasome [275]. As small molecule-based proteasome inhibitors, chloroquine and the secondary fungal metabolite, gliotoxin, were shown to non-competitively inhibit the activity of 20S proteasome, but both have issues of toxicity [278, 279]. Although 5-amino-8-hydroxyquinoline (5AHQ) was also reported to selectively inhibit the proteasome in myeloma and leukemia cells, no direct evidence for interaction between 5AHQ and the proteasome was provided [280]. Recently, Tepe and co-workers described the substrate selectivity of proteasome mediated proteolysis induced by small molecule imidazoline scaffolds, TCH-013 and its derivatives, via a non-competitive protein/ligand interaction and with nanomolar potency [276, 277]. This class of small molecules represents a promising direction for the development of novel non-competitive proteasome inhibitors which overcome the limitations caused by competitive proteasome inhibition. However, little is known about the site(s) at which the non-competitive inhibitor binds to the proteasome, or their mechanism(s) of biological activity.

MS-based quantitative proteomic strategies are widely used to elucidate the mode of action by which a drug exerts its pharmacological effect by providing information on drug-induced regulation of functional proteins and/or their PTMs [281]. For example, the mechanism of action of Lenalidomide, another effective drug for MM, is not fully understood [282]; through large scale quantitative proteomic analysis, Krönke *et al.* reported that two essential transcription factors of MM cells, IKZF1 and IKZF3, were selectively ubiquitinated and degraded by CRBN-CRL4 ubiquitin ligase, providing a novel mode of action for lenalidomide [283]. For any successful proteomics study, a

broad coverage of identification and sufficient depth of quantification is critical for unbiased searching of stimuli-induced changes in protein and PTM abundance [50, 64]. Therefore, reducing the sample complexity through enrichment and/or fractionation techniques is usually required [50]. Basic pH reversed-phase fractionation is gaining popularity due to the availability of reversed-phase columns tolerable to a wide pH range, better resolving power of hydrophobicity-dependent separation compared to that of other separation techniques (e.g., strong cation ion exchange) and more affordable cost compared to antibody-based enrichment [284]. To enable large scale MS-based quantitative proteomic analysis of animal or human samples where spiking stable isotope labeled analogue standards and metabolic labeling of stable isotopes are not applicable, chemical labeling with isotope-coded tags followed by sample pooling before down-stream analysis is commonly used as discussed in Chapter 1, section 1.2.1.3.3. Relying on the advantages of inexpensive reagents, fast reactions and applicability to a broad range of sample quantities, dimethyl labeling is one of the frequently used chemical labeling methods for quantitative proteomic studies [188]. In this chapter, a strategy involving stable isotope-containing dimethyl labeling, basic reversed-phase fractionation and quantitative LC-MS/MS was employed for quantitative proteomic analysis of TCH-013 (imidazoline scaffold)-, Bortezomib- and vehicle control- (DMSO) treated human RPMI-8226 cells, to gain insights into the mechanism of non-competitive proteasome inhibition.

6.2 Results and Discussion

6.2.1 Quantitative Proteomic Analysis Workflow

A quantitative proteomic analysis workflow (Figure 6.1) using enzymatic digestion, dimethyl labeling, basic reversed-phase fractionation, LC-MS/MS and bioinformatic analysis was designed to characterize the effect of TCH-013 on cellular protein abundance to help elucidate its mechanism of action. In detail, after drug (i.e., TCH-013, Bortezomib and DMSO vehicle control) treatment to RPMI-8226 cells, protein extraction and protein concentration measurement, the crude protein samples were reduced, alkylated and digested by trypsin to generate peptide samples. To enable duplexed quantitative analysis using MS, peptides from samples at each treatment condition were differentially labeled by deuterated formaldehyde (CD_2O) or formaldehyde (CH_2O) as the alkylation reagent and NaBH_3CN as the reduction reagent. In this study, TCH-013 treated samples were labeled by CD_2O while Bortezomib and DMSO treated samples were labeled with CH_2O . Then, the CD_2O labeled (TCH-013 treated) sample was mixed with the CH_2O labeled (Bortezomib or DMSO treated) sample at ratio of 1:1 (normalized to protein quantity). To improve the coverage of identification and depth of quantification, basic pH reversed-phase fractionation was used to separate the sample mixture into 10 less complex fractionations based on their hydrophobicity at high pH conditions which is orthogonal to that at low pH conditions used for subsequent data-dependent LC-MS/MS analysis of each fraction [284]. For the acquired data, MaxQuant software was employed for database search-based peptide identification, protein assignment and extraction of quantitative information from the intensity ratios of CD_2O -labeled (heavy) and CH_2O -labeled (light) peptide duplet peaks. Quantitative analysis at a protein level

was achieved by an in-house C++ script. A heavy/light ratio for each protein was expressed as the median value of the normalized, \log_2 transformed and grouped heavy/light ratio of each peptide assigned to that protein. As mentioned in Chapter 1, section 1.2.1.3.3, dimethyl labeling can lead to peptide retention time shifts caused by deuterium isotope effects [190]. The accuracy of quantifying based on the intensity ratios of heavy/light peptide duplet peaks may be compromised by this phenomenon which occurred during first and second dimensional separations in the designed workflow [190]. To correct this type of systematic error, peptides identified in multiple fractions were not used for quantification. Also, the intensity ratios of heavy/light peptide duplet peaks were analyzed collectively over the whole chromatographic peak by plotting the peak intensity of heavy peptide over that of light peptide and calculating the slope (i.e., heavy/light ratio) using a linear fit model [285].

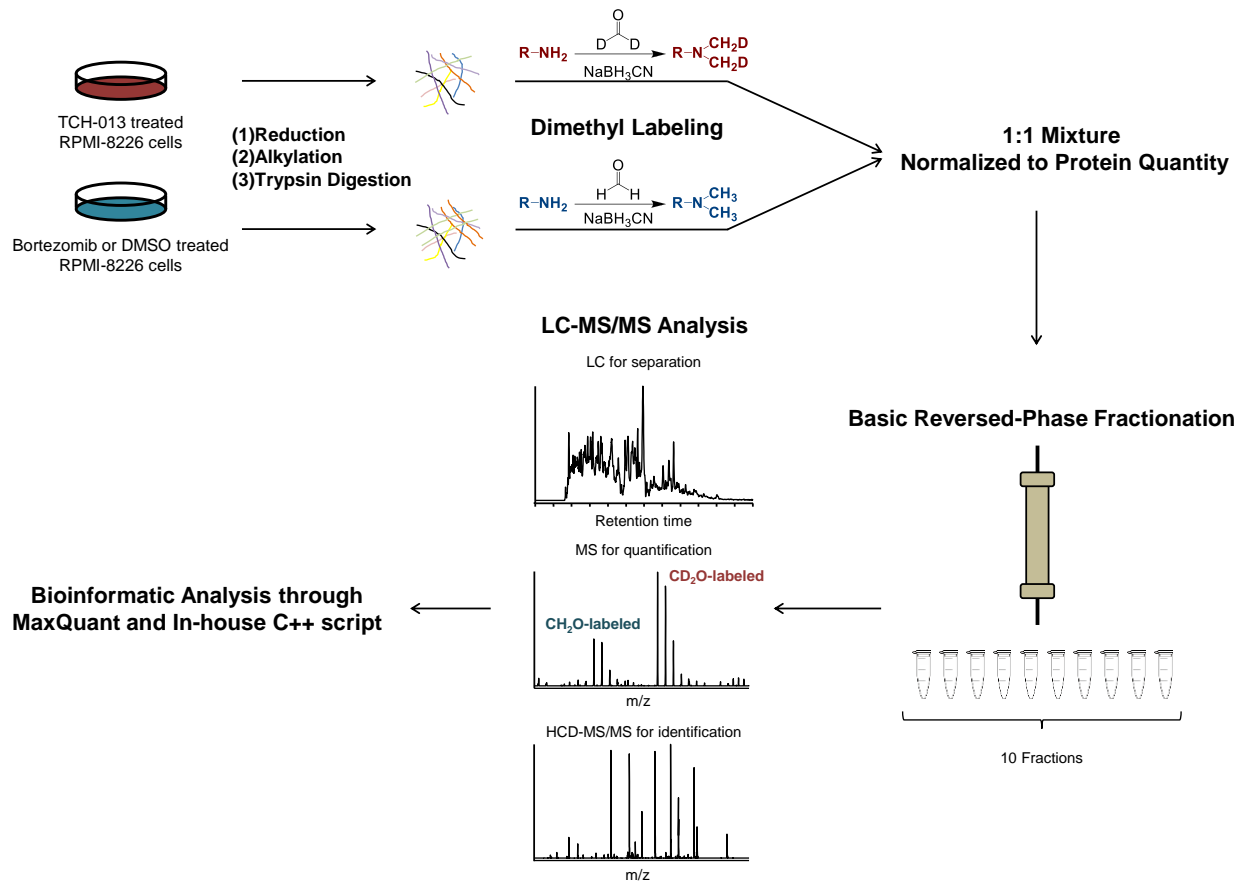


Figure 6.1 A workflow using tryptic digestion, dimethyl labeling, basic reversed-phase fractionation, LC-MS/MS and bioinformatic analysis for quantitative proteomic analysis of TCH-013, Bortezomib and DMSO (vehicle control) treated human RPMI-8226 cells.

6.2.2 Coverage of Protein Identification and Selection Criteria During Protein Quantification

Proteomic analysis of TCH-013-, Bortezomib- and DMSO-treated RPMI-8226 cells using the workflow described above revealed >1200 proteins with at least 2 peptides identified in each of the three treatments and in all three biological replicates. The coverage of protein identities acquired by this workflow is illustrated in Figure 6.2A-B. From TCH-013-treated (heavy) and Bortezomib-treated (light) samples (Figure 6.2A), 1721 proteins were identified in total from three biological replicates in which 78.4% (1350) of them are common in at least two biological replicates and 59.4% (1022) of them are common for all three biological replicates. Similarly, from TCH-013 treated (heavy) and DMSO treated (light) cells (Figure 6.2B), 1788 proteins were identified in all three biological replicates where 81.5% (1457) and 65.8% (1176) were identified in two and three biological replicates, respectively. The good overlap of identified proteins between biological replicates demonstrates that the designed workflow has a broad enough coverage of identification for subsequent large scale quantitative analysis. The influence of selection criteria (i.e., minimum number of peptides for each protein) on the number of quantified proteins common in all three biological replicates was shown in Figure 6.2C and D for the two sample mixtures. Although more heavy/light peptide pairs assigned to each protein is desired to acquire a more reproducible heavy/light protein ratio, the number of relatively quantified proteins decreases at the same time, which limits the ability to find possible drug-regulated proteins with less peptides assigned. In this study, stringent criteria was applied i.e. only proteins with ≥ 4 peptides from each of the three treatments and in all three biological replicates were used for a more

reproducible quantification at protein level. After applying the selected criteria, 402 heavy/light protein pairs was considered to be relatively quantified in the sample mixtures consisting of cellular proteins under TCH-013 and Bortezomib treatment and 472 heavy/light protein pairs was considered to be relatively quantified in the sample mixtures consisting of cellular proteins under TCH-013 and DMSO treatment. Ubiquitination was not quantified in this study due to the much lower number of identified and quantified ubiquitinated peptides compared to their unmodified counterparts.

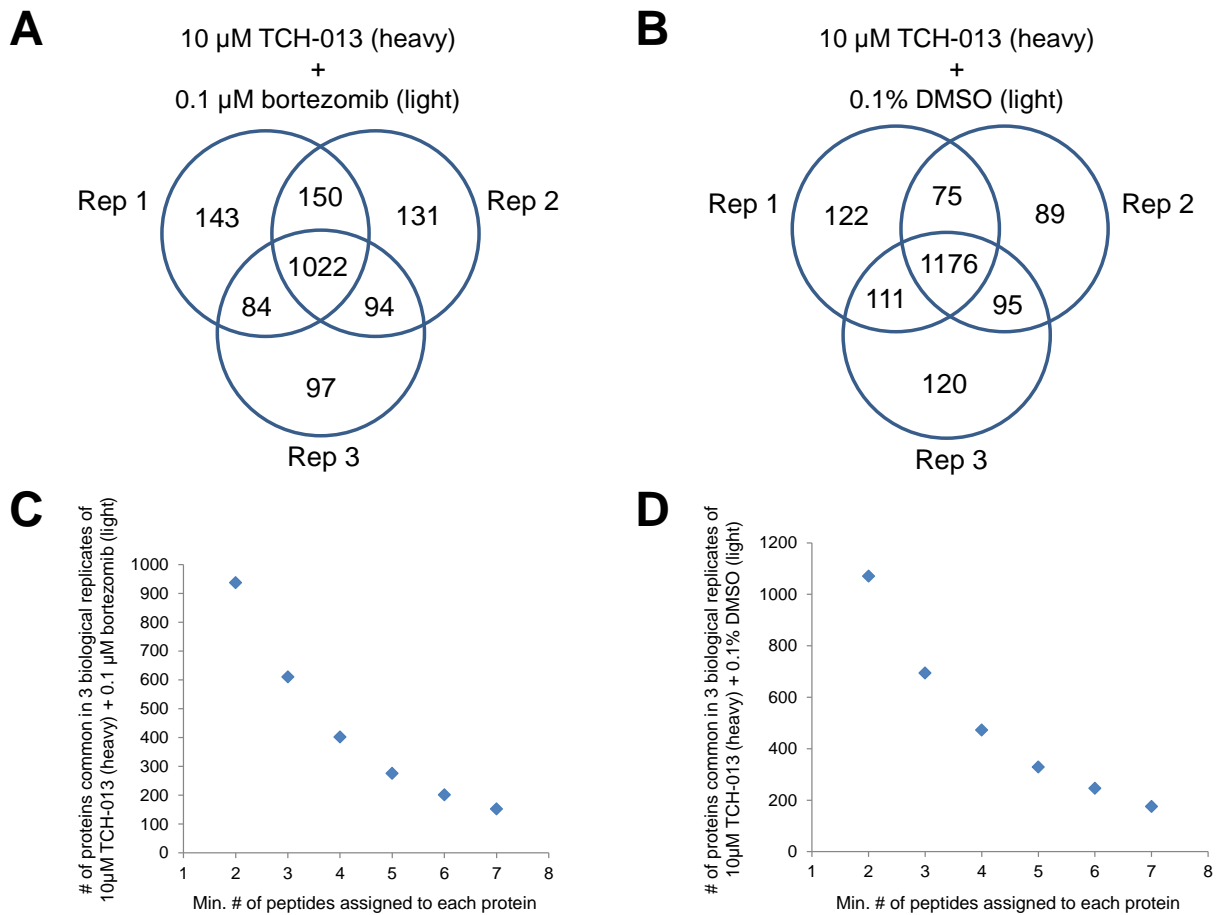


Figure 6.2 Overlapping of identified heavy/light proteins in three biological replicate sample mixtures consisting of (A) a heavy-labeled TCH-013 (10 μM) treated sample mixed with a light-labeled Bortezomib (0.1 μM) treated sample; (B) a heavy-labeled TCH-013 (10 μM) treated sample mixed with a light-labeled DMSO (0.1%, v/v) treated sample. The influence of selection criteria (i.e., minimum of peptides assigned to each protein) on the number of relatively quantified proteins common in three biological replicates of sample mixture A (C) and B (D).

6.2.3 Protein Regulation in Human RPMI-8226 Cells Induced by TCH-013

Following relative quantification of the proteins from human RPMI-8226 cells subjected to different treatments, the histograms of averaged \log_2 heavy/light proteins ratios ($n=3$) for quantified proteins after TCH-013 (heavy) treatment vs Bortezomib (light) treatment or TCH-013 (heavy) treatment vs DMSO (light) treatment were plotted (Figure 6.3A and B). In general, protein abundance appeared to be unaffected by the selective proteasome inhibitor, TCH-013 as well as the non-selective proteasome inhibitor, Bortezomib. This steady-state level of proteins was consistent with previous large scale proteomic studies involving human 293T and HCT116 cells treated with Bortezomib and human Jurkat cells treated with another competitive proteasome inhibitor, MG-132 [286, 287]. In addition, although both Bortezomib and TCH-013 have been demonstrated to induce accumulation of ubiquitinated proteins as the substrates of the ubiquitin-proteasome protein degradation pathway, no proteins were significantly (near 2 folds) up-regulated in TCH-013 treated samples compared to those treated with Bortezomib or DMSO (control), possibly due to the low stoichiometry of ubiquitination [286, 287]. However, in the present study TCH-013, but not Bortezomib or DMSO, treatment was associated with significant (near 2 folds) down-regulation of four proteins (Table 6.1) namely prohibitin-2, NAD(P) transhydrogenase, NADH-ubiquinone oxidoreductase and ADP/ATP translocate 2. Surprisingly, they are all closely involved in regulation of the mitochondrial respiration for production of ATP or the detoxification of reactive oxygen species (ROS), both of which are usually increasingly demanded for growth and division of cancer cells having higher rates of metabolism [288-291]. For example, knockdown of prohibitin-1 and prohibitin-2 together or prohibitin-2 alone

have been reported to suppress tumor growth [288, 292, 293]. Also, the key roles of mitochondrial ADP/ATP translocate 2 in the almost exclusive metabolism pathway (i.e., glycolysis) in many cancer cells were also summarized in a recent review [290]. To further elucidate the mechanism of observed selective protein down-regulation induced by TCH-013 and how it is related to TCH-induced activity changes of proteasome and/or cell apoptosis, more targeted biological studies on protein ubiquitination and protein interactions are required.

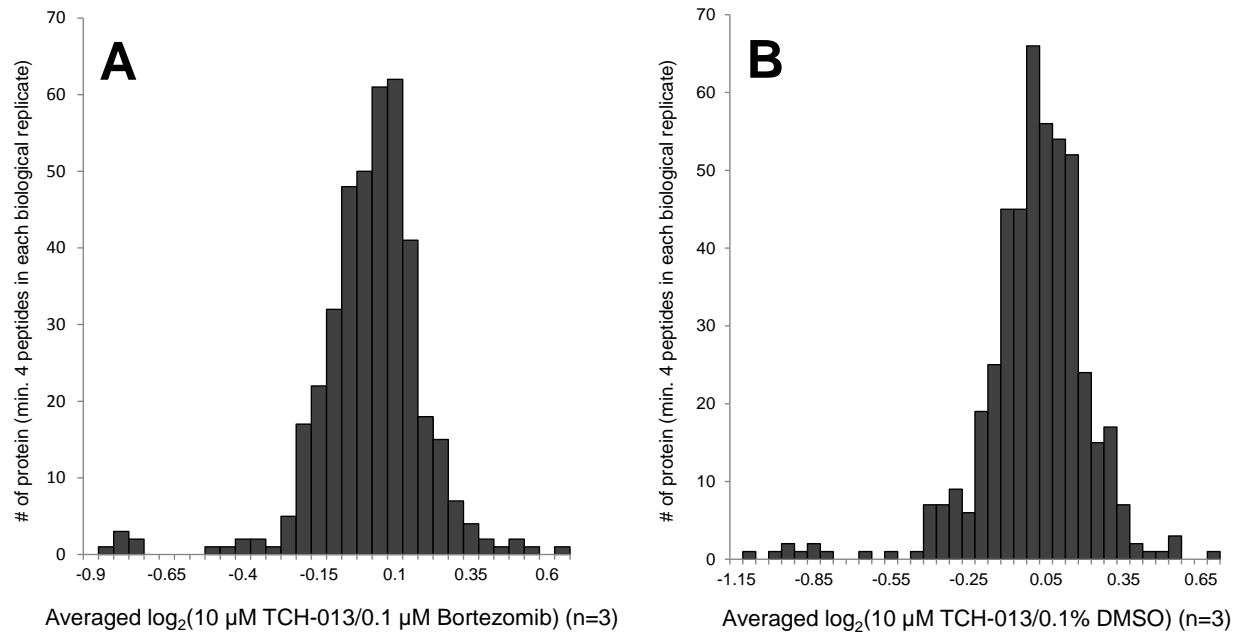


Figure 6.3 Histograms of averaged \log_2 heavy/light proteins ratios (n=3) for quantified proteins after (A) TCH-013 (heavy) treatment vs Bortezomib (light) treatment and (B) TCH-013 (heavy) treatment vs DMSO (light) treatment.

Protein name	log ₂ (10 μM TCH-013/ 0.1 μM bortezomib)			log ₂ (10 μM TCH-013/ 0.1% DMSO)			log ₂ (0.1 μM bortezomib/ 0.1% DMSO)		
	Rep 1	Rep 2	Rep 3	Rep 1	Rep 2	Rep 3	Rep 1	Rep 2	Rep 3
	Prohibitin-2	-0.93	-1.20	-0.74	-1.04	-1.19	-0.91	-0.11	0.01
NAD(P) transhydrogenase	-0.83	-0.98	-0.64	-0.96	-1.06	-0.83	-0.13	-0.08	-0.19
NADH-ubiquinone oxidoreductase	-0.78	-1.00	-0.71	-1.04	-1.08	-0.87	-0.26	-0.08	-0.16
ADP/ATP translocase 2	-0.67	-1.14	-0.57	-0.95	-1.04	-0.65	-0.28	0.10	-0.08

Table 6.1 Protein down-regulation (near 2 folds) expressed in log₂ heavy/light protein ratios in three biological replicates of TCH-013 (heavy) treated RPMI-8226 cells compared to that treated with Bortezomib (light) and DMSO control (light).

6.3 Conclusions

A quantitative proteomics strategy comprising human RPMI-8226 cells treated with either the non-competitive proteasome inhibitor, TCH-013, the competitive proteasome inhibitor, Bortezomib or DMSO (vehicle control), tryptic digestion, dimethyl labeling, basic pH reversed-phase fractionation, LC-MS/MS and bioinformatic tools were employed to study the mechanism of action of TCH-013. To minimize the errors of quantification caused by retention time shifts of CD₂O-labeled peptides compared to their CH₂O-labeled counterparts, peptides identified in multiple fractions were excluded for quantitative analysis and the integral intensity ratios of CD₂O/CH₂O-labeled peptide duplet peaks were calculated collectively over their chromatographic peaks. In each of three treatments and in all three biological replicates >1200 proteins with at least two peptides were identified and >400 proteins with at least 4 peptides were quantified. Although no significantly up-regulated proteins were observed, 4 proteins including prohibitin-2, NAD(P) transhydrogenase, NADH-ubiquinone oxidoreductase and ADP/ATP translocate 2 were found to be down-regulated by at least two fold. Interestingly, down-regulated proteins were all closely related to the regulation of mitochondrial functions which are critical to growth and division of many cancer cells [288-293]. While the exact mechanism of selective protein down-regulation induced by TCH-013 in the present study remains unclear, this work provides candidate protein targets for future more targeted TCH-013 mechanistic studies.

CHAPTER SEVEN

Experimental Methods for Chapters Five and Six

7.1 Materials

Acetic acid (99%) and formic acid (FA, 99%) were purchased from Thermo Fisher Scientific (San Jose, CA), trifluoroacetic acid (TFA, LC grade) from Applied Biosystems (Waltham, MA) and acetonitrile (ACN, HPLC grade) and 25% ammonia solution from EMD Millipore (Billerica, MA). Trypsin (sequencing grade), iodoacetamide, ammonium formate, triethylammonium bicarbonate (TEAB) buffer solution, 37% formaldehyde (CH₂O) in water (H₂O) and 20% deuterium-labeled formaldehyde (CD₂O) in deuterium-labeled water (D₂O) were purchased from Sigma-Aldrich (St. Louis, MO). Urea, methanol, chloroform and tris(2-carboxyethyl)phosphine (TCEP) solution were purchased from Thermo Fisher Scientific (San Jose, CA). HPLC grade H₂O was provided by a Milli-Q A10 water purification system (EMD Millipore, Billerica, MA). Sodium bicarbonate (NaHCO₃) was purchased from Chem Supply (Gillman, Australia). Oasis solid phase extraction (SPE) cartridges (10 mg sorbent, 30 μM particle size) were from Waters Corporation (Milford, MA). ¹⁵N-labeled recombinant human parathyroid hormone (PTH) 1-84 internal standard was purchased from Cell Sciences (Canton, MA) and its concentration was determined by amino acid analysis. World health organization (WHO) international standard human recombinant PTH 1-84 was from National Institute for Biological Standards and Control (NIBSC, Potters Bar, UK). Isotope-labeled oxidized PTH 1-20 and 7-20 internal standard peptides, both with methionine sulfoxide (M(O)) at residue 8 and 18 as well as ¹³C₆¹⁵N₁-labeled leucine (¹³C₆¹⁵N₁Leu) at residue 7 and 15 were purchased from Sigma-Aldrich (St. Louis, MO). Bortezomib was purchased from

Selleck Biochemicals (Houston, TX). TCH-013 was synthesized by the Tepe lab at Michigan State University (East Lansing, MI) as previously described [294]. All other reagents were commercially available and used without further purification.

7.2 Biological Samples

7.2.1 Patient Information and Immuno-Affinity Enrichment of PTH Proteins

Plasma samples were collected and prepared from patients with high concentrations of PTH 1-84 (500 to 1500 pg/mL as previously measured by chemiluminescent immunoassay) by the Martin lab at Saint Louis University (St. Louis, MO). For 1 mL of patient plasma, 20 μ L of PTH-depleted plasma containing 25 pg/ μ L 15 N-labeled PTH 1-84 was added immediately after blood draw and centrifuging separation for plasma. Then patient plasmas were frozen, shipped, stored at -80 $^{\circ}$ C and thawed at room temperature before immuno-affinity enrichment at DiaSorin (Stillwater, MN). As previously described [264], 350 μ g of magnetic beads coated with goat anti-PTH (39-84) antibody were added in 1 mL of plasma before incubation at room temperature with gentle rotation for immuno-affinity enrichment. The plasma was then removed using a DynaMag-2 Magnet (Life Technologies, Grand Island, NY) to capture the beads and washed with 1 mL each of phosphate-buffered saline (PBS) buffer, 35% ACN and PBS buffer followed by a final wash with 1 mL of 10 mM NH_4HCO_3 . Bound PTH was then eluted with 100 μ L of 3.5% ACN/0.9% FA after 10 min incubation with gentle rotation. The eluent was dried down under vacuum.

7.2.2 Cell Culture and Treatment Using TCH-013, Bortezomib and DMSO

Cell lysates from Human RPMI-8226 cells treated with TCH-013, Bortezomib or DMSO were provided by Tepe lab at Michigan State University (East Lansing, MI). The

conditions for cell culture were described previously [276]. RPMI-8226 cells were incubated with DMSO, Bortezomib or TCH-013 to final a concentrations of 0.1% (v/v), 0.1 μ M and 10 μ M, respectively, for 1 hour at 37 $^{\circ}$ C and 5% CO₂ before harvest and measurement of total protein concentration using BCA reagent.

7.3 Protein Digestion

7.3.1 Trypsin Digestion of PTH Standards and Immuno-Enriched Samples from Patient Plasmas

To each dried sample containing eluted PTH from 1 mL of patient plasma, 47.5 μ L of 10 mM NH₄HCO₃ and 500 ng trypsin dissolved in 2 μ L of H₂O were added. The solution was incubated at 37 $^{\circ}$ C for 4 h, and the digestion was quenched by adding 0.5 μ L of acetic acid. ¹³C₆¹⁵N₁Leu-labeled PTH 1-20 M8(O)M18(O) mixed with equal molar amount of ¹³C₆¹⁵N₁Leu-labeled PTH 7-20 M8(O)M18(O) was digested using the same conditions described above (trypsin : peptide = 1 : 1) to prepare a stock solution of internal standards containing 1 μ M ¹³C₆¹⁵N₁Leu-labeled PTH 1-13 M(O) and 7-13 M(O) as well as 2 μ M ¹³C₆¹⁵N₁Leu-labeled PTH 14-20 M(O). After dilution with H₂O, 5 nM ¹³C₆¹⁵N₁Leu-labeled PTH 1-13 M(O) and 7-13 M(O) as well as 10 nM ¹³C₆¹⁵N₁Leu-labeled PTH 14-20 M(O) in 10 μ L H₂O was spiked into the digested patient sample. After drying down under vacuum, the patient sample was reconstituted in 50 μ L of 0.1% TFA/2% ACN in H₂O and 5 μ L of each sample solution was used for LC-MS/MS analysis (described below). WHO PTH 1-84 standard was also digested with the same conditions to facilitate optimization of MS parameters for PTH peptides as described below.

7.3.2 Trypsin Digestion of Proteins in Lysates of TCH-013, Bortezomib and DMSO Treated RPMI-8226 Cells

Following a methanol/chloroform precipitation, 50 µg of TCH-013, Bortezomib or DMSO treated samples from each of three biological replicates were dried under vacuum, separately. Thereafter, each sample was dissolved in 8 M urea in 50 mM TEAB buffer (pH=8) and incubated at 37 °C for 30 min followed by reduction in 10 mM TCEP at 37 °C for 45 min and alkylation in 55 mM iodoacetamide at 37 °C for 45 min. Samples were then diluted to 1 M urea with 25 mM TEAB (pH=8) and digested for 18 hours at 37 °C with trypsin (1:40). Following digestion, samples were acidified to 1% FA, desalted using an Oasis SPE cartridge and then dried under vacuum.

7.4 Dimethyl Labeling of Digested Proteins from TCH-013, Bortezomib and DMSO Treated RPMI-8226 Cells

Each of the digested or desalted samples was re-dissolved in 200 µL of 100 mM TEAB buffer (pH=8). TCH-013 treated samples were labeled by adding 8 µL of 4% (v/v) CD₂O in 100 mM TEAB buffer (pH=8) while Bortezomib and DMSO treated samples were labeled by adding 8 µL of 4% (v/v) CH₂O in 100 mM TEAB buffer (pH=8), separately. 8 µL of 0.6 M NaBH₃CN was added to each sample before incubation for 1 hour at room temperature while mixing. Thereafter 32 µL of 1% (v/v) ammonia solution was added, vortexed, and 16 µL of formic acid was added to further quench the reaction. Each sample was dried under vacuum and reconstituted with 100 µL of 5mM ammonium formate/2% ACN, after which 50 µL of CD₂O labeled TCH-013 treated sample was mixed with either 50 µL of CH₂O labeled Bortezomib treated sample or 50 µL of CH₂O labeled DMSO treated sample.

7.5 Basic pH Reversed-Phase Fractionation of Digested and Dimethyl Labeled Proteins

Off-line basic reversed-phase fractionation was completed using an Alltima HP AQ C18 column (2.1 X 100 mm, 3 μ M, Grace Corporate, Columbia, MD) and an Agilent 1100 series HPLC system (Agilent Technologies, Santa Clara, CA). Solvent A is 5mM ammonium formate/2% ACN (pH=10) and solvent B is 5mM ammonium formate/90% ACN (pH=10). The flow rate of the LC system is 0.1 mL/min. 100 μ L of sample mixture consisting of equal amount of TCH-013 treated sample with either Bortezomib or DMSO treated sample in solvent A was injected. Then the percentage of solvent B in the mobile phase was increased from 0% with a gradient of 1.2% B/min for 5 min, 1% B/min for 2 min, 0.5% B/min for 19 min, 1% B/min for 4 min, 2% B/min for 8 min and 3% B/min for 7 min. Finally, the percentage of solvent B was increased to 95% within 1 min, kept for 4 min, decreased to 0% within 1 min and kept for 24 min for column cleaning and re-equilibration. Across the entire gradient, the first fraction was collected from 0 - 17.5 min. From 17.5 to 57.5 min, fractions were collected every 5 min. From 57.5 to 77.5 min, the last fraction was collected. Each of the total 10 fractions for each injected sample was dried under vacuum.

7.6 Mass Spectrometry

7.6.1 LC-MS/MS Analysis of Digested PTH standards and Immuno-Affinity Enriched Samples from Patient Plasmas

LC-ESI-MS and HCD-MS/MS analyses were performed using a Thermo Scientific Q Exactive Plus Orbitrap mass spectrometer (Thermo Fisher Scientific, San Jose, CA) coupled to an Agilent 1200 Infinity Binary LC System (Agilent Technologies,

Santa Clara, CA). Analyses were performed using automated methods created by the Xcalibur software (Thermo Fisher Scientific, San Jose, CA). Samples in 0.1 % TFA/2% ACN were loaded onto an IntegraFrit Sample Trap Magic AQ C18 Column (3 μm , 200 \AA , 150 μm I.D. x 25 mm in length, New Objective, Woburn, MA) at a flow rate of 2 $\mu\text{L}/\text{min}$ for 5 min using 0.1% FA/2% ACN as the loading buffer. The peptides concentrated on the trap column were eluted onto a PicoChip Magic AQ C18 Column (3 μm , 200 \AA , 150 μm I.D. x 105 mm in length, New Objective, Woburn, MA) at a flow rate of 800 nL/min using a linear 20 min gradient from 2% to 60% solvent B (Solvent A is 0.1% FA and solvent B is 0.1% FA/95% ACN). After gradient separation, the columns were cleaned with 90% solvent B for 6 min followed by re-equilibrium with 98% solvent A for 10 min. The spray voltage of the Q Exactive Plus Orbitrap mass spectrometer was maintained at 2.7 kV. The ion transfer tube of the mass spectrometer was set at 300 $^{\circ}\text{C}$, and the S-lens was at 60%. Full MS scans were acquired at m/z 250 – 2000, a resolving power of 70,000, an auto gain control (AGC) target value of 1.0×10^6 and a maximum injection time of 100 ms. HCD-MS/MS scans were taken at resolving power of 17,500, AGC target value of 5.0×10^4 ; maximum injection time of 50 ms and an isolation window of m/z 1.5. The resolving power of HCD-MS/MS scans was increased to 140,000 from 12.5 min to 13.9 min within the 20 min gradient to distinguish monitored fragment ions from artefact ions in patient samples. All spectra were recorded in profile mode. Targeted HCD-MS/MS analysis was performed based on the information listed in Table 5.1 where charge states of precursor ions, normalized collision energy (NCE) and monitored fragment ions have been optimized for optimal sensitivity by LC-ESI-HCD-

MS/MS analysis of PTH peptides from digested WHO PTH 1-84, $^{13}\text{C}_6^{15}\text{N}_1$ Leu-labeled PTH 1-20 M8(O)M18(O) and $^{13}\text{C}_6^{15}\text{N}_1$ Leu-labeled PTH 7-20 M8(O)M18(O).

7.6.2 LC-MS/MS Analysis of Digested, Dimethyl Labeled and Fractionated Proteins from TCH-013, Bortezomib and DMSO Treated RPMI-8226 Cells

Each of 10 fractions from each sample reconstituted in 120 μL 0.1% FA/2% ACN was analyzed by LC-MS/MS using a Q Exactive Plus mass spectrometer coupled to an Ultimate 3000 UHPLC (Thermo Fisher Scientific, San Jose, CA). Solvent A is 0.1% FA/2% ACN and solvent B is 0.1% FA in ACN. 6.4 μL of each fraction was injected onto a PepMap C18 trap column (75 μM X 2 cm, 3 μM , 100 \AA , Thermo Fisher Scientific, San Jose, CA) at 2 $\mu\text{L}/\text{min}$ for 15 min using 2% ACN and then separated through a PepMap C18 analytical column (75 μM X 15 cm, 2 μM , 100 \AA , Thermo Fisher Scientific, San Jose, CA) at a flow rate of 300 nL/min. During separation, the percentage of solvent B in mobile phase was increased from 2% to 10% in 1 min, from 10% to 35% in 50 min, from 35% to 60% in 1 min and from 60% to 90% in 1 min. Then the columns were cleaned at 90% B for 7 min before decreasing the % B to 2% in 1 min and re-equilibrating for 6 min. The spray voltage, temperature of ion transfer tube and S-lens of the Q Exactive Plus Orbitrap mass spectrometer was set at 1.8 kV, 250 $^\circ\text{C}$ and 50%, respectively. The full MS scans were acquired at m/z 300 – 2000, a resolving power of 70,000, an AGC target value of 3.0×10^6 and a maximum injection time of 30 ms. HCD-MS/MS scans were acquired at a resolving power of 17,500, AGC target value of 5.0×10^4 , maximum injection time of 120 ms, isolation window of m/z 1.4 and NCE of 25% for the top 12 most abundant ions in the MS spectra. All spectra were recorded in profile mode.

7.7 Data Analysis

7.7.1 Quantification of Full Length, Oxidized and Truncated PTH Variants in Patient Plasma

PTH 1-13 M(O) and PTH 1-13 represent any form of PTH 1-84 with and without oxidation within residue 1-13, respectively, while PTH 7-13 M(O) and PTH 7-13 represent any form of PTH 7-84 with and without oxidation, respectively, within residue 7-13. PTH 14-20 M(O) and PTH 14-20 represent any form of residue 14-84 containing-PTH (i.e., PTH 1-84 and 7-84) with and without oxidation within residue 14-20. PTH 27-44, 45-52, 53-65, 66-72 and 73-80 were also quantified using targeted HCD-MS/MS and ¹⁵N-labeled standards from digestion of ¹⁵N-labeled PTH 1-84.

For each of the PTH peptides listed in Table 5.1, its HCD-MS/MS spectra were averaged across the extracted ion current (XIC) chromatogram peak of the corresponding representative fragment ion. For each unoxidized peptide, the concentration ($C_{\text{non_ox}}$) was calculated using the equation (1),

$$C_{\text{non_ox}} = \frac{I_{\text{non_ox}}}{I_{^{15}\text{N_non_ox}}} \frac{C_{^{15}\text{N}}}{V} \quad (1)$$

where $I_{\text{non_ox}}$ and $I_{^{15}\text{N_non_ox}}$ are intensities of isotopic clusters of the representative product ion of the unoxidized PTH peptide and unoxidized ¹⁵N-labeled PTH peptide internal standard. $C_{^{15}\text{N}}$ is concentration of ¹⁵N-labeled PTH 1-84 or 7-84 internal standard spiked in plasma and V is the volume of original plasma sample. Concentrations of *in vivo* oxidized PTH peptides (C_{ox}) were determined using the equation (2),

$$C_{\text{ox}} = \frac{I_{\text{ox}} - \frac{I_{^{15}\text{N_ox}}}{I_{^{15}\text{N_non_ox}}} I_{\text{non_ox}}}{I_{^{13}\text{C}^{15}\text{N}}} \frac{C_{^{13}\text{C}^{15}\text{N}}}{V} \frac{1}{Y_{\text{recovery}}} \quad (2)$$

where I_{ox} , $I_{15N_{ox}}$, I_{13C15N} are the intensities of isotopic clusters of the representative product ion of the oxidized PTH peptide, oxidized ^{15}N -labeled PTH peptide internal standard and $^{13}C_6^{15}N_1$ Leu-labeled oxidized PTH peptide internal standard. C_{13C15N} is concentration of $^{13}C_6^{15}N_1$ Leu-labeled oxidized PTH peptide internal standard spiked in sample before LC-MS/MS analysis and $y_{recovery}$ is the recovery yield (66%) of the immuno LC-MS/MS method [264].

7.3.3 Bioinformatic Analysis for Proteomic Profiling of Proteins in TCH-013, Bortezomib and DMSO Treated RPMI-8226 Cells

Peptides and proteins were identified and quantified using the MaxQuant software package, version 1.5.3.30 [285, 295]. The terminology described below is specific to this software. Data was searched against human Uniprot protein database containing 78,909 entries. For searching, the enzyme specificity was set to be trypsin with the maximum number of missed cleavages set to be 2. The MS and MS/MS tolerance were set to be 4.5 ppm and 20 ppm, respectively. Fixed modifications were set as two-plex dimethyl labeling of lysine residues and peptide N-termini and carbamidomethylation of cysteine residues. Variable modifications were set as oxidation of methionine residues, acetylation of protein N termini and glycine-glycine addition (Gly-Gly) on the side chains of lysine residues. The false discovery rate (FDR) for peptide and protein identification was set to 1%. The minimum peptide length was set to be 6 and peptide re-quantification functions were enabled. Following a MaxQuant search, reverse and potential contaminant peptides and proteins were removed. Only proteins identified with at least 2 unique/razor peptides were considered as identified. In-house C++ script was written by David Perkins in the Bio21 Mass Spectrometry and

Proteomics Facility at the University of Melbourne and used to process the data in MaxQuant Evidence table for quantitative analysis. Briefly, for each experiment, peptides with same 'Mod. Peptide ID' but having different 'Fraction' numbers were removed to avoid incorrect H/L peptide ratios caused by shifted retention times of CH₂O and CD₂O labeled peptides in the basic reversed-phase fractionation. Then, to correct errors from sample mixing, H/L ratios of the remaining peptides were normalized so that the median ratio was 1. The normalized peptide H/L ratios were log₂ transformed and the median values were calculated for peptides with the same sequence as their grouped H/L ratios. A H/L ratio of protein group was derived by calculating a median value over normalized, log₂ transformed and grouped H/L ratio of peptides assigned to that protein group.

BIBLIOGRAPHY

BIBLIOGRAPHY

1. Bensimon, A., Heck, A.J.R., Aebersold, R., Mass spectrometry–based proteomics and network biology. *Annual Review of Biochemistry* **2012**, 81, 379.
2. Murphy, R.C., Tandem mass spectrometry of lipids: Molecular analysis of complex lipids, Royal Society of Chemistry, Cambridge, UK, **2014**.
3. Gabelica, V., Nucleic acids in the gas phase, in: *Physical Chemistry in Action*, Springer-Verlag Berlin Heidelberg, **2014**.
4. Kailemia, M.J., Ruhaak, L.R., Lebrilla, C.B., Amster, I.J., Oligosaccharide analysis by mass spectrometry: A review of recent developments. *Analytical Chemistry* **2014**, 86, 196.
5. Theodoridis, G., Gika, H.G., Wilson, I.D., Mass spectrometry-based holistic analytical approaches for metabolite profiling in systems biology studies. *Mass Spectrometry Reviews* **2011**, 30, 884.
6. Piez, K.A., Molecular weight determination of random coil polypeptides from collagen by molecular sieve chromatography. *Analytical Biochemistry* **1968**, 26, 305.
7. Grefrath, S.P., Reynolds, J.A., The molecular weight of the major glycoprotein from the human erythrocyte membrane. *Proceedings of the National Academy of Sciences of the United States of America* **1974**, 71, 3913.
8. Siegel, L.M., Monty, K.J., Determination of molecular weights and frictional ratios of proteins in impure systems by use of gel filtration and density gradient centrifugation. Application to crude preparations of sulfite and hydroxylamine reductases. *Biochimica et Biophysica Acta* **1966**, 112, 346.
9. Hoffmann, E.D., Stroobant, V., Mass spectrometry: Principles and applications, Third edition, John Wiley & Sons Ltd, The Atrium, Southern Gate, Chichester, West Sussex, England, **2007**.
10. Fenn, J.B., Mann, M., Meng, C.K., Wong, S.F., Whitehouse, C.M., Electrospray ionization for mass-spectrometry of large biomolecules. *Science* **1989**, 246, 64.
11. Tanaka, K., Waki, H., Ido, Y., Akita, S., Yoshida, Y., Yoshida, T., Matsuo, T., Protein and polymer analyses up to m/z 100 000 by laser ionization time-of-flight mass spectrometry. *Rapid Communications in Mass Spectrometry* **1988**, 2, 151.
12. Hilton, G.R., Benesch, J.L.P., Two decades of studying non-covalent biomolecular assemblies by means of electrospray ionization mass spectrometry. *Journal of the Royal Society Interface* **2012**, 9, 801.

13. Seeley, E.H., Schwamborn, K., Caprioli, R.M., Imaging of intact tissue sections: Moving beyond the microscope. *Journal of Biological Chemistry* **2011**, 286, 25459.
14. Seeley, E.H., Caprioli, R.M., 3D imaging by mass spectrometry: A new frontier. *Analytical Chemistry* **2012**, 84, 2105.
15. Cheng, C., Gross, M.L., Pittenauer, E., Complete structural elucidation of triacylglycerols by tandem sector mass spectrometry. *Analytical Chemistry* **1998**, 70, 4417.
16. Pittenauer, E., Allmaier, G., The renaissance of high-energy CID for structural elucidation of complex lipids: MALDI-TOF/RTOF-MS of alkali cationized triacylglycerols. *Journal of the American Society for Mass Spectrometry* **2009**, 20, 1037.
17. Shushan, B., A review of clinical diagnostic applications of liquid chromatography-tandem mass spectrometry. *Mass Spectrometry Reviews* **2010**, 29, 930.
18. Parker, C., Domanski, D., Percy, A., Chambers, A., Camenzind, A., Smith, D., Borchers, C., Mass spectrometry in high-throughput clinical biomarker assays: Multiple reaction monitoring in: L.S. Tang, N., Poon, T. (Eds.) *Chemical Diagnostics*, Springer Berlin Heidelberg, **2014**, 117.
19. Xia, Y., McLuckey, S.A., Evolution of instrumentation for the study of gas-phase ion/ion chemistry via mass spectrometry. *Journal of the American Society for Mass Spectrometry* **2008**, 19, 173.
20. Marshall, A.G., Chen, T., 40 years of Fourier transform ion cyclotron resonance mass spectrometry. *International Journal of Mass Spectrometry* **2015**, 377, 410.
21. Eliuk, S., Makarov, A., Evolution of Orbitrap mass spectrometry instrumentation. *Annual Review of Analytical Chemistry* **2015**, 8, 61.
22. Hendrickson, C., Quinn, J., Kaiser, N., Smith, D., Blakney, G., Chen, T., Marshall, A., Weisbrod, C., Beu, S., 21 tesla Fourier transform ion cyclotron resonance mass spectrometer: A national resource for ultrahigh resolution mass analysis. *Journal of the American Society for Mass Spectrometry* **2015**, 26, 1626.
23. Almeida, R., Pauling, J., Sokol, E., Hannibal-Bach, H., Ejsing, C., Comprehensive lipidome analysis by shotgun lipidomics on a hybrid quadrupole-Orbitrap-linear ion trap mass spectrometer. *Journal of the American Society for Mass Spectrometry* **2015**, 26, 133.
24. Fhaner, C.J., Liu, S., Ji, H., Simpson, R.J., Reid, G.E., Comprehensive lipidome profiling of isogenic primary and metastatic colon adenocarcinoma cell lines. *Analytical Chemistry* **2012**, 84, 8917.

25. Hebert, A.S., Merrill, A.E., Bailey, D.J., Still, A.J., Westphall, M.S., Strieter, E.R., Pagliarini, D.J., Coon, J.J., Neutron-encoded mass signatures for multiplexed proteome quantification. *Nature Methods* **2013**, 10, 332.
26. Zhurov, K.O., Fornelli, L., Wodrich, M.D., Laskay, U.A., Tsybin, Y.O., Principles of electron capture and transfer dissociation mass spectrometry applied to peptide and protein structure analysis. *Chemical Society Reviews* **2013**, 42, 5014.
27. Cox, J., Marginean, I., Kelly, R., Smith, R., Tang, K., Improving the sensitivity of mass spectrometry by using a new sheath flow electrospray emitter array at subambient pressures. *Journal of the American Society for Mass Spectrometry* **2014**, 25, 2028.
28. Kim, T., Udseth, H.R., Smith, R.D., Improved ion transmission from atmospheric pressure to high vacuum using a multicapillary inlet and electrodynamic ion funnel interface. *Analytical Chemistry* **2000**, 72, 5014.
29. Krutchinsky, A., Padovan, J., Cohen, H., Chait, B., Maximizing ion transmission from atmospheric pressure into the vacuum of mass spectrometers with a novel electrospray interface. *Journal of the American Society for Mass Spectrometry* **2015**, 26, 649.
30. Krutchinsky, A., Padovan, J., Cohen, H., Chait, B., Optimizing electrospray interfaces using slowly diverging conical duct (ConDuct) electrodes. *Journal of the American Society for Mass Spectrometry* **2015**, 26, 659.
31. Jääntti, S., Kivilompolo, M., Öhrnberg, L., Pietiläinen, K., Nygren, H., Orešič, M., Hyötyläinen, T., Quantitative profiling of bile acids in blood, adipose tissue, intestine, and gall bladder samples using ultra high performance liquid chromatography-tandem mass spectrometry. *Analytical and Bioanalytical Chemistry* **2014**, 406, 7799.
32. Damen, C.W.N., Isaac, G., Langridge, J., Hankemeier, T., Vreeken, R.J., Enhanced lipid isomer separation in human plasma using reversed-phase UPLC with ion-mobility/high-resolution MS detection. *Journal of Lipid Research* **2014**, 55, 1772.
33. Harris, G.A., Galhena, A.S., Fernández, F.M., Ambient sampling/ionization mass spectrometry: Applications and current trends. *Analytical Chemistry* **2011**, 83, 4508.
34. McLuckey, S.A., Goeringer, D.E., Slow heating methods in tandem mass spectrometry. *Journal of Mass Spectrometry* **1997**, 32, 461.
35. Sleno, L., Volmer, D.A., Ion activation methods for tandem mass spectrometry. *Journal of Mass Spectrometry* **2004**, 39, 1091.

36. Palumbo, A.M., Reid, G.E., Evaluation of gas-phase rearrangement and competing fragmentation reactions on protein phosphorylation site assignment using collision induced dissociation-MS/MS and MS³. *Analytical Chemistry* **2008**, 80, 9735.
37. Mikesch, L.M., Ueberheide, B., Chi, A., Coon, J.J., Syka, J.E.P., Shabanowitz, J., Hunt, D.F., The utility of ETD mass spectrometry in proteomic analysis. *Biochimica et Biophysica Acta (BBA) - Proteins and Proteomics* **2006**, 1764, 1811.
38. Zubarev, R.A., Kelleher, N.L., McLafferty, F.W., Electron capture dissociation of multiply charged protein cations. A nonergodic process. *Journal of the American Chemical Society* **1998**, 120, 3265.
39. Zhang, H., Cui, W., Wen, J., Blankenship, R.E., Gross, M.L., Native electrospray and electron-capture dissociation FTICR mass spectrometry for top-down studies of protein assemblies. *Analytical Chemistry* **2011**, 83, 5598.
40. Shaw, J.B., Li, W., Holden, D.D., Zhang, Y., Griep-Raming, J., Fellers, R.T., Early, B.P., Thomas, P.M., Kelleher, N.L., Brodbelt, J.S., Complete protein characterization using top-down mass spectrometry and ultraviolet photodissociation. *Journal of the American Chemical Society* **2013**, 135, 12646.
41. O'Brien, J.P., Needham, B.D., Henderson, J.C., Nowicki, E.M., Trent, M.S., Brodbelt, J.S., 193 nm ultraviolet photodissociation mass spectrometry for the structural elucidation of lipid A compounds in complex mixtures. *Analytical Chemistry* **2014**, 86, 2138.
42. Ko, B.J., Brodbelt, J.S., 193 nm ultraviolet photodissociation of deprotonated sialylated oligosaccharides. *Analytical Chemistry* **2011**, 83, 8192.
43. Smith, S.I., Brodbelt, J.S., Characterization of oligodeoxynucleotides and modifications by 193 nm photodissociation and electron photodetachment dissociation. *Analytical Chemistry* **2010**, 82, 7218.
44. O'Brien, J.P., Brodbelt, J.S., Structural characterization of gangliosides and glycolipids via ultraviolet photodissociation mass spectrometry. *Analytical Chemistry* **2013**, 85, 10399.
45. Aponte, J.R., Vasicek, L., Swaminathan, J., Xu, H., Koag, M.C., Lee, S., Brodbelt, J.S., Streamlining bottom-up protein identification based on selective ultraviolet photodissociation (UVPD) of chromophore-tagged histidine- and tyrosine-containing peptides. *Analytical Chemistry* **2014**, 86, 6237.
46. Brodbelt, J.S., Photodissociation mass spectrometry: New tools for characterization of biological molecules. *Chemical Society Reviews* **2014**, 43, 2757.
47. Lodish, H.F., Molecular cell biology, 6th edition., W.H. Freeman, New York, **2008**.

48. Feng, X., Liu, X., Luo, Q., Liu, B., Mass spectrometry in systems biology: An overview. *Mass Spectrometry Reviews* **2008**, 27, 635.
49. Brugger, B., Lipidomics: Analysis of the lipid composition of cells and subcellular organelles by electrospray ionization mass spectrometry. *Annual Review of Biochemistry* **2014**, 83, 79.
50. Angel, T.E., Aryal, U.K., Hengel, S.M., Baker, E.S., Kelly, R.T., Robinson, E.W., Smith, R.D., Mass spectrometry based proteomics: Existing capabilities and future directions. *Chemical Society Reviews* **2012**, 41, 3912.
51. Swaney, D.L., Wenger, C.D., Coon, J.J., The value of using multiple proteases for large-scale mass spectrometry-based proteomics. *Journal of Proteome Research* **2010**, 9, 1323.
52. Zhong, X., Zhang, Z., Jiang, S., Li, L., Recent advances in coupling capillary electrophoresis based separation techniques to ESI and MALDI MS. *Electrophoresis* **2014**, 35, 1214.
53. Kalli, A., Smith, G.T., Sweredoski, M.J., Hess, S., Evaluation and optimization of mass spectrometric settings during data-dependent acquisition mode: Focus on LTQ-Orbitrap mass analyzers. *Journal of Proteome Research* **2013**, 12, 3071.
54. Law, K.P., Lim, Y.P., Recent advances in mass spectrometry: Data independent analysis and hyper reaction monitoring. *Expert Review of Proteomics* **2013**, 10, 551.
55. Shi, T., Su, D., Liu, T., Tang, K., Camp, D.G., Qian, W.-J., Smith, R.D., Advancing the sensitivity of selected reaction monitoring-based targeted quantitative proteomics. *Proteomics* **2012**, 12, 1074.
56. McHugh, L., Arthur, J.W., Computational methods for protein identification from mass spectrometry data. *PLoS Computational Biology* **2008**, 4, e12.
57. Heck, A.J.R., Native mass spectrometry: A bridge between interactomics and structural biology. *Nature Methods* **2008**, 5, 927.
58. Nahnsen, S., Bielow, C., Reinert, K., Kohlbacher, O., Tools for label-free peptide quantification. *Molecular & Cellular Proteomics* **2013**, 12, 549.
59. Schilling, B., Rardin, M.J., MacLean, B.X., Zawadzka, A.M., Frewen, B.E., Cusack, M.P., Sorensen, D.J., Bereman, M.S., Jing, E., Wu, C.C., Verdin, E., Kahn, C.R., MacCoss, M.J., Gibson, B.W., Platform-independent and label-free quantitation of proteomic data using MS1 extracted ion chromatograms in Skyline: Application to protein acetylation and phosphorylation. *Molecular & Cellular Proteomics* **2012**, 11, 202.

60. Bantscheff, M., Lemeer, S., Savitski, M., Kuster, B., Quantitative mass spectrometry in proteomics: Critical review update from 2007 to the present. *Analytical and Bioanalytical Chemistry* **2012**, 404, 939.
61. Fonslow, B.R., Carvalho, P.C., Academia, K., Freeby, S., Xu, T., Nakorchevsky, A., Paulus, A., Yates, J.R., Improvements in proteomic metrics of low abundance proteins through proteome equalization using proteoMiner prior to MudPIT. *Journal of Proteome Research* **2011**, 10, 3690.
62. Rundlett, K.L., Armstrong, D.W., Mechanism of signal suppression by anionic surfactants in capillary electrophoresis–electrospray ionization mass spectrometry. *Analytical Chemistry* **1996**, 68, 3493.
63. Gropengiesser, J., Varadarajan, B.T., Stephanowitz, H., Krause, E., The relative influence of phosphorylation and methylation on responsiveness of peptides to MALDI and ESI mass spectrometry. *Journal of Mass Spectrometry* **2009**, 44, 821.
64. Olsen, J.V., Mann, M., Status of large-scale analysis of post-translational modifications by mass spectrometry. *Molecular & Cellular Proteomics* **2013**, 12, 3444.
65. Fahy, E., Subramaniam, S., Brown, H.A., Glass, C.K., Merrill, A.H., Murphy, R.C., Raetz, C.R.H., Russell, D.W., Seyama, Y., Shaw, W., Shimizu, T., Spener, F., van Meer, G., VanNieuwenhze, M.S., White, S.H., Witztum, J.L., Dennis, E.A., A comprehensive classification system for lipids. *Journal of Lipid Research* **2005**, 46, 839.
66. Ekroos, K., Lipidomics perspective: From molecular lipidomics to validated clinical diagnostics, in, Wiley-VCH Verlag GmbH & Co. KGaA, Weinheim, Germany, 2012.
67. Rainville, P.D., Stumpf, C.L., Shockcor, J.P., Plumb, R.S., Nicholson, J.K., Novel application of reversed-phase UPLC-oeTOF-MS for lipid analysis in complex biological mixtures: A new tool for lipidomics. *Journal of Proteome Research* **2007**, 6, 552.
68. Schuhmann, K., Almeida, R., Baumert, M., Herzog, R., Bornstein, S.R., Shevchenko, A., Shotgun lipidomics on a LTQ Orbitrap mass spectrometer by successive switching between acquisition polarity modes. *Journal of Mass Spectrometry* **2012**, 47, 96.
69. Han, X., Yang, K., Gross, R.W., Multi-dimensional mass spectrometry-based shotgun lipidomics and novel strategies for lipidomic analyses. *Mass Spectrometry Reviews* **2012**, 31, 134.
70. Ejsing, C.S., Sampaio, J.L., Surendranath, V., Duchoslav, E., Ekroos, K., Klemm, R.W., Simons, K., Shevchenko, A., Global analysis of the yeast lipidome by quantitative shotgun mass spectrometry. *Proceedings of the National Academy of Sciences* **2009**,

71. Murphy, R.C., Gaskell, S.J., New applications of mass spectrometry in lipid analysis. *Journal of Biological Chemistry* **2011**, 286, 25427.
72. Hsu, F., Turk, J., Electrospray ionization multiple-stage linear ion-trap mass spectrometry for structural elucidation of triacylglycerols: Assignment of fatty acyl groups on the glycerol backbone and location of double bonds. *Journal of the American Society for Mass Spectrometry* **2010**, 21, 657.
73. Hsu, F., Turk, J., Structural characterization of unsaturated glycerophospholipids by multiple-stage linear ion-trap mass spectrometry with electrospray ionization. *Journal of the American Society for Mass Spectrometry* **2008**, 19, 1681.
74. Hsu, F., Turk, J., Toward total structural analysis of cardiolipins: Multiple-stage linear ion-trap mass spectrometry on the $[M - 2H + 3Li]^+$ ions. *Journal of the American Society for Mass Spectrometry* **2010**, 21, 1863.
75. Taucher, M., Breuker, K., Characterization of modified RNA by top-down mass spectrometry. *Angewandte Chemie International Edition* **2012**, 51, 11289.
76. Tretyakova, N., Goggin, M., Sangaraju, D., Janis, G., Quantitation of DNA adducts by stable isotope dilution mass spectrometry. *Chemical Research in Toxicology* **2012**, 25, 2007.
77. Beck, J.L., Developments in electrospray ionization mass spectrometry of non-covalent DNA–ligand complexes. *Australian Journal of Chemistry* **2011**, 64, 705.
78. Varki, A., Biological roles of oligosaccharides: All of the theories are correct. *Glycobiology* **1993**, 3, 97.
79. Zaikin, V., Halket, J., A handbook of derivatives for mass spectrometry, in, IM Publications LLP, Charlton, Chichester, UK, 2009.
80. Oss, M., Krueve, A., Herodes, K., Leito, I., Electrospray ionization efficiency scale of organic compounds. *Analytical Chemistry* **2010**, 82, 2865.
81. Mirzaei, H., Regnier, F., Enhancing electrospray ionization efficiency of peptides by derivatization. *Analytical Chemistry* **2006**, 78, 4175.
82. Lu, Y., Zhou, X., Stemmer, P.M., Reid, G.E., Sulfonium ion derivatization, isobaric stable isotope labeling and data dependent CID- and ETD-MS/MS for enhanced phosphopeptide quantitation, identification and phosphorylation site characterization. *Journal of the American Society for Mass Spectrometry* **2012**, 23, 577.
83. Kulevich, S.E., Frey, B.L., Kreitinger, G., Smith, L.M., Alkylating tryptic peptides to enhance electrospray ionization mass spectrometry analysis. *Analytical Chemistry* **2010**, 82, 10135.

84. Lecchi, P., Olson, M., Brancia, F.L., The role of esterification on detection of protonated and deprotonated peptide ions in matrix assisted laser desorption/ionization (MALDI) mass spectrometry (MS). *Journal of the American Society for Mass Spectrometry* **2005**, 16, 1269.
85. Brancia, F.L., Oliver, S.G., Gaskell, S.J., Improved matrix-assisted laser desorption/ionization mass spectrometric analysis of tryptic hydrolysates of proteins following guanidination of lysine-containing peptides. *Rapid Communications in Mass Spectrometry* **2000**, 14, 2070.
86. Frahm, J.L., Bori, I.D., Comins, D.L., Hawkrigde, A.M., Muddiman, D.C., Achieving augmented limits of detection for peptides with hydrophobic alkyl tags. *Analytical Chemistry* **2007**, 79, 3989.
87. Yang, W., Adamec, J., Regnier, F.E., Enhancement of the LC/MS analysis of fatty acids through derivatization and stable isotope coding. *Analytical Chemistry* **2007**, 79, 5150.
88. Li, Y.L., Su, X., Stahl, P.D., Gross, M.L., Quantification of diacylglycerol molecular species in biological samples by electrospray ionization mass spectrometry after one-step derivatization. *Analytical Chemistry* **2007**, 79, 1569.
89. Woo, H., Go, E.P., Hoang, L., Trauger, S.A., Bowen, B., Siuzdak, G., Northen, T.R., Phosphonium labeling for increasing metabolomic coverage of neutral lipids using electrospray ionization mass spectrometry. *Rapid Communications in Mass Spectrometry* **2009**, 23, 1849.
90. Sandhoff, R., Brügger, B., Jeckel, D., Lehmann, W.D., Wieland, F.T., Determination of cholesterol at the low picomole level by nano-electrospray ionization tandem mass spectrometry. *Journal of Lipid Research* **1999**, 40, 126.
91. Han, X., Yang, K., Cheng, H., Fikes, K.N., Gross, R.W., Shotgun lipidomics of phosphoethanolamine-containing lipids in biological samples after one-step *in situ* derivatization. *Journal of Lipid Research* **2005**, 46, 1548.
92. Pham, H.T., Julian, R.R., Mass shifting and radical delivery with crown ether attachment for separation and analysis of phosphatidylethanolamine lipids. *Analytical Chemistry* **2014**, 86, 3020.
93. Julian, R.R., Beauchamp, J.L., Site specific sequestering and stabilization of charge in peptides by supramolecular adduct formation with 18-crown-6 ether by way of electrospray ionization. *International Journal of Mass Spectrometry* **2001**, 210–211, 613.
94. Dell, A., Preparation and desorption mass spectrometry of permethyl and peracetyl derivatives of oligosaccharides in: *Methods in Enzymology*, Academic Press, **1990**, 647.

95. Lamari, F.N., Kuhn, R., Karamanos, N.K., Derivatization of carbohydrates for chromatographic, electrophoretic and mass spectrometric structure analysis. *Journal of Chromatography B* **2003**, 793, 15.
96. Bereman, M.S., Comins, D.L., Muddiman, D.C., Increasing the hydrophobicity and electrospray response of glycans through derivatization with novel cationic hydrazides. *Chemical Communications* **2010**, 46, 237.
97. Walker, S.H., Papas, B.N., Comins, D.L., Muddiman, D.C., Interplay of permanent charge and hydrophobicity in the electrospray ionization of glycans. *Analytical Chemistry* **2010**, 82, 6636.
98. Nordström, A., Tarkowski, P., Tarkowska, D., Dolezal, K., Åstot, C., Sandberg, G., Moritz, T., Derivatization for LC-electrospray ionization-MS: A tool for improving reversed-phase separation and ESI responses of bases, ribosides, and intact nucleotides. *Analytical Chemistry* **2004**, 76, 2869.
99. Flarakos, J., Xiong, W., Glick, J., Vouros, P., A deoxynucleotide derivatization methodology for improving LC-ESI-MS detection. *Analytical Chemistry* **2005**, 77, 2373.
100. Null, A.P., Nepomuceno, A.I., Muddiman, D.C., Implications of hydrophobicity and free energy of solvation for characterization of nucleic acids by electrospray ionization mass spectrometry. *Analytical Chemistry* **2003**, 75, 1331.
101. Yang, W., Mirzaei, H., Liu, X., Regnier, F.E., Enhancement of amino acid detection and quantification by electrospray ionization mass spectrometry. *Analytical Chemistry* **2006**, 78, 4702.
102. Biemann, K., Contributions of mass spectrometry to peptide and protein structure. *Biological Mass Spectrometry* **1988**, 16, 99.
103. Ko, B., Brodbelt, J., Enhanced electron transfer dissociation of peptides modified at C-terminus with fixed charges. *Journal of the American Society for Mass Spectrometry* **2012**, 23, 1991.
104. Setner, B., Rudowska, M., Klem, E., Cebrat, M., Szewczuk, Z., Peptides derivatized with bicyclic quaternary ammonium ionization tags. Sequencing via tandem mass spectrometry. *Journal of Mass Spectrometry* **2014**, 49, 995.
105. Sadagopan, N., Watson, J.T., Investigation of the tris(trimethoxyphenyl)phosphonium acetyl charged derivatives of peptides by electrospray ionization mass spectrometry and tandem mass spectrometry. *Journal of the American Society for Mass Spectrometry* **2000**, 11, 107.
106. Stutzman, J.R., McLuckey, S.A., Ion/Ion reactions of MALDI-derived peptide ions: Increased sequence coverage via covalent and electrostatic modification upon charge inversion. *Analytical Chemistry* **2012**, 84, 10679.

107. Gunawardena, H.P., Emory, J.F., McLuckey, S.A., Phosphopeptide anion characterization via sequential charge inversion and electron-transfer dissociation. *Analytical Chemistry* **2006**, 78, 3788.
108. Gao, X., Wu, H., Lee, K.-C., Liu, H., Zhao, Y., Cai, Z., Jiang, Y., Stable isotope N-phosphorylation labeling for peptide *de novo* sequencing and protein quantification based on organic phosphorus chemistry. *Analytical Chemistry* **2012**, 84, 10236.
109. Stutzman, J.R., Hassell, K.M., McLuckey, S.A., Dissociation behavior of tryptic and intramolecular disulfide-linked peptide ions modified in the gas phase via ion/ion reactions. *International Journal of Mass Spectrometry* **2012**, 312, 195.
110. Robotham, S.A., Kluwe, C., Cannon, J.R., Ellington, A., Brodbelt, J.S., *De Novo* sequencing of peptides using selective 351 nm ultraviolet photodissociation mass spectrometry. *Analytical Chemistry* **2013**, 85, 9832.
111. O'Brien, J.P., Pruet, J.M., Brodbelt, J.S., Chromogenic chemical probe for protein structural characterization via ultraviolet photodissociation mass spectrometry. *Analytical Chemistry* **2013**, 85, 7391.
112. Cotham, V.C., Wine, Y., Brodbelt, J.S., Selective 351 nm photodissociation of cysteine-containing peptides for discrimination of antigen-binding regions of IgG fragments in bottom-up liquid chromatography–tandem mass spectrometry workflows. *Analytical Chemistry* **2013**, 85, 5577.
113. Ko, B., Brodbelt, J., Ultraviolet photodissociation of carboxylate-derivatized peptides in a quadrupole ion trap. *Journal of the American Society for Mass Spectrometry* **2011**, 22, 49.
114. Vasicek, L., Wilson, J., Brodbelt, J., Improved infrared multiphoton dissociation of peptides through N-terminal phosphonite derivatization. *Journal of the American Society for Mass Spectrometry* **2009**, 20, 377.
115. Ly, T., Julian, R.R., Residue-specific radical-directed dissociation of whole proteins in the gas phase. *Journal of the American Chemical Society* **2008**, 130, 351.
116. Diedrich, J.K., Julian, R.R., Site-specific radical directed dissociation of peptides at phosphorylated residues. *Journal of the American Chemical Society* **2008**, 130, 12212.
117. Marshall, D.L., Hansen, C.S., Trevitt, A.J., Oh, H.B., Blanksby, S.J., Photodissociation of TEMPO-modified peptides: new approaches to radical-directed dissociation of biomolecules. *Physical Chemistry Chemical Physics* **2014**, 16, 4871.
118. Hodyss, R., Cox, H.A., Beauchamp, J.L., Bioconjugates for tunable peptide fragmentation: Free radical Initiated peptide sequencing (FRIPS). *Journal of the American Chemical Society* **2005**, 127, 12436.

119. Lee, S., Glover, M.S., Reilly, J.P., Clemmer, D.E., Photosynthesis of a combinatorial peptide library in the gas phase. *Analytical Chemistry* **2015**, 87, 9384.
120. McGee, W.M., McLuckey, S.A., Efficient and directed peptide bond formation in the gas phase via ion/ion reactions. *Proceedings of the National Academy of Sciences* **2014**, 111, 1288.
121. Krishna, R.G., Wold, F., Identification of common post-translational modifications, in: Protein structure: A practical approach, Oxford University Press, Oxford, **1997**, 91.
122. Seo, J., Lee, K.J., Post-translational modifications and their biological functions: proteomic analysis and systematic approaches. *Journal of Biochemistry Molecular Biology* **2004**, 37, 35.
123. Oda, Y., Nagasu, T., Chait, B.T., Enrichment analysis of phosphorylated proteins as a tool for probing the phosphoproteome. *Nature Biotechnology* **2001**, 19, 379.
124. Wells, L., Gao, Y., Mahoney, J.A., Vosseller, K., Chen, C., Rosen, A., Hart, G.W., Dynamic O-glycosylation of nuclear and cytosolic proteins: Future characterization of the nucleocytoplasmic β -N-acetylglucosaminidase, O-GlcNAcase. *Journal of Biological Chemistry* **2002**, 277, 1755.
125. Diedrich, J.K., Julian, R.R., Facile identification of phosphorylation sites in peptides by radical directed dissociation. *Analytical Chemistry* **2011**, 83, 6818.
126. Mendoza, V.L., Vachet, R.W., Probing protein structure by amino acid-specific covalent labeling and mass spectrometry. *Mass Spectrometry Reviews* **2009**, 28, 785.
127. Zhou, X., Lu, Y., Wang, W., Borhan, B., Reid, G.E., 'Fixed charge' chemical derivatization and data dependant multistage tandem mass spectrometry for mapping protein surface residue accessibility. *Journal of the American Society for Mass Spectrometry* **2010**, 21, 1339.
128. Zhou, X., Mester, C., Stemmer, P.M., Reid, G.E., Oxidation-induced conformational changes in calcineurin determined by covalent labeling and tandem mass spectrometry. *Biochemistry* **2014**, 53, 6754.
129. Whitehurst, C.B., Soderblom, E.J., West, M.L., Hernandez, R., Goshe, M.B., Brown, D.T., Location and role of free cysteinyl residues in the sindbis virus E1 and E2 glycoproteins. *Journal of Virology* **2007**, 81, 6231.
130. Liu, Y., Kvaratskhelia, M., Hess, S., Qu, Y., Zou, Y., Modulation of replication protein A function by its hyperphosphorylation-induced conformational change involving DNA binding domain B. *Journal of Biological Chemistry* **2005**, 280, 32775.

131. Mendoza, V.L., Vachet, R.W., Protein surface mapping using diethylpyrocarbonate with mass spectrometric detection. *Analytical Chemistry* **2008**, 80, 2895.
132. Cammarata, M., Lin, K.-Y., Pruet, J., Liu, H.-w., Brodbelt, J., Probing the unfolding of myoglobin and domain C of PARP-1 with covalent labeling and top-down ultraviolet photodissociation mass spectrometry. *Analytical Chemistry* **2014**, 86, 2534.
133. Rappsilber, J., The beginning of a beautiful friendship: cross-linking/mass spectrometry and modelling of proteins and multi-protein complexes. *Journal of structural biology* **2011**, 173, 530.
134. Pham, N.D., Parker, R.B., Kohler, J.J., Photocrosslinking approaches to interactome mapping. *Current Opinion in Chemical Biology* **2013**, 17, 90.
135. Liu, F., Rijkers, D.T.S., Post, H., Heck, A.J.R., Proteome-wide profiling of protein assemblies by cross-linking mass spectrometry. *Nature Methods* **2015**, advance online publication,
136. Webb, I., Mentinova, M., McGee, W., McLuckey, S., Gas-phase intramolecular protein crosslinking via ion/ion reactions: Ubiquitin and a homobifunctional sulfo-NHS ester. *Journal of the American Society for Mass Spectrometry* **2013**, 24, 733.
137. Fhaner, C.J., Liu, S., Zhou, X., Reid, G.E., Functional group selective derivatization and gas-phase fragmentation reactions of plasmalogen glycerophospholipids. *Mass Spectrom (Tokyo)* **2013**, 2, S0015.
138. Lydic, T.A., Townsend, S., Adda, C.G., Collins, C., Mathivanan, S., Reid, G.E., Rapid and comprehensive 'shotgun' lipidome profiling of colorectal cancer cell derived exosomes. *Methods* **2015**,
139. Brown, S.H.J., Mitchell, T.W., Blanksby, S.J., Analysis of unsaturated lipids by ozone-induced dissociation. *Biochimica et Biophysica Acta (BBA) - Molecular and Cell Biology of Lipids* **2011**, 1811, 807.
140. Lemmon, M.A., Membrane recognition by phospholipid-binding domains. *Nature Reviews Molecular Cell Biology* **2008**, 9, 99.
141. Mitchell, T.W., Pham, H., Thomas, M.C., Blanksby, S.J., Identification of double bond position in lipids: From GC to OzID. *Journal of Chromatography B* **2009**, 877, 2722.
142. Hsu, F., Bohrer, A., Turk, J., Formation of lithiated adducts of glycerophosphocholine lipids facilitates their identification by electrospray ionization tandem mass spectrometry. *Journal of the American Society for Mass Spectrometry* **1998**, 9, 516.

143. Ekroos, K., Ejsing, C.S., Bahr, U., Karas, M., Simons, K., Shevchenko, A., Charting molecular composition of phosphatidylcholines by fatty acid scanning and ion trap MS³ fragmentation. *Journal of Lipid Research* **2003**, 44, 2181.
144. Stutzman, J.R., Blanksby, S.J., McLuckey, S.A., Gas-phase transformation of phosphatidylcholine cations to structurally informative anions via ion/ion chemistry. *Analytical Chemistry* **2013**, 85, 3752.
145. Pham, H.T., Maccarone, A.T., Thomas, M.C., Campbell, J.L., Mitchell, T.W., Blanksby, S.J., Structural characterization of glycerophospholipids by combinations of ozone- and collision-induced dissociation mass spectrometry: The next step towards "top-down" lipidomics. *Analyst* **2014**, 139, 204.
146. Huang, C., Lin, H., Li, S., Wang, G., Influence of the positions of *cis* double bonds in the sn-2-acyl chain of phosphatidylethanolamine on the bilayer's melting behavior. *Journal of Biological Chemistry* **1997**, 272, 21917.
147. Lin, Y., Schuurbiens, E., Van der Veen, S., De Deckere, E.A.M., Conjugated linoleic acid isomers have differential effects on triglyceride secretion in Hep G2 cells. *Biochimica et Biophysica Acta (BBA) - Molecular and Cell Biology of Lipids* **2001**, 1533, 38.
148. Heipieper, H.J., Meinhardt, F., Segura, A., The *cis*-*trans* isomerase of unsaturated fatty acids in *Pseudomonas* and *Vibrio*: Biochemistry, molecular biology and physiological function of a unique stress adaptive mechanism. *FEMS Microbiology Letters* **2003**, 229, 1.
149. Hsu, F., Turk, J., Elucidation of the double-bond position of long-chain unsaturated fatty acids by multiple-stage linear ion-trap mass spectrometry with electrospray ionization. *Journal of the American Society for Mass Spectrometry* **2008**, 19, 1673.
150. Xu, Y., Brenna, J.T., Atmospheric pressure covalent adduct chemical ionization tandem mass spectrometry for double bond localization in monoene- and diene-containing triacylglycerols. *Analytical Chemistry* **2007**, 79, 2525.
151. Ma, X., Xia, Y., Pinpointing double bonds in lipids by Paternò-Büchi reactions and mass spectrometry. *Angewandte Chemie International Edition* **2014**, 53, 2592.
152. Pham, H.T., Trevitt, A.J., Mitchell, T.W., Blanksby, S.J., Rapid differentiation of isomeric lipids by photodissociation mass spectrometry of fatty acid derivatives. *Rapid Communications in Mass Spectrometry* **2013**, 27, 805.
153. Pham, H.T., Ly, T., Trevitt, A.J., Mitchell, T.W., Blanksby, S.J., Differentiation of complex lipid isomers by radical-directed dissociation mass spectrometry. *Analytical Chemistry* **2012**, 84, 7525.
154. Pham, H.T., Prendergast, M.B., Dunstan, C.W., Trevitt, A.J., Mitchell, T.W., Julian, R.R., Blanksby, S.J., Dissociation of proton-bound complexes reveals geometry

- and arrangement of double bonds in unsaturated lipids. *International Journal of Mass Spectrometry* **2015**, doi:10.1016/j.ijms.2015.07.006,
155. Shendure, J., Ji, H., Next-generation DNA sequencing. *Nature Biotechnology* **2008**, 26, 1135.
 156. Wilson, J.J., Brodbelt, J.S., Ultraviolet photodissociation at 355 nm of fluorescently labeled oligosaccharides. *Analytical Chemistry* **2008**, 80, 5186.
 157. Zhang, X., Julian, R.R., Radical mediated dissection of oligosaccharides. *International Journal of Mass Spectrometry* **2014**, 372, 22.
 158. Konermann, L., Pan, J., Liu, Y.-H., Hydrogen exchange mass spectrometry for studying protein structure and dynamics. *Chemical Society Reviews* **2011**, 40, 1224.
 159. Reid, G.E., Simpson, R.J., O'Hair, R.A.J., Probing the fragmentation reactions of protonated glycine oligomers via multistage mass spectrometry and gas phase ion molecule hydrogen/deuterium exchange. *International Journal of Mass Spectrometry* **1999**, 190–191, 209.
 160. Polce, M.J., Ren, D., Wesdemiotis, C., Dissociation of the peptide bond in protonated peptides. *Journal of Mass Spectrometry* **2000**, 35, 1391.
 161. Cui, L., Yapici, I., Borhan, B., Reid, G.E., Quantification of competing H_3PO_4 Versus $\text{HPO}_3 + \text{H}_2\text{O}$ neutral losses from regioselective ^{18}O -labeled phosphopeptides. *Journal of the American Society for Mass Spectrometry* **2014**, 25, 141.
 162. Riba Garcia, I., Giles, K., Bateman, R.H., Gaskell, S.J., Studies of peptide a- and b-type fragment ions using stable isotope labeling and integrated ion mobility/tandem mass spectrometry. *Journal of the American Society for Mass Spectrometry* **2008**, 19, 1781.
 163. Zhang, X., Fhaner, C.J., Ferguson-Miller, S.M., Reid, G.E., Evaluation of ion activation strategies and mechanisms for the gas-phase fragmentation of sulfoquinovosyldiacylglycerol lipids from *Rhodobacter sphaeroides*. *International Journal of Mass Spectrometry* **2012**, 316-318, 100.
 164. Andersen, T.E., Kirpekar, F., Haselmann, K.F., RNA fragmentation in MALDI mass spectrometry studied by H/D-exchange: Mechanisms of general applicability to nucleic acids. *Journal of the American Society for Mass Spectrometry* **2006**, 17, 1353.
 165. Saad, O.M., Leary, J.A., Delineating mechanisms of dissociation for isomeric heparin disaccharides using isotope labeling and ion trap tandem mass spectrometry. *Journal of the American Society for Mass Spectrometry* **2004**, 15, 1274.

166. Dookeran, N.N., Yalcin, T., Harrison, A.G., Fragmentation reactions of protonated α -amino acids. *Journal of Mass Spectrometry* **1996**, 31, 500.
167. Chalmers, M.J., Busby, S.A., Pascal, B.D., He, Y., Hendrickson, C.L., Marshall, A.G., Griffin, P.R., Probing protein ligand interactions by automated hydrogen/deuterium exchange mass spectrometry. *Analytical Chemistry* **2006**, 78, 1005.
168. Jørgensen, T.J.D., Gårdsvoll, H., Ploug, M., Roepstorff, P., Intramolecular migration of amide hydrogens in protonated peptides upon collisional activation. *Journal of the American Chemical Society* **2005**, 127, 2785.
169. Rand, K.D., Zehl, M., Jensen, O.N., Jørgensen, T.J.D., Protein hydrogen exchange measured at single-residue resolution by electron transfer dissociation mass spectrometry. *Analytical Chemistry* **2009**, 81, 5577.
170. Rand, K.D., Adams, C.M., Zubarev, R.A., Jørgensen, T.J.D., Electron capture dissociation proceeds with a low degree of intramolecular migration of peptide amide hydrogens. *Journal of the American Chemical Society* **2008**, 130, 1341.
171. Pan, J., Han, J., Borchers, C.H., Konermann, L., Conformer-specific hydrogen exchange analysis of A β (1–42) oligomers by top-down electron capture dissociation mass spectrometry. *Analytical Chemistry* **2011**, 83, 5386.
172. Abzalimov, R.R., Kaplan, D.A., Easterling, M.L., Kaltashov, I.A., Protein conformations can be probed in top-down HDX MS experiments utilizing electron transfer dissociation of protein ions without hydrogen scrambling. *Journal of the American Society for Mass Spectrometry* **2009**, 20, 1514.
173. Kirkpatrick, D.S., Gerber, S.A., Gygi, S.P., The absolute quantification strategy: A general procedure for the quantification of proteins and post-translational modifications. *Methods* **2005**, 35, 265.
174. Krötz, F., Riexinger, T., Buerkle, M.A., Nithipatikom, K., Gloe, T., Sohn, H.Y., Campbell, W.B., Pohl, U., Membrane potential-dependent inhibition of platelet adhesion to endothelial cells by epoxyeicosatrienoic acids. *Arteriosclerosis, Thrombosis, and Vascular Biology* **2004**, 24, 595.
175. Chan, W., Chen, B., Wang, L., Taghizadeh, K., Demott, M.S., Dedon, P.C., Quantification of the 2-deoxyribonolactone and nucleoside 5'-aldehyde products of 2-deoxyribose oxidation in DNA and cells by isotope-dilution gas chromatography mass spectrometry: Differential effects of γ -radiation and Fe²⁺-EDTA. *Journal of the American Chemical Society* **2010**, 132, 6145.
176. Merrifield, R.B., Solid phase synthesis (Nobel Lecture). *Angewandte Chemie International Edition* **1985**, 24, 799.

177. Gerber, S.A., Rush, J., Stemman, O., Kirschner, M.W., Gygi, S.P., Absolute quantification of proteins and phosphoproteins from cell lysates by tandem MS. *Proceedings of the National Academy of Sciences* **2003**, 100, 6940.
178. Brun, V., Dupuis, A., Adrait, A., Marcellin, M., Thomas, D., Court, M., Vandenesch, F., Garin, J., Isotope-labeled protein standards: Toward absolute quantitative proteomics. *Molecular & Cellular Proteomics* **2007**, 6, 2139.
179. Hanke, S., Besir, H., Oesterhelt, D., Mann, M., Absolute SILAC for accurate quantitation of proteins in complex mixtures down to the attomole level. *Journal of Proteome Research* **2008**, 7, 1118.
180. Carroll, K.M., Simpson, D.M., Eyers, C.E., Knight, C.G., Brownridge, P., Dunn, W.B., Winder, C.L., Lanthaler, K., Pir, P., Malys, N., Kell, D.B., Oliver, S.G., Gaskell, S.J., Beynon, R.J., Absolute quantification of the glycolytic pathway in yeast: Deployment of a complete QconCAT approach. *Molecular & Cellular Proteomics* **2011**, 10, M111.007633.
181. Singh, S., Springer, M., Steen, J., Kirschner, M.W., Steen, H., FLEXIQuant: A novel tool for the absolute quantification of proteins, and the simultaneous identification and quantification of potentially modified peptides. *Journal of Proteome Research* **2009**, 8, 2201.
182. Gold, H., Mirzaian, M., Dekker, N., Joao Ferraz, M., Lugtenburg, J., Codée, J.D.C., van der Marel, G.A., Overkleeft, H.S., Linthorst, G.E., Groener, J.E.M., Aerts, J.M., Poorthuis, B.J.H.M., Quantification of globotriaosylsphingosine in plasma and urine of fabry patients by stable isotope ultraperformance liquid chromatography–Tandem mass spectrometry. *Clinical Chemistry* **2013**, 59, 547.
183. Noack, S., Wiechert, W., Quantitative metabolomics: A phantom? *Trends in Biotechnology* **2014**, 32, 238.
184. Orlando, R., Lim, J.-M., Atwood, J.A., Angel, P.M., Fang, M., Aoki, K., Alvarez-Manilla, G., Moremen, K.W., York, W.S., Tiemeyer, M., Pierce, M., Dalton, S., Wells, L., IDAWG: Metabolic incorporation of stable isotope labels for quantitative glycomics of cultured cells. *Journal of Proteome Research* **2009**, 8, 3816.
185. Ong, S., Blagoev, B., Kratchmarova, I., Kristensen, D.B., Steen, H., Pandey, A., Mann, M., Stable isotope labeling by amino acids in cell culture, SILAC, as a simple and accurate approach to expression proteomics. *Molecular & Cellular Proteomics* **2002**, 1, 376.
186. Cambridge, S.B., Gnad, F., Nguyen, C., Bermejo, J.L., Krüger, M., Mann, M., Systems-wide proteomic analysis in mammalian cells reveals conserved, functional protein turnover. *Journal of Proteome Research* **2011**, 10, 5275.

187. Geiger, T., Wisniewski, J.R., Cox, J., Zanivan, S., Kruger, M., Ishihama, Y., Mann, M., Use of stable isotope labeling by amino acids in cell culture as a spike-in standard in quantitative proteomics. *Nature Protocols* **2011**, 6, 147.
188. Boersema, P.J., Raijmakers, R., Lemeer, S., Mohammed, S., Heck, A.J.R., Multiplex peptide stable isotope dimethyl labeling for quantitative proteomics. *Nature Protocols* **2009**, 4, 484.
189. Shiio, Y., Aebersold, R., Quantitative proteome analysis using isotope-coded affinity tags and mass spectrometry. *Nature Protocols* **2006**, 1, 139.
190. Zhang, R., Sioma, C.S., Wang, S., Regnier, F.E., Fractionation of isotopically labeled peptides in quantitative proteomics. *Analytical Chemistry* **2001**, 73, 5142.
191. Werner, T., Sweetman, G., Savitski, M.F., Mathieson, T., Bantscheff, M., Savitski, M.M., Ion coalescence of neutron encoded TMT 10-plex reporter ions. *Analytical Chemistry* **2014**, 86, 3594.
192. Pottiez, G., Wiederin, J., Fox, H.S., Ciborowski, P., Comparison of 4-plex to 8-plex iTRAQ quantitative measurements of proteins in human plasma samples. *Journal of Proteome Research* **2012**, 11, 3774.
193. Gu, L., Evans, A., Robinson, R.S., Sample multiplexing with cysteine-selective approaches: cysDML and cPILOT. *Journal of the American Society for Mass Spectrometry* **2015**, 26, 615.
194. Berry, K.A.Z., Murphy, R.C., Analysis of cell membrane aminophospholipids as isotope-tagged derivatives. *Journal of Lipid Research* **2005**, 46, 1038.
195. Berry, K.A.Z., Murphy, R.C., Analysis of polyunsaturated aminophospholipid molecular species using isotope-tagged derivatives and tandem mass spectrometry/mass spectrometry/mass spectrometry. *Analytical Biochemistry* **2006**, 349, 118.
196. Berry, K.A.Z., Turner, W.W., VanNieuwenhze, M.S., Murphy, R.C., Stable isotope labeled 4-(dimethylamino)benzoic acid derivatives of glycerophosphoethanolamine lipids. *Analytical Chemistry* **2009**, 81, 6633.
197. Nabetani, T., Makino, A., Hullin-Matsuda, F., Hirakawa, T.A., Takeoka, S., Okino, N., Ito, M., Kobayashi, T., Hirabayashi, Y., Multiplex analysis of sphingolipids using amine-reactive tags (iTRAQ). *Journal of Lipid Research* **2011**, 52, 1294.
198. Hahne, H., Neubert, P., Kuhn, K., Etienne, C., Bomgarden, R., Rogers, J.C., Kuster, B., Carbonyl-reactive tandem mass tags for the proteome-wide quantification of N-linked glycans. *Analytical Chemistry* **2012**, 84, 3716.

199. Ow, S.Y., Salim, M., Noirel, J., Evans, C., Rehman, I., Wright, P.C., iTRAQ underestimation in simple and complex Mixtures: "The good, the bad and the ugly". *Journal of Proteome Research* **2009**, 8, 5347.
200. Karp, N.A., Huber, W., Sadowski, P.G., Charles, P.D., Hester, S.V., Lilley, K.S., Addressing Accuracy and Precision Issues in iTRAQ Quantitation. *Molecular and Cellular Proteomics* **2010**, 9, 1885.
201. Ting, L., Rad, R., Gygi, S.P., Haas, W., MS³ eliminates ratio distortion in isobaric multiplexed quantitative proteomics. *Nature Methods* **2011**, 8, 937.
202. Wenger, C.D., Lee, M.V., Hebert, A.S., McAlister, G.C., Phanstiel, D.H., Westphall, M.S., Coon, J.J., Gas-phase purification enables accurate, multiplexed proteome quantification with isobaric tagging. *Nature Methods* **2011**, 8, 933.
203. Sturm, R.M., Lietz, C.B., Li, L.J., Improved isobaric tandem mass tag quantification by ion mobility mass spectrometry. *Rapid Communications in Mass Spectrometry* **2014**, 28, 1051.
204. Lligadas, G., Ronda, J.C., Galia, M., Cadiz, V., Renewable polymeric materials from vegetable oils: a perspective. *Materials Today* **2013**, 16, 337.
205. Martin-Polvillo, M., Marquez-Ruiz, G., Dobarganes, M.C., Oxidative stability of sunflower oils differing in unsaturation degree during long-term storage at room temperature. *Journal of the American Oil Chemists Society* **2004**, 81, 577.
206. Aladedunye, F.A., Przybylski, R., Protecting oil during frying: A comparative study. *European Journal of Lipid Science and Technology* **2009**, 111, 893.
207. Zlatanic, A., Lava, C., Zhang, W., Petrovic, Z.S., Effect of structure on properties of polyols and polyurethanes based on different vegetable oils. *Journal of Polymer Science Part B-Polymer Physics* **2004**, 42, 809.
208. Shogren, R.L., Petrovic, Z., Liu, Z.S., Erhan, S.Z., Biodegradation behavior of some vegetable oil-based polymers. *Journal of Polymers and the Environment* **2004**, 12, 173.
209. Mallegol, J., Gardette, J.L., Lemaire, J., Long-term behavior of oil-based varnishes and paints I. Spectroscopic analysis of curing drying oils. *Journal of the American Oil Chemists Society* **1999**, 76, 967.
210. Neff, W.E., List, G.R., Oxidative stability of natural and randomized high-palmitic- and high-stearic-acid oils from genetically modified soybean varieties. *Journal of the American Oil Chemists Society* **1999**, 76, 825.
211. Asadauskas, S., Erhan, S.Z., Thin-film test to investigate liquid oxypolymerization of nonvolatile analytes: Assessment of vegetable oils and biodegradable lubricants. *Journal of the American Oil Chemists Society* **2001**, 78, 1029.

212. Wesdemiotis, C., Solak, N., Polce, M.J., Dabney, D.E., Chaicharoen, K., Katzenmeyer, B.C., Fragmentation pathways of polymer ions. *Mass Spectrometry Reviews* **2011**, 30, 523.
213. Mentinova, M., McLuckey, S.A., Intra- and inter-molecular cross-linking of peptide ions in the gas phase: Reagents and conditions. *Journal of the American Society for Mass Spectrometry* **2011**, 22, 912.
214. Lee, S., Julian, R.R., Valentine, S.J., Reilly, J.P., Clemmer, D.E., Biomolecular condensation via ultraviolet excitation in vacuo. *International Journal of Mass Spectrometry* **2012**, 316, 6.
215. Muller, C., Kanawati, B., Rock, T.M., Forcisi, S., Moritz, F., Schmitt-Kopplin, P., Dimer ion formation and intermolecular fragmentation of 1,2-diacylglycerols revealed by electrospray ionization Fourier transform ion cyclotron resonance mass spectrometry for more comprehensive lipid analysis. *Rapid Communications in Mass Spectrometry* **2014**, 28, 1735.
216. Meier, M.A.R., Metzger, J.O., Schubert, U.S., Plant oil renewable resources as green alternatives in polymer science. *Chemical Society Reviews* **2007**, 36, 1788.
217. Osburn, S., O'Hair, R.A.J., Unleashing radical sites in non-covalent complexes: The case of the protonated S-nitrosocysteine/18-crown-6 complex. *Rapid Communications in Mass Spectrometry* **2013**, 27, 2783.
218. Barlow, C.K., McFadyen, W.D., O'Hair, R.A.J., Formation of cationic peptide radicals by gas-phase redox reactions with trivalent chromium, manganese, iron, and cobalt complexes. *Journal of the American Chemical Society* **2005**, 127, 6109.
219. Kong, R.P.W., Quan, Q., Hao, Q., Lai, C.K., Siu, C.K., Chu, I.K., Formation and dissociation of phosphorylated peptide radical cations. *Journal of the American Society for Mass Spectrometry* **2012**, 23, 2094.
220. Bird, S.S., Marur, V.R., Sniatynski, M.J., Greenberg, H.K., Kristal, B.S., Serum lipidomics profiling using LC-MS and high-energy collisional dissociation fragmentation: Focus on triglyceride detection and characterization. *Analytical Chemistry* **2011**, 83, 6648.
221. McClellan, J.E., Murphy, J.P., Mulholland, J.J., Yost, R.A., Effects of fragile ions on mass resolution and on isolation for tandem mass spectrometry in the quadrupole ion trap mass spectrometer. *Analytical Chemistry* **2002**, 74, 402.
222. Wells, J.M., Plass, W.R., Patterson, G.E., Zheng, O.Y., Badman, E.R., Cooks, R.G., Chemical mass shifts in ion trap mass spectrometry: Experiments and simulations. *Analytical Chemistry* **1999**, 71, 3405.
223. Blanksby, S.J., Ellison, G.B., Bond dissociation energies of organic molecules. *Accounts of Chemical Research* **2003**, 36, 255.

224. McAnoy, A.M., Wu, C.C., Murphy, R.C., Direct qualitative analysis of triacylglycerols by electrospray mass spectrometry using a linear ion trap. *Journal of the American Society for Mass Spectrometry* **2005**, 16, 1498.
225. Pellissier, H., Santelli, M., The use of arynes in organic synthesis. *Tetrahedron* **2003**, 59, 701.
226. Wenthold, P.G., Squires, R.R., Lineberger, W.C., Ultraviolet photoelectron spectroscopy of the *o*-, *m*-, and *p*-benzyne negative ions. Electron affinities and singlet-triplet splittings for *o*-, *m*-, and *p*-benzyne. *Journal of the American Chemical Society* **1998**, 120, 5279.
227. Fadeel, B., Xue, D., The ins and outs of phospholipid asymmetry in the plasma membrane: Roles in health and disease. *Critical Reviews in Biochemistry and Molecular Biology* **2009**, 44, 264.
228. Vance, J.E., Tasseva, G., Formation and function of phosphatidylserine and phosphatidylethanolamine in mammalian cells. *Biochimica Et Biophysica Acta-Molecular and Cell Biology of Lipids* **2013**, 1831, 543.
229. Chaurio, R.A., Janko, C., Munoz, L.E., Frey, B., Herrmann, M., Gaipf, U.S., Phospholipids: Key players in apoptosis and immune regulation. *Molecules* **2009**, 14, 4892.
230. Zhang, W., Tsan, R., Schroit, A.J., Fidler, I.J., Apoptotic cells initiate endothelial cell sprouting via electrostatic signaling. *Cancer Research* **2005**, 65, 11529.
231. Min, H.K., Lim, S., Chung, B.C., Moon, M.H., Shotgun lipidomics for candidate biomarkers of urinary phospholipids in prostate cancer. *Analytical and Bioanalytical Chemistry* **2011**, 399, 823.
232. Zhu, C., Liang, Q., Hu, P., Wang, Y., Luo, G., Phospholipidomic identification of potential plasma biomarkers associated with type 2 diabetes mellitus and diabetic nephropathy. *Talanta* **2011**, 85, 1711.
233. Donovan, E.L., Pettine, S.M., Hickey, M.S., Hamilton, K.L., Miller, B.F., Lipidomic analysis of human plasma reveals ether-linked lipids that are elevated in morbidly obese humans compared to lean. *Diabetology & Metabolic Syndrome* **2013**, 5,
234. Han, X., Multi-dimensional mass spectrometry-based shotgun lipidomics and the altered lipids at the mild cognitive impairment stage of Alzheimer's disease. *Biochimica Et Biophysica Acta-Molecular and Cell Biology of Lipids* **2010**, 1801, 774.
235. Wang, X., Li, N., Liu, B., Sun, H., Chen, T., Li, H.Z., Qiu, J., Zhang, L., Wan, T., Cao, X., A novel human phosphatidylethanolamine-binding protein resists tumor necrosis factor alpha-induced apoptosis by inhibiting mitogen-activated protein

- kinase pathway activation and phosphatidylethanolamine externalization. *Journal of Biological Chemistry* **2004**, 279, 45855.
236. Rappley, I., Myers, D.S., Milne, S.B., Ivanova, P.T., LaVoie, M.J., Brown, H.A., Selkoe, D.J., Lipidomic profiling in mouse brain reveals differences between ages and genders, with smaller changes associated with alpha-synuclein genotype. *Journal of Neurochemistry* **2009**, 111, 15.
237. Hein, E.M., Blank, L.M., Heyland, J., Baumbach, J.I., Schmid, A., Hayen, H., Glycerophospholipid profiling by high-performance liquid chromatography/mass spectrometry using exact mass measurements and multi-stage mass spectrometric fragmentation experiments in parallel. *Rapid Communications in Mass Spectrometry* **2009**, 23, 1636.
238. Lydic, T.A., Busik, J.V., Reid, G.E., A monophasic extraction strategy for the simultaneous lipidome analysis of polar and nonpolar retina lipids. *Journal of Lipid Research* **2014**, 55, 1797.
239. Christoforou, A.L., Lilley, K.S., Isobaric tagging approaches in quantitative proteomics: The ups and downs. *Analytical and Bioanalytical Chemistry* **2012**, 404, 1029.
240. Hsu, F., Turk, J., Characterization of phosphatidylethanolamine as a lithiated adduct by triple quadrupole tandem mass spectrometry with electrospray ionization. *Journal of Mass Spectrometry* **2000**, 35, 596.
241. Hsu, F., Turk, J., Electrospray ionization with low-energy collisionally activated dissociation tandem mass spectrometry of glycerophospholipids: Mechanisms of fragmentation and structural characterization. *Journal of Chromatography B-Analytical Technologies in the Biomedical and Life Sciences* **2009**, 877, 2673.
242. Liebisch, G., Vizcaino, J.A., Kofeler, H., Trotschmuller, M., Griffiths, W.J., Schmitz, G., Spener, F., Wakelam, M.J., Shorthand notation for lipid structures derived from mass spectrometry. *Journal of Lipid Research* **2013**, 54, 1523.
243. Haimi, P., Uphoff, A., Hermansson, M., Somerharju, P., Software tools for analysis of mass spectrometric lipidome data. *Analytical Chemistry* **2006**, 78, 8324.
244. Isaia, G., Marchetti, M., PTH and PTH-related peptides in: Brandi, M. L., Brown, E. M. (Eds.) Hypoparathyroidism, Springer Milan, 2015, pp. 19.
245. Bushinsky, D.A., Monk, R.D., Electrolyte quintet: Calcium. *Lancet* **1998**, 352, 306.
246. Fraser, W.D., Hyperparathyroidism. *Lancet* **2009**, 374, 145.
247. Couchman, L., Taylor, D.R., Krastins, B., Lopez, M.F., Moniz, C.F., LC-MS candidate reference methods for the harmonisation of parathyroid hormone (PTH)

- measurement: A review of recent developments and future considerations. *Clinical Chemistry and Laboratory Medicine* **2014**, 52, 1251.
248. D'Amour, P., Acute and chronic regulation of circulating PTH: Significance in health and in disease. *Clinical Biochemistry* **2012**, 45, 964.
249. Lopez, M.F., Rezai, T., Sarracino, D.A., Prakash, A., Krastins, B., Athanas, M., Singh, R.J., Barnidge, D.R., Oran, P., Borges, C., Nelson, R.W., Selected reaction monitoring-mass spectrometric immunoassay responsive to parathyroid hormone and related variants. *Clinical Chemistry* **2010**, 56, 281.
250. Zhang, C., Weber, B.V., Thammavong, J., Grover, T.A., Wells, D.S., Identification of carboxyl-terminal peptide fragments of parathyroid hormone in human plasma at low-picomolar levels by mass spectrometry. *Analytical Chemistry* **2006**, 78, 1636.
251. Pines, M., Adams, A.E., Stueckle, S., Bessalle, R., Rashti-Behar, V., Chorev, M., Rosenblatt, M., Suva, L.J., Generation and characterization of human kidney cell lines stably expressing recombinant human PTH/PTHrP receptor: Lack of interaction with a C-terminal human PTH peptide. *Endocrinology* **1994**, 135, 1713.
252. Segre, G.V., Habener, J.F., Powell, D., Tregear, G.W., Potts, J.T., Parathyroid hormone in human plasma: Immunochemical characterization and biological implications. *Journal of Clinical Investigation* **1972**, 51, 3163.
253. Murray, T.M., Rao, L.G., Divieti, P., Bringhurst, F.R., Parathyroid hormone secretion and action: Evidence for discrete receptors for the carboxyl-terminal region and related biological actions of carboxyl-terminal ligands. *Endocrine Reviews* **2005**, 26, 78.
254. Ji, J.A., Zhang, B., Cheng, W., Wang, Y.J., Methionine, tryptophan, and histidine oxidation in a model protein, PTH: Mechanisms and stabilization. *Journal of Pharmaceutical Sciences* **2009**, 98, 4485.
255. Frelinger, A.L., 3rd, Zull, J.E., The role of the methionine residues in the structure and function of parathyroid hormone. *Archives of Biochemistry and Biophysics* **1986**, 244, 641.
256. Zull, J.E., Smith, S.K., Wiltshire, R., Effect of methionine oxidation and deletion of amino-terminal residues on the conformation of parathyroid hormone. Circular dichroism studies. *Journal of Biological Chemistry* **1990**, 265, 5671.
257. Hocher, B., Armbruster, F.P., Stoeva, S., Reichetzedler, C., Gron, H.J., Lieker, I., Khadzhynov, D., Slowinski, T., Roth, H.J., Measuring parathyroid hormone (PTH) in patients with oxidative stress - do we need a fourth generation parathyroid hormone assay? *PLoS One* **2012**, 7, e40242.
258. Vieira, J.G., PTH assays: Understanding what we have and forecasting what we will have. *Journal of Osteoporosis* **2012**, 2012, 523246.

259. Gao, P., Scheibel, S., D'Amour, P., John, M.R., Rao, S.D., Schmidt-Gayk, H., Cantor, T.L., Development of a novel immunoradiometric assay exclusively for biologically active whole parathyroid hormone 1-84: Implications for improvement of accurate assessment of parathyroid function. *Journal of Bone and Mineral Research* **2001**, 16, 605.
260. John, M.R., Goodman, W.G., Gao, P., Cantor, T.L., Salusky, I.B., Juppner, H., A novel immunoradiometric assay detects full-length human PTH but not aminotermi-nally truncated fragments: implications for PTH measurements in renal failure. *Journal of Clinical Endocrinology & Metabolism* **1999**, 84, 4287.
261. Brossard, J.H., Lepage, R., Cardinal, H., Roy, L., Rousseau, L., Dorais, C., D'Amour, P., Influence of glomerular filtration rate on non-(1-84) parathyroid hormone (PTH) detected by intact PTH assays. *Clinical Chemistry* **2000**, 46, 697.
262. Lafferty, F.W., Hamlin, C.R., Corrado, K.R., Arnold, A., Shuck, J.M., Primary hyperparathyroidism with a low-normal, atypical serum parathyroid hormone as shown by discordant immunoassay curves. *Journal of Clinical Endocrinology & Metabolism* **2006**, 91, 3826.
263. Kumar, V., Barnidge, D.R., Chen, L.S., Twentyman, J.M., Cradic, K.W., Grebe, S.K., Singh, R.J., Quantification of serum 1-84 parathyroid hormone in patients with hyperparathyroidism by immunocapture in situ digestion liquid chromatography-tandem mass spectrometry. *Clinical Chemistry* **2010**, 56, 306.
264. Cui, L., Evaluation and improvement of mass spectrometry based strategies for protein post-translational modification analysis, Michigan State University, Ann Arbor, **2014**, 243.
265. Monier-Faugere, M.C., Geng, Z., Mawad, H., Friedler, R.M., Gao, P., Cantor, T.L., Malluche, H.H., Improved assessment of bone turnover by the PTH-(1-84)/large C-PTH fragments ratio in ESRD patients. *Kidney International* **2001**, 60, 1460.
266. Salusky, I.B., Goodman, W.G., Adynamic renal osteodystrophy: is there a problem? *Journal of the American Society of Nephrology* **2001**, 12, 1978.
267. Singh, R.J., Hines, J.M., Lopez, M.F., Krastins, B., Hoofnagle, A.N., Mass spectrometric immunoassay raises doubt for the existence of parathyroid hormone fragment 7-84. *Clinical Chemistry* **2015**, 61, 558.
268. Murata, S., Yashiroda, H., Tanaka, K., Molecular mechanisms of proteasome assembly. *Nature Reviews Molecular Cell Biology* **2009**, 10, 104.
269. Kisselev, A.F., van der Linden, W.A., Overkleeft, H.S., Proteasome inhibitors: An expanding army attacking a unique target. *Chemistry & biology* **2012**, 19, 99.
270. Beck, P., Dubiella, C., Groll, M., Covalent and non-covalent reversible proteasome inhibition. *Biological Chemistry* **2012**, 393, 1101.

271. Chapman, M.A., Lawrence, M.S., Keats, J.J., Cibulskis, K., Sougnez, C., Schinzel, A.C., Harview, C.L., Brunet, J.-P., Ahmann, G.J., Adli, M., Anderson, K.C., Ardlie, K.G., Auclair, D., Baker, A., Bergsagel, P.L., Bernstein, B.E., Drier, Y., Fonseca, R., Gabriel, S.B., Hofmeister, C.C., Jagannath, S., Jakubowiak, A.J., Krishnan, A., Levy, J., Liefeld, T., Lonial, S., Mahan, S., Mfuko, B., Monti, S., Perkins, L.M., Onofrio, R., Pugh, T.J., Rajkumar, S.V., Ramos, A.H., Siegel, D.S., Sivachenko, A., Stewart, A.K., Trudel, S., Vij, R., Voet, D., Winckler, W., Zimmerman, T., Carpten, J., Trent, J., Hahn, W.C., Garraway, L.A., Meyerson, M., Lander, E.S., Getz, G., Golub, T.R., Initial genome sequencing and analysis of multiple myeloma. *Nature* **2011**, 471, 467.
272. Alexanian, R., Delasalle, K., Wang, M., Thomas, S., Weber, D., Curability of multiple myeloma. *Bone Marrow Research* **2012**, 2012, 916479.
273. de Wilt, L.H.A.M., Jansen, G., Assaraf, Y.G., van Meerloo, J., Cloos, J., Schimmer, A.D., Chan, E.T., Kirk, C.J., Peters, G.J., Kruyt, F.A.E., Proteasome-based mechanisms of intrinsic and acquired bortezomib resistance in non-small cell lung cancer. *Biochemical Pharmacology* **2012**, 83, 207.
274. Franke, N.E., Niewerth, D., Assaraf, Y.G., van Meerloo, J., Vojtekova, K., van Zantwijk, C.H., Zweegman, S., Chan, E.T., Kirk, C.J., Geerke, D.P., Schimmer, A.D., Kaspers, G.J.L., Jansen, G., Cloos, J., Impaired bortezomib binding to mutant $\beta 5$ subunit of the proteasome is the underlying basis for bortezomib resistance in leukemia cells. *Leukemia* **2012**, 26, 757.
275. Anbanandam, A., Albarado, D.C., Tirziu, D.C., Simons, M., Veeraraghavan, S., Molecular basis for proline- and arginine-rich peptide inhibition of proteasome. *Journal of molecular biology* **2008**, 384, 219.
276. Lansdell, T.A., Hurchla, M.A., Xiang, J., Hovde, S., Weilbaecher, K.N., Henry, R.W., Tepe, J.J., Noncompetitive modulation of the proteasome by imidazoline scaffolds overcomes bortezomib resistance and delays MM tumor growth *in vivo*. *ACS Chemical Biology* **2013**, 8, 578.
277. Azevedo, L.M., Lansdell, T.A., Ludwig, J.R., Mosey, R.A., Woloch, D.K., Cogan, D.P., Patten, G.P., Kuszpit, M.R., Fisk, J.S., Tepe, J.J., Inhibition of the human proteasome by imidazoline scaffolds. *Journal of Medicinal Chemistry* **2013**, 56, 5974.
278. Sprangers, R., Li, X., Mao, X., Rubinstein, J.L., Schimmer, A.D., Kay, L.E., TROSY-based NMR evidence for a novel class of 20S proteasome inhibitors. *Biochemistry* **2008**, 47, 6727.
279. Kroll, M., Arenzana-Seisdedos, F., Bachelier, F., Thomas, D., Friguet, B., Conconi, M., The secondary fungal metabolite gliotoxin targets proteolytic activities of the proteasome. *Chemistry & biology* **1999**, 6, 689.

280. Li, X., Wood, T.E., Sprangers, R., Jansen, G., Franke, N.E., Mao, X., Wang, X., Zhang, Y., Verbrugge, S.E., Adomat, H., Li, Z.H., Trudel, S., Chen, C., Religa, T.L., Jamal, N., Messner, H., Cloos, J., Rose, D.R., Navon, A., Guns, E., Batey, R.A., Kay, L.E., Schimmer, A.D., Effect of noncompetitive proteasome inhibition on bortezomib resistance. *Journal of the National Cancer Institute* **2010**, 102, 1069.
281. Schirle, M., Bantscheff, M., Kuster, B., Mass spectrometry-based proteomics in preclinical drug discovery. *Chemistry & biology* **2012**, 19, 72.
282. Rajkumar, S.V., Hayman, S.R., Lacy, M.Q., Dispenzieri, A., Geyer, S.M., Kabat, B., Zeldenrust, S.R., Kumar, S., Greipp, P.R., Fonseca, R., Lust, J.A., Russell, S.J., Kyle, R.A., Witzig, T.E., Gertz, M.A., Combination therapy with lenalidomide plus dexamethasone (Rev/Dex) for newly diagnosed myeloma. *Blood* **2005**, 106, 4050.
283. Krönke, J., Udeshi, N.D., Narla, A., Grauman, P., Hurst, S.N., McConkey, M., Svinkina, T., Heckl, D., Comer, E., Li, X., Ciarlo, C., Hartman, E., Munshi, N., Schenone, M., Schreiber, S.L., Carr, S.A., Ebert, B.L., Lenalidomide causes selective degradation of IKZF1 and IKZF3 in multiple myeloma cells. *Science* **2014**, 343, 301.
284. Batth, T.S., Francavilla, C., Olsen, J.V., Off-line high-pH reversed-phase fractionation for in-depth phosphoproteomics. *Journal of Proteome Research* **2014**, 13, 6176.
285. Cox, J., Mann, M., MaxQuant enables high peptide identification rates, individualized p.p.b.-range mass accuracies and proteome-wide protein quantification. *Nature Biotechnology* **2008**, 26, 1367.
286. Udeshi, N.D., Mani, D.R., Eisenhaure, T., Mertins, P., Jaffe, J.D., Clauser, K.R., Hachohen, N., Carr, S.A., Methods for quantification of *in vivo* changes in protein ubiquitination following proteasome and ubiquitinase inhibition. *Molecular & Cellular Proteomics* **2012**, 11, 148.
287. Kim, W., Bennett, E.J., Huttlin, E.L., Guo, A., Li, J., Possemato, A., Sowa, M.E., Rad, R., Rush, J., Comb, M.J., Harper, J.W., Gygi, S.P., Systematic and quantitative assessment of the ubiquitin modified proteome. *Molecular cell* **2011**, 44, 325.
288. Bavelloni, A., Piazzini, M., Raffini, M., Faenza, I., Blalock, W.L., Prohibitin 2: At a communications crossroads. *IUBMB Life* **2015**, 67, 239.
289. Rydström, J., Mitochondrial NADPH, transhydrogenase and disease. *Biochimica et Biophysica Acta (BBA) - Bioenergetics* **2006**, 1757, 721.
290. Chevrollier, A., Loiseau, D., Reynier, P., Stepien, G., Adenine nucleotide translocase 2 is a key mitochondrial protein in cancer metabolism. *Biochimica et Biophysica Acta (BBA) - Bioenergetics* **2011**, 1807, 562.

291. Bridges, Hannah R., Birrell, James A., Hirst, J., The mitochondrial-encoded subunits of respiratory complex I (NADH:ubiquinone oxidoreductase): Identifying residues important in mechanism and disease. *Biochemical Society Transactions* **2011**, 39, 799.
292. Polier, G., Neumann, J., Thuaud, F., Ribeiro, N., Gelhaus, C., Schmidt, H., Giaisi, M., Köhler, R., Müller, Wolfgang W., Proksch, P., Leippe, M., Janssen, O., Désaubry, L., Krammer, Peter H., Li-Weber, M., The natural anticancer compounds rocaglamides inhibit the Raf-MEK-ERK pathway by targeting prohibitin 1 and 2. *Chemistry & biology* **2012**, 19, 1093.
293. Cheng, J., Gao, F., Chen, X., Wu, J., Xing, C., Lv, Z., Xu, W., Xie, Q., Wu, L., Ye, S., Xie, H., Zheng, S., Zhou, L., Prohibitin-2 promotes hepatocellular carcinoma malignancy progression in hypoxia based on a label-free quantitative proteomics strategy. *Molecular Carcinogenesis* **2014**, 53, 820.
294. Kahlon, D.K., Lansdell, T.A., Fisk, J.S., Hupp, C.D., Friebe, T.L., Hovde, S., Jones, A.D., Dyer, R.D., Henry, R.W., Tepe, J.J., Nuclear factor-kappaB mediated inhibition of cytokine production by imidazoline scaffolds. *Journal of Medicinal Chemistry* **2009**, 52, 1302.
295. Cox, J., Neuhauser, N., Michalski, A., Scheltema, R.A., Olsen, J.V., Mann, M., Andromeda: A peptide search engine integrated into the MaxQuant environment. *Journal of Proteome Research* **2011**, 10, 1794.